EVOLUTION OF THE GALAPAGOS RISE AND THE BAUER MICROPLATE: IMPLICATIONS FOR THE NAZCA PLATE

A Dissertation

by

JENNIFER CATHERINE MCGUIRE WRIGHT

Submitted to the Office of Graduate Studies of
Texas A&M University
in partial fulfillment of the requirements for the degree of

DOCTOR OF PHILOSOPHY

December 2004

Major Subject: Geophysics

EVOLUTION OF THE GALAPAGOS RISE AND THE BAUER MICROPLATE: IMPLICATIONS FOR THE NAZCA PLATE

A Dissertation

by

JENNIFER CATHERINE MCGUIRE WRIGHT

Submitted to Texas A&M University
in partial fulfillment of the requirements
for the degree of

DOCTOR OF PHILOSOPHY

Approved as to style and content by:

Thomas W.C. Hilde (Chair of Committee)	Mark E. Everett (Member)
David Sparks (Member)	William W. Sager (Member)
William R. Bryant (Member)	Richard L. Carlson (Head of Department)

December 2004

Major Subject: Geophysics

ABSTRACT

Evolution of the Galapagos Rise and the Bauer Microplate: Implications for the Nazca Plate. (December 2004)

Jennifer Catherine McGuire Wright, B.S., State University of New York at Stony Brook

Chair of Advisory Committee: Dr. Thomas W.C. Hilde

Analysis of the satellite altimetry based predicted bathymetry, magnetic anomalies, and earthquake seismic data relating to the geophysical structure on the Nazca plate indicates that the Galapagos Rise system served as the transitional spreading system between Pacific-Farallon spreading and the current East Pacific Rise (EPR) system.

First order age/depth relationships for this area indicate that the Galapagos Rise, the most prominent extinct spreading system within the Nazca plate, accommodated most of the Pacific-Nazca plate separation from ~23 million years ago (Ma) to ~8 Ma. After this time, spreading was dominantly along the EPR, with probable ultra slow spreading along the Galapagos Rise continuing until very recent times (0-5 Ma). Magnetic lineations and depth trends across the Bauer Basin suggest that it was captured between the failing Galapagos Rise and the currently active EPR. Anomalously shallow ridge crests along the Galapagos Rise indicate that magmatic activity may have occurred

until very recent time (0-5 Ma). Tightly curved (concave southward) fracture zones offsetting Galapagos Rise ridge segments indicate a pole of rotation at the present day position of ~22.5°S and ~99.5°W. The curvature of the fracture zones and the fan-shaped spreading pattern of seafloor structures produced at the Galapagos Rise indicate that the Galapagos Rise initiated parallel to the Mendaña fracture zone. Consistent with the rotation of the Nazca plate after the fragmentation of the Farallon plate, the Galapagos Rise rotated counter-clockwise during its active phase. The Galapagos Rise initiated in the vicinity of Gallego fracture zones and propagated southward. Failure of the Galapagos Rise occurred as spreading jumped westward in stages to the East Pacific Rise.

DEDICATION

This work is dedicated to my family, for their constant encouragement and belief in my success, and to my son, whose smile inspires me.

ACKNOWLEDGMENTS

I would like to sincerely thank Dr. Thomas Hilde for his support and guidance during my pursuit of my graduate degree. I greatly appreciate his contributions to my research and my professional development. In addition, I would like to thank Dr. Mark Everett for his continual assistance and interest in my development as a scientist. I have benefited from their enthusiasm, advice, and support in my research pursuits.

Thanks are also due to Drs. David Sparks and William Sager, who provided a great deal of help in the form of critical review, and Dr. Gary Acton for his contribution and support in the operation of the magnetic anomaly modeling program.

Most important of all, I would like to thank my family for their unending support in all phases of my professional career and personal life. Most especially my parents, John Edward McGuire Sr. and Catherine Dolores McGuire, and my brother, John Edward McGuire, Jr., always show their confidence in my abilities and faith in my success. My husband, Granville Clay Wright, Jr., believes in me and supports me in more ways than I can count. My son, Granville Clay Wright IV, inspires me to always strive for the better. Without the love of my family, this work would not have been possible.

TABLE OF CONTENTS

	Page
ABSTRACT	iii
DEDICATION	v
ACKNOWLEDGMENTS	vi
TABLE OF CONTENTS	vii
LIST OF TABLES	ix
LIST OF FIGURES	x
INTRODUCTION	1
GEOLOGIC SETTING	9
The Nazca Plate	9
Previous Galapagos Rise Reconstructions	13
DATA AND METHODS	22
NGDC Ship track Bathymetry and Magnetic Anomaly Data	23
Predicted Bathymetry	33
Seafloor Fabric	36
Earthquakes	42
Euler Poles	46
Reconstructions	49
ANALYSIS	52
Age/Depth Relationships	52
Bathymetry and Seafloor Structure	55
Seafloor Fabric	70
Magnetic Anomalies	73
Reconstructions	82
The 23 Million Years Reconstruction	83
The 19.5 Million Years Reconstruction	91
The 14.7 Million Years Reconstruction	94
The 9.5 Million Years Reconstruction	95
The 5.9 Million Years Reconstruction	96

Page

The Present Day 97

DISCUSSION 99

CONCLUSIONS 106

REFERENCES 110

VITA 117

LIST OF TABLES

Table		Page
1	Identification numbers and source institutions of bathymetric and magnetic for ship track data obtained from the NGDC and used in this study	25
2	List of parameters used to calculate synthetic magnetic anomaly profile	32
3	List of parameters used in the tectonic reconstruction program	51

LIST OF FIGURES

Figure		Page
1	Location map of study area illustrating locations of significant morpho-tectonic features.	2
2	Predicted bathymetry [Smith and Sandwell, 1997] map illustrating depth variation within the study area	4
3	Magnetic anomaly lineations in the study area adapted from Herron [1972].	11
4	Reconstruction of the Galapagos Rise system adapted from Mammerickx et al. [1980].	16
5	Reconstruction of the Galapagos Rise system adapted from Lonsdale [1989].	18
6	Reconstruction of the Galapagos Rise system adapted from Goff and Cochran [1996].	19
7	Map illustrating coverage of ship track bathymetry and magnetic anomaly data in the study area.	24
8	Synthetic model of the total field magnetic reversal sequence	31
9	Comparison of ship track bathymetry locations from the *R/V Yaquina* cruise (1971) obtained from the NGDC plotted verses the same locations from the Smith and Sandwell (1997) predicted bathymetry grid.	35
10	Comparison of independent ship track bathymetry and predicted bathymetry extracted at the same locations from the Smith and Sandwell [1997] grid.	37
11	Shaded relief image of the predicted bathymetry data from Smith and Sandwell [1997], illuminated from an azimuth of 0°	39
12	Shaded relief image of the predicted bathymetry data from Smith and Sandwell [1997], illuminated from an azimuth of 45°.	40

Figure		Page
13	Shaded relief image of the predicted bathymetry data from Smith and Sandwell [1997], illuminated from an azimuth of 315°.....	41
14	Map of the focus centers of earthquakes from the NEIC and NOAA hydrophone network in the study area relative to the Smith and Sandwell [1997] predicted bathymetry grid..	44
15	Location map of study area illustrating locations of bathymetric features discussed in text and Figures 21-23 and 25-27.....	47
16	Equal area projection of graphically determined Euler pole locations based on curvature of Galapagos Rise fracture zones...	48
17	Predicted bathymetry map from the Smith and Sandwell [1997] grid showing the locations of the magnetic anomaly lineations used to determine the age/depth relationship for the study area.	53
18	Curve fit to age data obtained from Cande et al. [1989] magnetic anomaly lineations and associated depth values from the predicted bathymetry grid.....	54
19	Depth-predicted age map of the study area..	56
20	Depth-predicted age map filtered to a 25 km radius to better resolve age boundaries.....	57
21	a) Bathymetric profile stack from north (top) to south (bottom) of the GR1 ridge crest. b) Profiles were extracted from the gridded Smith and Sandwell [1997] predicted bathymetry set at 2-minute resolution along the profile path.	59
22	a) Bathymetric profile stack from north (top) to south (bottom) of the GR2 ridge crest. Blue lines indicate the ridge crest of the overlapping spreading centers. Red lines indicate the -1000 m contour on each profile for calibration with the depth scale. b) Profiles were extracted from the gridded Smith and Sandwell (1997) predicted bathymetry set at 2-minute resolution along the profile path.	61

Figure		Page
23	a) Bathymetric profile stack from north (top) to south (bottom) of the GR3 ridge crest. Red lines indicate the -2500 m contour on each profile for calibration with the depth scale. b) Profiles were extracted from the gridded Smith and Sandwell (1997) predicted bathymetry set at 2-minute resolution along the profile path.	63
24	Comparison of a) the Valdavia fracture zone system on the Chile Rise to b) the transition zone of the southern Galapagos Rise and c) the Gofar and Quebrada fracture zones on the EPR.	64
25	Stacked bathymetry profiles extracted from the predicted bathymetry grid to illustrate the morpho-structural features of the Bauer Scarp.	66
26	Stacked bathymetry profiles extracted from the predicted bathymetry grid to illustrate discontinuities present at the a) northern and b) eastern tectonic boundaries of the Galapagos Rise system. c) Locations of profiles plotted for reference	67
27	a) Stacked bathymetry profiles extracted from the predicted bathymetry grid to illustrate the morpho-structural features of the SEGR. b) Locations of profiles plotted for reference.	69
28	Magnetic anomaly trends from available ship track data in the study area	71
29	Index map for magnetic anomaly correlations in Figures 30, 31, 32, and 33.	74
30	Correlation of identified magnetic anomaly lineations mapped in the study area to synthetic magnetic reversal sequence.	76
31	Magnetic anomaly trends mapped in the Bauer Basin area	78
32	Magnetic anomaly trends mapped in the eastern portion of the Nazca plate.	79
33	Magnetic anomaly trends mapped in the SEGR region.....	81

Figure		Page
34	Reconstruction of the Galapagos Rise at 23 Ma	84
35	Reconstruction of the Galapagos Rise at 19.5 Ma	85
36	Reconstruction of the Galapagos Rise at 14.7 Ma	86
37	Reconstruction of the Galapagos Rise at 9.5 Ma	87
38	Reconstruction of the Galapagos Rise at 5.9 Ma	88
39	Present-day configuration of the study area	89

INTRODUCTION

The transfer of active spreading from one location to another following the reorientation of plate motion occurs by means of ridge jump and ridge propagation at new trends. The breakup of the Farallon plate into the Nazca and Cocos plates precipitated several major ridge jumps in the eastern Pacific. During the last 23 million years, the Galapagos Rise (Figure 1) represented a major component of the transition from the seafloor spreading between the Pacific and Farallon plates to the spreading between the Pacific and Nazca plates [Mammerickx et al., 1980, Hey, 1977, Hey et al., 1980, Lonsdale, 1989, Goff and Cochran, 1996].

The nature of the transition between the Pacific-Farallon spreading system and the East Pacific Rise (EPR) south of the equator has been a topic of inquiry since the discovery of the extremely shallow peak at the northern end of the Galapagos Rise [Menard et al., 1964]. Subsequent geophysical surveys and related attempts to explain the details of the spreading reorientation on the Nazca plate have revealed an increasingly complex history of the transition that yields insight into the nature of ridge jumps, microplate formation, and the processes of plate fragmentation.

Development of the global uniform gridded predicted bathymetry based

---

This dissertation follows the style of the *Journal of Geophysical Research*.

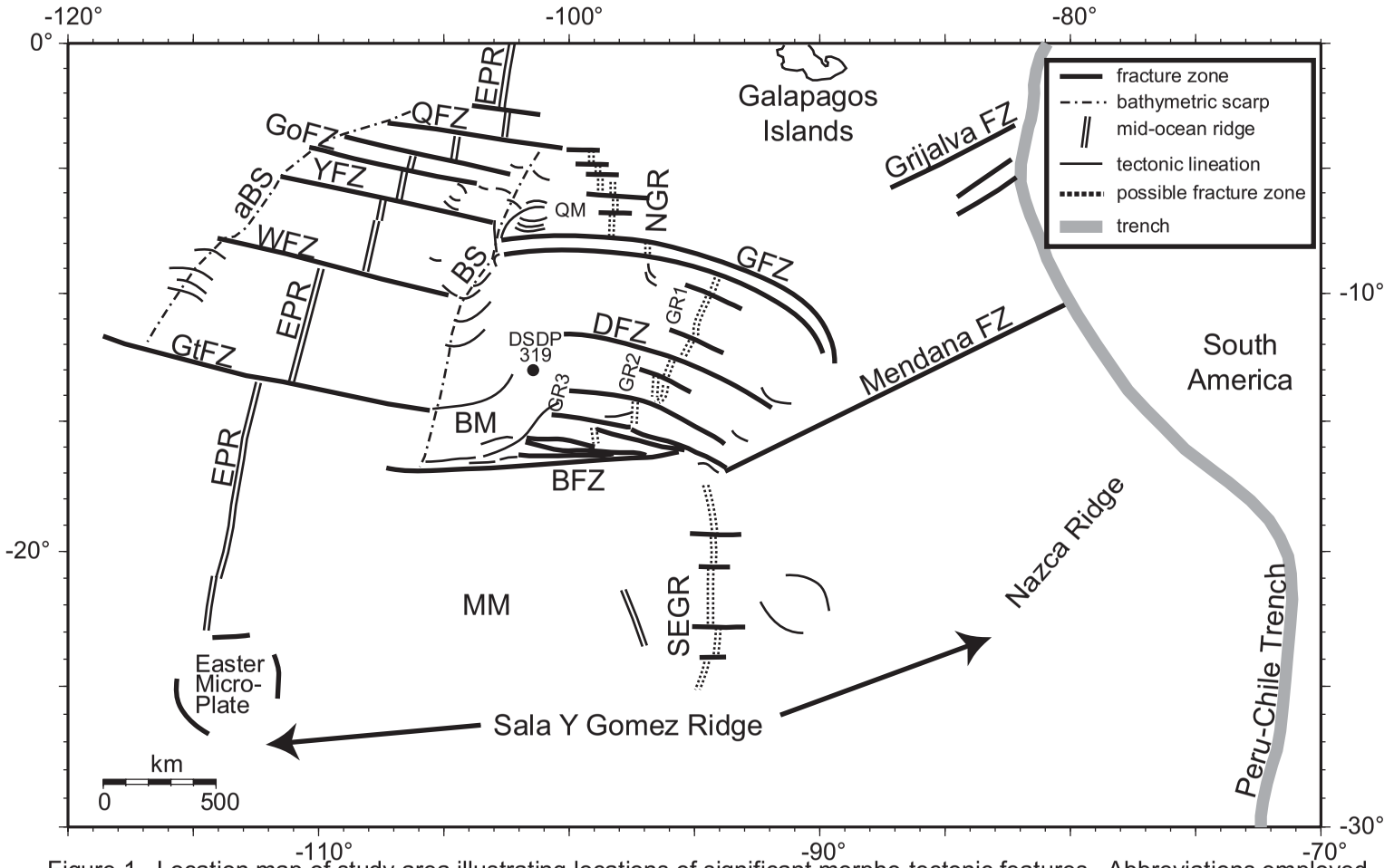

Figure 1. Location map of study area illustrating locations of significant morpho-tectonic features. Abbreviations employed are: EPR = East Pacific Rise, GR = Galapagos Rise, SEGR = Southeast Galapagos Rise, NGR = North Galapagos Rise, GFZ = Gallego Fracture Zone, DFZ = Dana Fracture Zone, QFZ = Quebrada Fracture Zone, GfFZ = Gofar Fracture Zone, YFZ = Yaquina Fracture Zone, WFZ = Wilkes Fracture Zone, GoFZ = Garrett Fracture Zone, BS = Bauer Scarp, aBS = anti-Bauer Scarp, BM = Bauer Microplate, BFZ = Bauer Fracture Zone, MM = Mendoza Microplate, QM = Quebrada Microplate Double dotted lines indicate extinct spreading centers. Dash-dot lines indicate bathymetric scarps.

on satellite altimetry data sets by Smith and Sandwell [1997] provides aerial resolution of seafloor morphology and structure with complete ocean coverage at two-minute spatial resolution. Greatly improved maps of seafloor depth and structures (Figure 2) thus present an opportunity to resolve uncertainties in the evolutionary details of the Galapagos Rise region.

The development of the predicted bathymetry data set by Smith and Sandwell [1997] yielded an unprecedented aerial view of the bathymetry by means of a high resolution, ocean-wide map of the seafloor. Previous gridded bathymetry was restricted to the limited areas with sufficient shipboard surveys. Some areas are densely populated with ship tracks that include depth measurements, while other areas contain only sparse ship tracks. Consequently, an ocean-wide uniform high resolution grid was impossible based solely on ship-collected data. Using satellite altimeter measurements of the sea surface, however, a gravity anomaly map of the oceans was made and used to create a predicted seafloor bathymetry map that is accurate to ~99% in correlation with subsequent shipboard surveys (see text in Data and Methods). In the region of the study area, the 2-minute resolution of the data makes it possible to trace the bathymetric character of seafloor structures, ridge segments and fracture zones across long distances of seafloor and creates the opportunity to infer the history of the seafloor in these areas based on morphological characteristics.

Satellite altimeter measurements are made using a radar-equipped

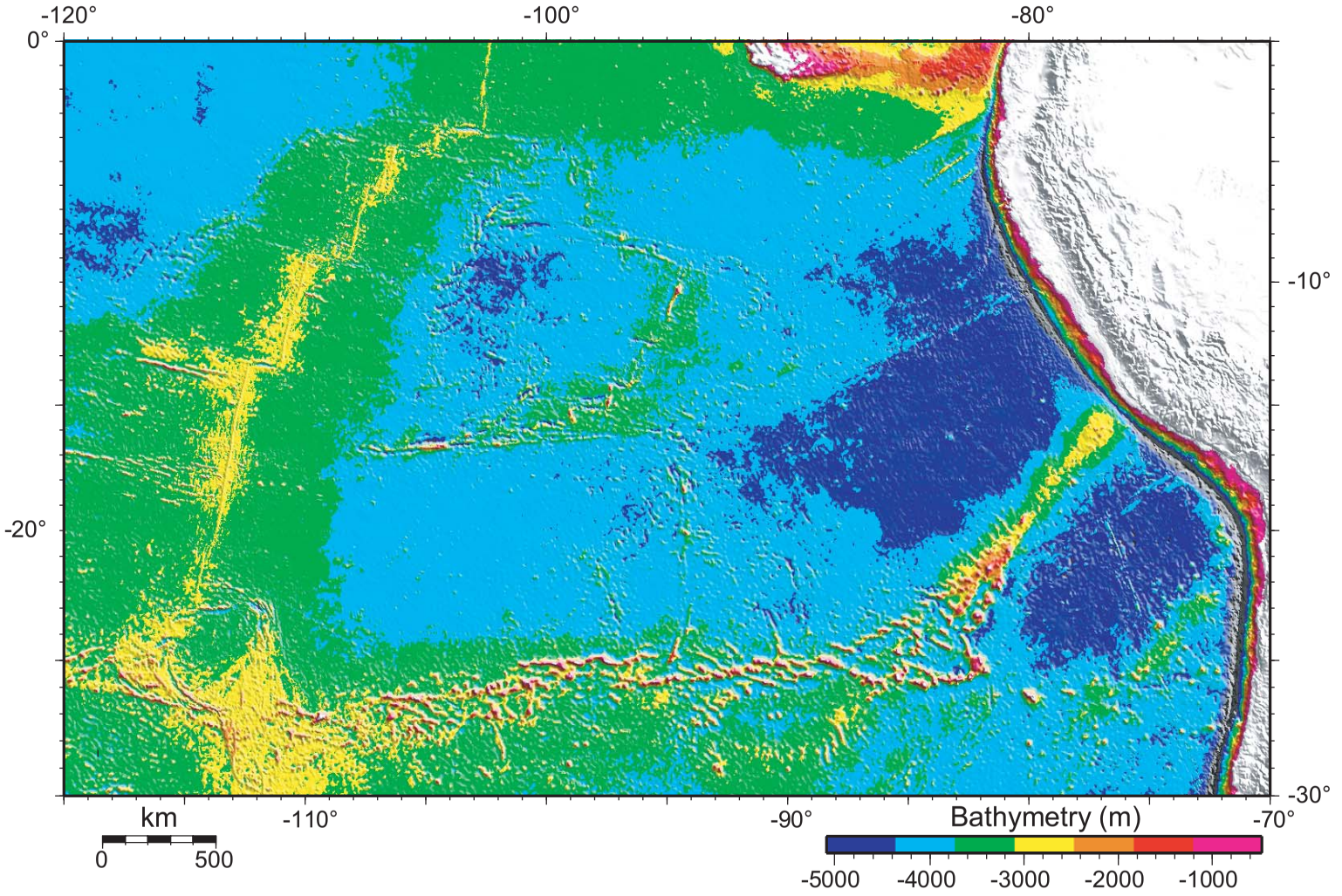

Figure 2. Predicted bathymetry [Smith and Sandwell, 1997] map illustrating depth variation within the study area.

satellites to measure the distances between the satellite and the sea surface. Stacking and averaging repeated orbital measurements allows the removal of higher-order transient effects such as waves and swells [Sandwell, 1990, Smith, 1993, and the National Oceanic and Atmospheric Administration website: http://www.ngdc.noaa.gov/mgg/bathymetry/predicted/explore.html].

The relationship between seafloor age and depth has been evaluated using several different models [Sclater et al., 1971, Davis and Lister, 1974, Parsons and Sclater, 1977, Stein and Stein, 1992, DeLaughter et al., 1999]. The relationship relies on the cooling and thickening of the lithosphere with distance from the ridge crest, and provides fundamental constraints to the evolution of oceanic lithosphere [Davis and Lister, 1974, Parsons and Sclater, 1977, Hayes, 1992, Phipps Morgan and Smith, 1992, Stein and Stein, 1992]. The age/depth models are valid only to predict the age of seafloor produced at mid-ocean ridges that have remained undisturbed by subsequent thermal or tectonic events. Locations that experience tectonic disturbances such as fracture zones or reheating events such as hot spots or off-ridge volcanism may alter the depth of the seafloor. In places where such disturbances have occurred, the depths of the seafloor cannot be considered a true predictor of age. The half-space cooling model predicts that depth increases linearly with the square root of age, as the plate cools and becomes increasingly thicker with age [Davis and Lister, 1974, Phipps Morgan and Smith, 1992]. Parsons and Sclater [1977] established that the relationship between age of the seafloor and

depth varies systematically by the square root of the age of the seafloor, but observed that the depth apparently approaches a constant value at older ages (and therefore the plate approaches a constant thickness). This relationship was developed to predict the global average of seafloor depth and heat flow as a function of the age of the seafloor. As noted by Stein and Stein [1992], the Parsons and Sclater [1977] relationship predicts lower heat flow and greater seafloor depths than observed values for seafloor greater than ~70 Ma because it assumes that only conductive cooling is responsible for the removal of heat.

Stein and Stein [1992] were able to use a much larger data set than Parsons and Sclater [1977], and were therefore able to construct a model that predicted heat flow and depth with a better fit to observed values, particularly at ages greater than ~70 Ma. The Stein and Stein [1992] model, referred to as GDH1 (Global Depth and Heat Flow) jointly fits the depth and heat flow data to develop a relationship between depth, heat flow, and age. Both the Parsons and Sclater [1977] and the Stein and Stein [1992] model yield relationships where depth varies by the square root of age. Both models are useful for predicting age values based on seafloor depth where little or no independent age data are available. The Stein and Stein [1992] model is particularly useful (due to better overall fit of observed depth and heat flow values) for predicted age in older seafloor.

Further studies, however, suggest that half-space cooling and global plate models predicting subsidence of the seafloor based on age are not complex

enough to reflect observed seafloor depths in many regions [Hayes, 1992, Calcagno and Cazenave, 1994, Marks and Stock, 1994, Levitt and Sandwell, 1996]. In particular, departures from the depth-square root of age trend in the central Pacific can occur at ages of less than 20 Ma [Calcagno and Cazenave, 1994]. This is significant for this study as most of the tectonic evolution of the Galapagos Rise takes place between 23 Ma and 1.95 Ma.

In this study, we first examined the morphology from the predicted bathymetry and the available magnetic anomaly data in order to establish the depth/age relationships across the region. Magnetic anomaly lineations were mapped across the study area to determine age trends in relation to morphological features. Euler poles were located based on the curvature of fracture zones in the Galapagos Rise system to examine the relative plate rotation that took place during the early stages of active spreading between the Nazca and Pacific plates. Earthquake data for the region were studied to identify active tectonic zones and plate boundaries. Finally, Pacific-Nazca reconstructions were made based on these data to demonstrate the details of the initiation, evolution, and eventual failure of the Galapagos Rise spreading system.

This analysis indicates that the Galapagos Rise represents a transitional spreading system in the transfer from stable spreading on the Pacific-Farallon system to the Pacific-Nazca spreading system, following breakup of the Farallon plate into the Cocos and Nazca plates. Rotation of the Galapagos Rise

spreading system occurred concurrently with the north-south component of separation of the Cocos and Nazca plates. The extremely shallow depths present along the northern ridge crest (GR1) of the Galapagos Rise (~550 m) indicate post-spreading magmatic activity. Active Pacific-Nazca spreading was fully transferred (in stages) to the northward-propagating East Pacific Rise between 1.95 and 8 Ma.

GEOLOGIC SETTING

The Nazca Plate

The distribution of seafloor depths in the study area yields insight into the tectonic history of the region. Seafloor produced by spreading centers and undisturbed by other events can be identified by the systematic increase of depth with distance from the spreading center [Sclater et al., 1971, Davis and Lister, 1974, Parsons and Sclater, 1977, Stein and Stein, 1992]. The departures from this relationship often represent the surface expression of regions where subsequent tectonic events have taken place, such as the initiation of new spreading [Mammerickx et al., 1980, Mammerickx and Sandwell, 1986, Goff and Cochran, 1996]. Other departures from the depth/age relationship in the study region can be attributed to hotspot swells, volcanic chains, off-ridge volcanism, etc. [Mammerickx et al., 1980, Mammerickx and Sandwell, 1986, Goff and Cochran, 1996, Calcagno and Cazenave, 1994].

Depth distribution patterns on the Nazca plate are primarily formed by the cooling, thickening, and subsidence of lithosphere associated with age and distance from current and past spreading center systems. Increasing depths across the seafloor on the Nazca plate correspond to the square root of age relationship, but there are significant asymmetries in subsidence on seafloor associated with Pacific-Nazca spreading [Perrot et al., 1998, Levitt and Sandwell, 1996, Marty and Cazenave, 1989, Cochran, 1986]. The asymmetries

in depth with distance and age from the ridge crest for areas of seafloor symmetric about the ridge crest are most prominent on the EPR from 3-18° S [Rea, 1978, Rea, 1981, Cochran, 1986, Lonsdale, 1989]. The west flank of the EPR in this region is significantly shallower than the east flank (300 m by 5 Ma) [Cochran, 1986, and Levitt and Sandwell, 1996]. This section of the EPR is parallel to the extinct Galapagos Rise on the Nazca plate (Figure 2).

The spreading history of the Nazca plate has been postulated based on the magnetic anomaly lineations and reversal ages and the analysis of the bathymetry associated with features such as extinct spreading ridges and transform regions on the Pacific and Nazca plates [Menard et al., 1964, Herron, 1972, Handschumacher, 1976, Mammerickx et al., 1975, Menard, 1978, Mammerickx et al., 1980, Engebretson et al., 1984, Cande and Leslie, 1986, Searle and Francheteau, 1986, Pardo-Casas and Molnar, 1987, Rosa and Molnar, 1988, Lonsdale, 1989, Searle, 1989, Mayes et al. 1990, Cande and Haxby, 1991, Goff and Cochran, 1996, Jordahl et al., 1998]. The first comprehensive mapping of the magnetic anomalies on the Nazca plate and on the Pacific plate was done by Herron [1972]. She concluded that they represent Pacific-Farallon and Pacific-Nazca spreading (Figure 3). This and later studies focused on conjugate sets of magnetic anomalies and bathymetric expressions of fracture zones that were used to postulate the spreading history of the Nazca (Farallon) plates, including breakup of the Farallon plate into the Cocos and Nazca plates, the initiation of EPR spreading, the presence of the Galapagos

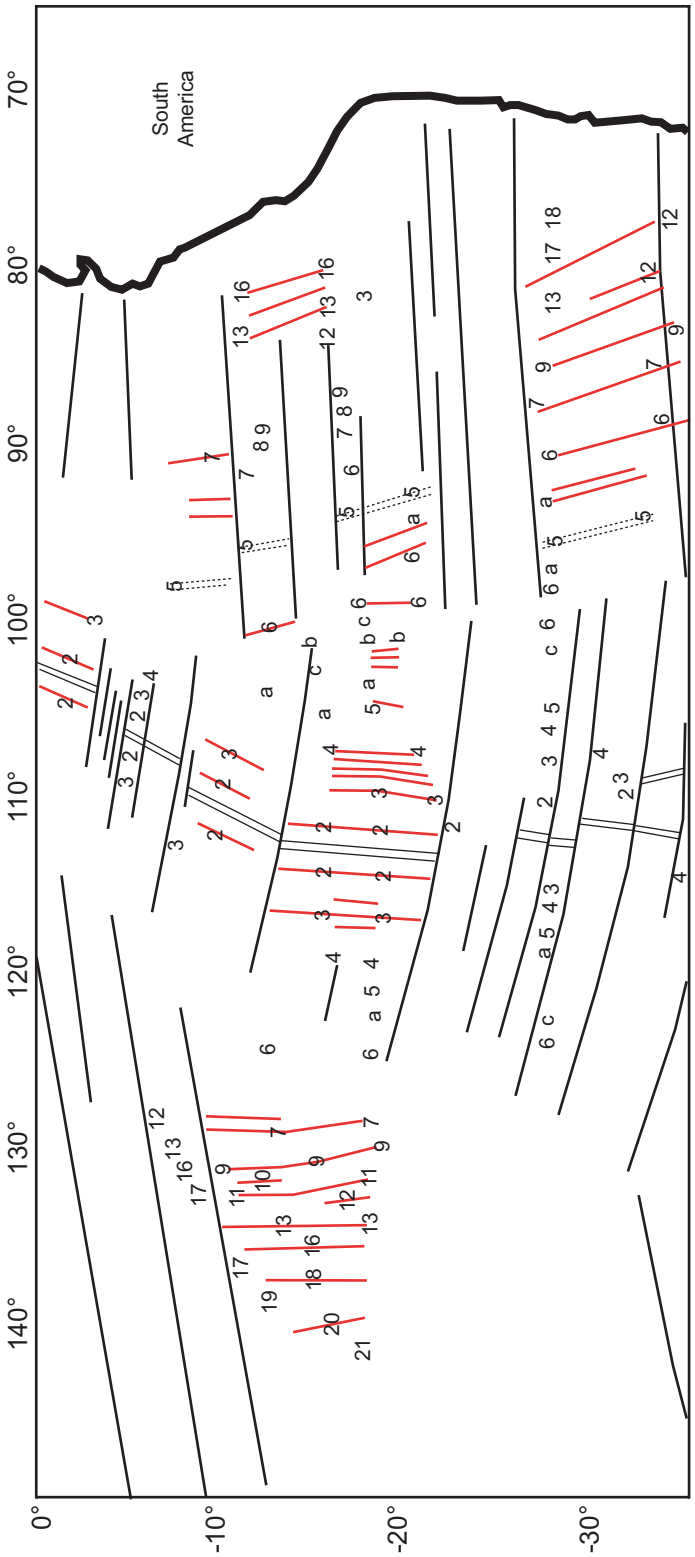

Figure 3. Magnetic anomaly lineations in the study area adapted from Herron [1972]. Double thin lines indicate active spreading centers. Double dashed lines indicate inactive spreading centers. Single black lines indicate fracture zones. Red lines indicate identified magnetic anomalies.

Rise system and several smaller ridge jumps [Mammerickx et al., 1980, Rosa and Molnar, 1988, Lonsdale, 1989, Mayes et al., 1990, Cande and Haxby, 1991, Goff and Cochran, 1996].

Wortel and Cloetingh [1983] constructed a finite element analysis based on age-dependant subduction to address the past and present stresses associated with the breakup of the Farallon plate. Their results predict that both the Cocos and Nazca plates rotated into their respective subduction zones in a way that caused the highest tensional stresses to be created perpendicular to the ridge segment trends of the current Galapagos Ridge. The reconstructions of Meschede and Barckhausen [2000] indicated that propagation of the Galapagos Ridge westward into the Pacific Basin slightly predated the initiation of the Galapagos Rise. The reconstructions of Meschede and Barckhausen [2000] indicate that the Galapagos Ridge underwent several ridge reconfigurations after its initiation ~23 Ma.

The Bauer Basin region, located between the Galapagos Rise and the EPR is covered by a thick layer of pelagic sediments, as identified by the drilling at Deep Sea Drilling Project (DSDP) Site 319 located in the western Bauer Basin (Figure 1). While some of the ages determined from these samples are as recent as 7-10 Ma [Hogan and Dymond, 1976, Reynolds, 1976, Seidemann, 1976] or as old as 24-40 Ma [Lanphere and Dalrymple, 1976, Reynolds, 1976], there is general agreement that the samples that produced these age determinations were altered. The enrichment of potassium or the depletion of

^{40}Ar in the sample would result in an age that is lower than those the ages determined by other experiments [Hogan and Dymond, 1976, Reynolds, 1976, Seidemann, 1976]. The age determinations with lower error estimates place the DSDP Site 319 basalts within the 15-19 Ma range. The oldest sediments recovered were determined to be 14-14.5 Ma at basement [Yeats et al., 1976]. Barrett and Friedrichsen [1982] constructed sediment thickness isopach maps to show the variations of sediment across the Nazca plate. They concluded that the thickest sediments were present on the areas of oldest crust, and in areas of high pelagic sediment productivity (such as the northern part of Bauer Basin). The thinnest sediments were present on the youngest crust, most recently found at the EPR and Galapagos Rise ridge crests.

Previous Galapagos Rise Reconstructions

The evolution of the Nazca Plate has involved three distinct sets of spreading centers in the southeast Pacific Ocean: the EPR system, the Galapagos Rise system, and the Pacific-Farallon system. The East Pacific Rise is the most recent and currently active spreading system, with the fastest recorded spreading rates in the world. The Galapagos Rise system was originally identified by [Menard et al., 1964] as a set of northeast-trending bathymetric rises in the southeastern Pacific. Herron [1972] used magnetic anomaly identifications to suggest that the Galapagos Rise system actually trended northwest, based on the identification of magnetic anomaly 7 on both

sides of the EPR (Figure 3). Rea [1978] and Rea [1981] used this determination to identify the Galapagos Rise as a part of the Farallon-Pacific spreading system. Mammerickx et al. [1980] later identified a fossil ridge called the Gallego Rise (5° S 120° W) west of the current EPR that trends parallel to the anomaly 7 identifications. The orientation of the postulated Gallego Rise is consistent with other fossil rises identified on the Nazca plate (such as the Mendoza, Roggeveen, and Selkirk Rises). These rises are suggested to be the remains of the Farallon-Pacific spreading system that was active prior to the breakup of the Farallon plate around 25 Ma [Mammerickx et al., 1975, Mammerickx et al., 1975, and Mammerickx et al., 1980]. The Gallego Rise is difficult to identify in the bathymetry data used in this study, as confirmed by Goff and Cochran [1996].

The Galapagos Rise was identified as a narrow ridge trending N10°E with a “huge seamount” [Mammerickx et al., 1980] at the northern end of the Galapagos Rise system, located at ~10.3°S latitude and ~95.8°W longitude (see Figure 2). These bathymetric features were identified using data collected by the 1977 R/V *Wecoma* and compiled data from other widely-spaced ship tracks. The identified “seamount” is resolved much more clearly in the predicted bathymetry data set [Smith and Sandwell, 1997], and is not an independent seamount, but rather the northern termination of the prominent ridge section at the Gallego double fracture zones (see Figure 2). Its extremely shallow depth was identified at ~550 meters below sea level at its peak [Mammerickx et al.,

1980] and is part of the continuous Galapagos Rise as defined in the predicted bathymetry data [Smith and Sandwell, 1997].

The EPR was initiated in the southeast Pacific after the progressive abandonment of several northwest-trending spreading centers north of 13°S in favor of the north- to northeast-trending system that is currently the EPR [Mammerickx et al., 1980, Rea, 1978, Rea, 1981, and Lonsdale, 1989]. This progression of ridge jumps followed the reorganization of plate motion during the Cenozoic and the subsequent breakup of the Farallon plate into the Cocos and Nazca plates. Specifically, [Mammerickx et al., 1980] identified the Galapagos Rise as the site of spreading along a proto-EPR between 7°S and 17°S (Figure 4). A ridge jump, occurring between 8.5 and 6.2 Ma, caused the locus of spreading along the Galapagos Rise to jump westward to the feature identified in the bathymetry as the Bauer Scarp. The distinct roughness of the Bauer Scarp was a result of slow initial spreading along the EPR segments [Mammerickx et al., 1980] and developed over approximately 0.9 Ma based on the bathymetric width of the zone of roughness [Rea, 1978]. The relief across the Bauer Scarp is primarily caused by the difference in age of the seafloor (and therefore depth) between the seafloor in the Bauer Deep and the 8.5-6.2 Ma seafloor produced by the EPR (see Figure 2). Between Wilkes fracture zone and 6.2°S, the distance from the EPR to Bauer Scarp was used to predict a 6.5 Ma age for the initiation of spreading along the EPR [Mammerickx et al., 1980]. The Bauer Deep (region east of the Bauer Scarp, identified by substantially

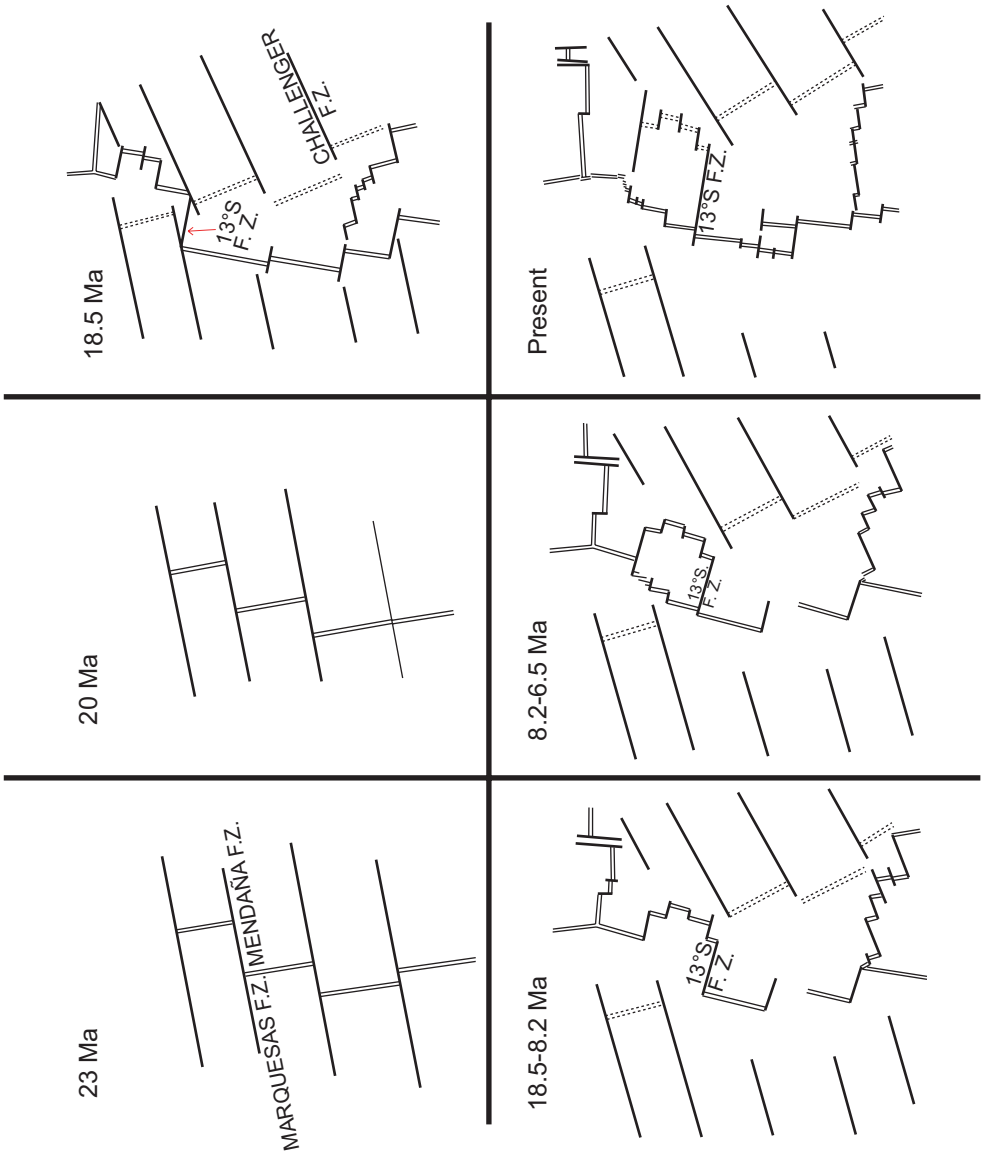

Figure 4. Reconstruction of the Galapagos Rise system adapted from Mammerickx et al. [1980]. Double thin lines indicate active spreading centers. Double dashed lines indicate inactive spreading centers. Single black lines indicate fracture zones.

deeper seafloor than that of EPR spreading in Figure 2) contains northwest trending magnetic anomalies identified by Lonsdale [1989] to be 16 Ma. When the Galapagos Rise segments ceased active spreading, the full fast spreading rate was transferred to the EPR in a series of ridge jumps and resulted in smoother bathymetric features between Bauer Scarp and the EPR ridge crests [Rea, 1978]. Wilkes fracture zone appears to have served as a temporary boundary between these spreading center jumps and connected the still-active parts of the Galapagos Rise with the newly active portions of the EPR.

A critical component of Rea's reconstruction is that, for a brief period, spreading existed on both the current EPR ridge system and the Galapagos Rise ridge system, creating a microplate between them known as the Bauer microplate [Rea, 1978 and Rea, 1981]. Subsequent interpretations of the Galapagos Rise evolution [Lonsdale, 1989, Goff and Cochran, 1996] have included the Bauer microplate as an important component of the reconstruction hypothesis. The Lonsdale [1989] reconstruction in particular, suggested that the Bauer microplate rotated counterclockwise as the EPR propagated northward from the Garrett fracture zone (Figure 5).

An alternate hypothesis for the evolution of the Galapagos Rise and EPR from 7°S and 17°S was proposed by Goff and Cochran [1996]. In this suggested evolution (Figure 6), two northward-propagating ridges initiated at the same time from the Garrett fracture zone, with the ridge to the east spreading fast and the ridge to the west spreading slowly. The eastern ridge became Galapagos Rise

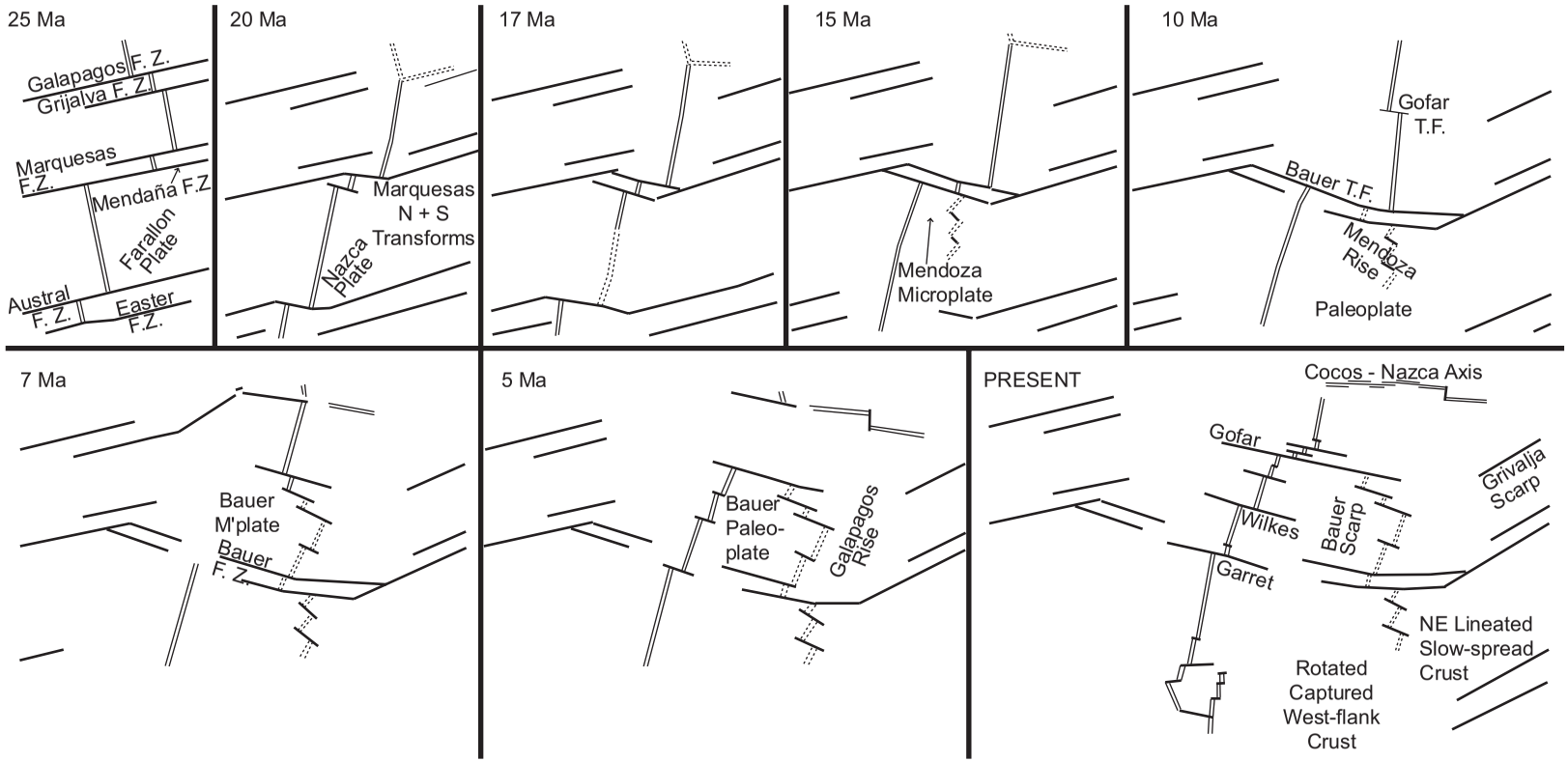

Figure 5. Reconstruction of the Galapagos Rise system adapted from Lonsdale [1989]. Double thin lines indicate active spreading centers. Double dashed lines indicate inactive spreading centers. Single black lines indicate fracture zones. GR indicates the location of the Galapagos Rise.

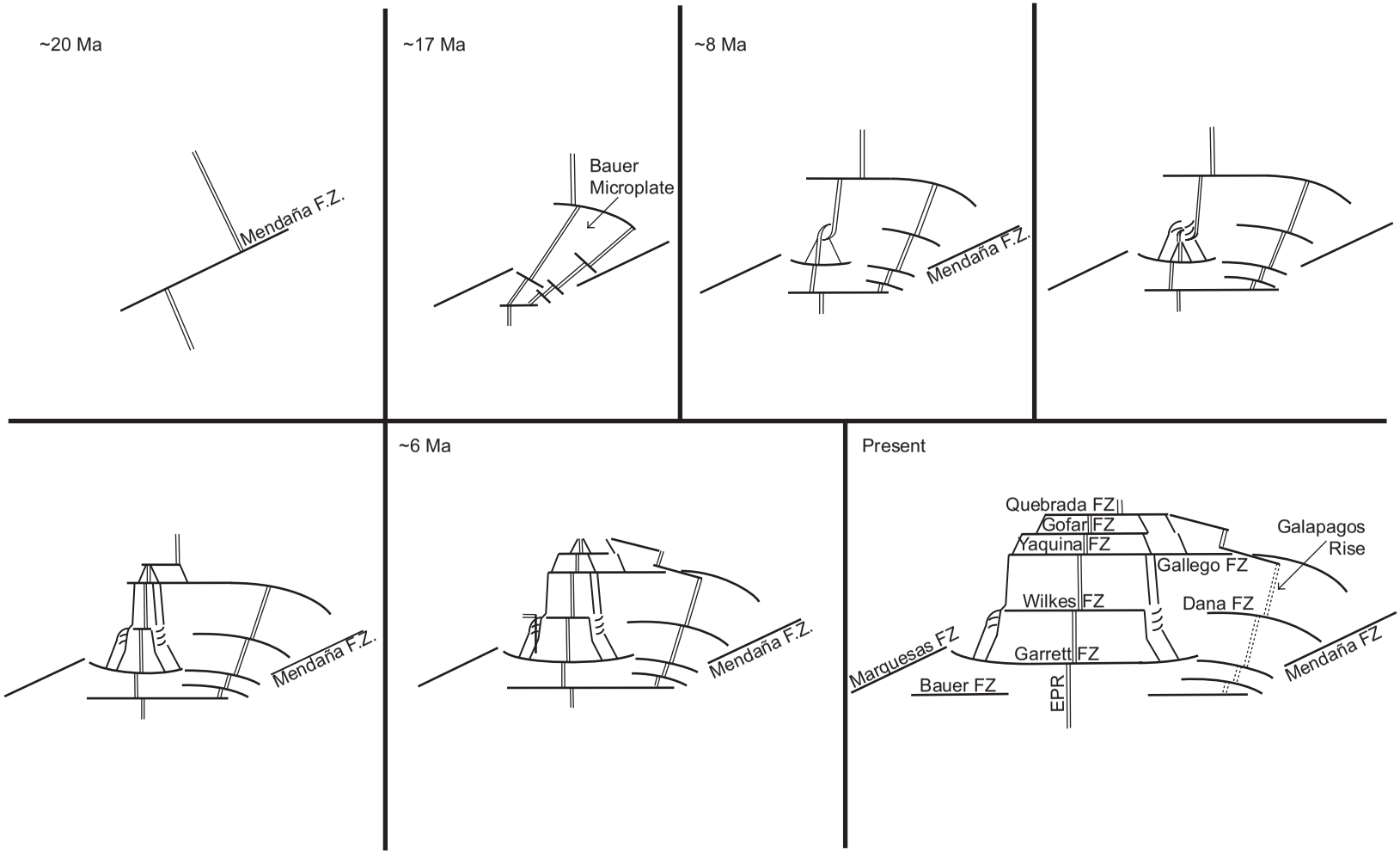

Figure 6. Reconstruction of the Galapagos Rise system adapted from Goff and Cochran [1996]. Double thin lines indicate active spreading centers. Double dashed lines indicate inactive spreading centers. Single black lines indicate fracture zones.

and the western ridge evolved into the EPR as spreading ceased along the Galapagos Rise (both ridges rotated counter-clockwise with time, creating the curved Gallego and Dana fracture zones on the Galapagos Rise, and the tightly curved bathymetric lineations on the borders of EPR spreading). The topographic roughness along Bauer Scarp is attributed to this initially slow-spreading western ridge system [Goff and Cochran, 1996, Mammerickx and Sandwell, 1986, and Mammerickx et al., 1980]. The trapped lithosphere between the simultaneous ridges created the proposed Bauer microplate extending from Garrett fracture zone in the south to the Gallego fracture zone in the north.

Typically, extinct spreading ridges exhibit morphology distinct from active spreading ridges in several aspects [Mammerickx and Sandwell, 1986]. The most common of these characteristics are: subsidence of the ridge axis due to cooling and contraction, and the cessation of fresh magma supply [Sclater et al., 1971], a deep axial rift along the ridge axis [Mammerickx and Sandwell, 1986], lack of frequent seismic activity, and identification of magnetic anomalies or dating of basement samples near the ridge axis that date spreading cessation. Axial rift valleys, similar to those found at slow spreading ridges evolve from the failure of magma supply to the ridge. Spreading slows dramatically and eventually ceases. The axial topographic high can not be supported, and a rift valley forms at the center of the ridge, elongated in the direction of the axis.

Ridge jump situations can create a pair of conjugate troughs bounding the

spreading of the currently active ridge system [Mammerickx and Sandwell, 1986]. In this case, Bauer Scarp and the distal trough, or “anti-Bauer Scarp” [Mammerickx and Sandwell, 1986] represent the troughs (proximal and distal, respectively) formed when the Galapagos Rise spreading transferred ~900 km west to the current location of Bauer Scarp, creating the currently spreading EPR. The Bauer and anti-Bauer escarpments are identified as troughs in the bathymetric profiles occurring sub-parallel to the ridge axis segments. The proximal and distal escarpments are markedly similar in morphology. As spreading progressed along the EPR, the escarpments moved apart marking the extent of EPR spreading in the region. Other such pairs of conjugate troughs are: the Hudson and Henry troughs in the southeast Pacific, identified by [Cande et al., 1982]; and the Moctezuma Trough west of Mathematician Ridge [Mammerickx and Sandwell, 1986]. Rough topography is consistently associated with these escarpments and likely indicative of the earliest stage of spreading at the new location.

DATA AND METHODS

The objectives of this dissertation were to establish age/depth relationships across the study area, map magnetic anomaly trends, and integrate available data to develop reconstructions of the study area. Age/depth relationships were investigated using available locations of previously mapped and dated magnetic anomalies and their associated depths from the Smith and Sandwell [1997] predicted bathymetry data. The predicted bathymetry data were used to evaluate the morphologic features of the area to examine the probable boundaries and seafloor structures related to Galapagos Rise spreading, as well as the northern and southern limits of the Galapagos Rise system.

Additionally, shaded relief images of the study area were used to relate morphological features on the seafloor to the evolution of the Galapagos Rise system. Magnetic anomaly patterns in the region were studied to establish possible lineation trends and correlated to the magnetic reversal sequence [Cande and Kent, 1992, Cande and Kent, 1995] to determine independent ages of the seafloor. Reconstructions using the above determined seafloor age distribution were then developed to create an improved evolution of the Galapagos Rise region that incorporated the available data in the study area.

The primary data sets used in this study were 1) ship track bathymetry and magnetic data, available for download from the National Geophysical Data

Center (http://www.ngdc.noaa.gov/), 2) satellite-derived gravity and bathymetry [Smith and Sandwell, 1997], and 3) micro-earthquake T-wave source locations obtained from hydrophone arrays, available for download from the NOAA VENTS project [Fox et al., 2001]. Each of these data sets is described below.

NGDC Ship track Bathymetry and Magnetic Anomaly Data

Depth and magnetic field measurements collected from ship surveys were obtained from the National Geophysical Data Center (NGDC) for the study region (Figure 7). The NGDC compiles worldwide shipboard bathymetric, gravity, magnetic, seismic, and digital navigation data from marine research cruises from 1953 to the present (http://www.ngdc.noaa.gov/mgg/gdas/gd_sys.html). These data are considered public domain and are obtained from both United States and foreign oceanographic institutions and governments. Table 1 shows the NGDC number for each data set and the source institution of the research vessel. The data sets in this study are referenced using the NGDC identification number. The data were selected for the study region using the interactive program GEODAS, available from the NGDC. Each data point is given with its corresponding navigational coordinates. The data for each cruise were downloaded in the NGDC's MGD77 format and the bathymetric and magnetic values and corresponding navigation points were extracted from the files. Each file was reviewed, and obviously erroneous data points were removed. Ship-collected

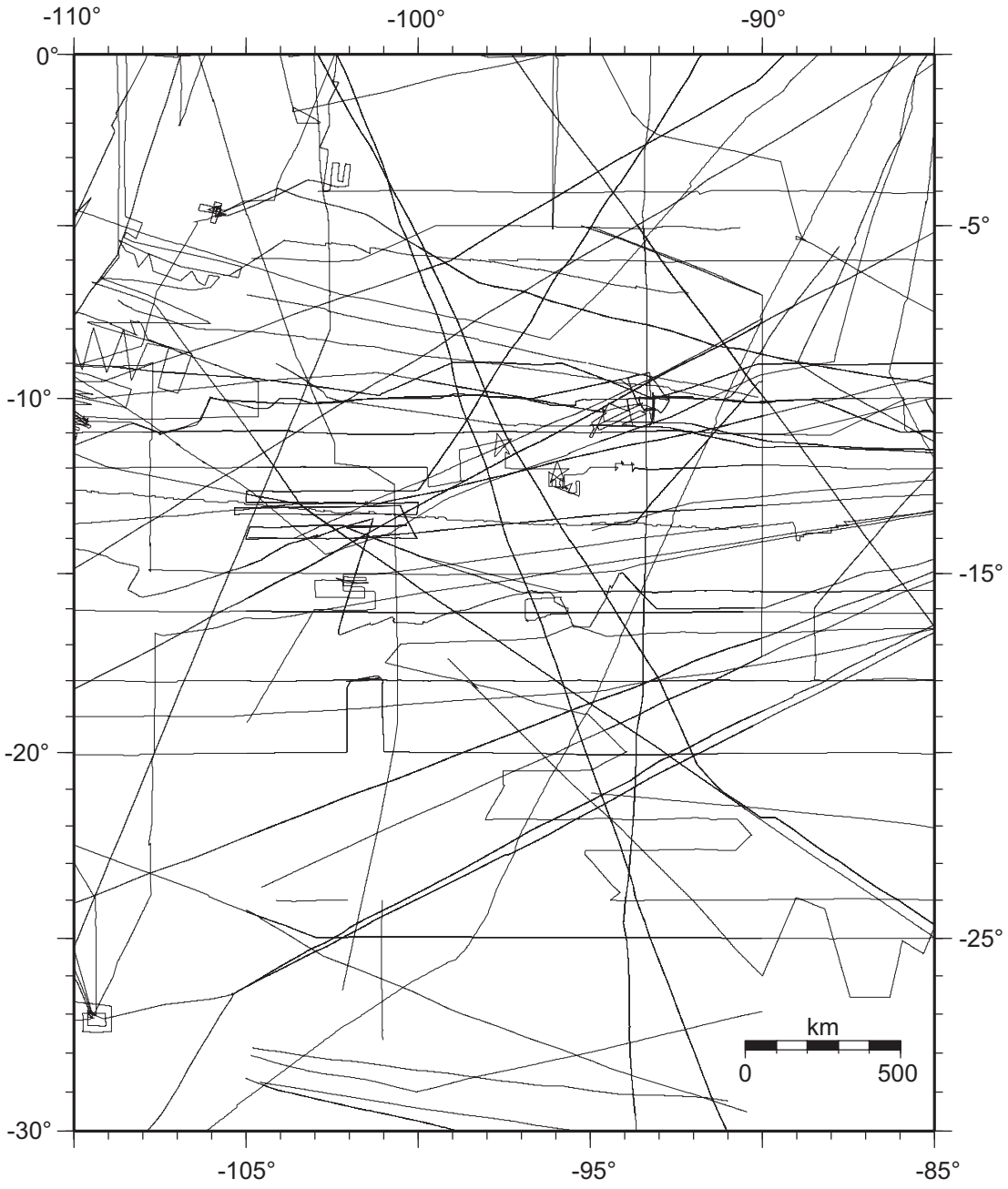

Figure 7. Map illustrating coverage of shiptrack bathymetry and magnetic anomaly data in the study area.

Table 1. Identification numbers and source institutions of bathymetric and magnetic ship track data obtained from the NGDC and used in this study. Depth values for these cruises were generally recorded at 0.5-1.0 km spacing.

NGDC ID Number	Number of Magnetic Survey Points	Source Institution or Country
1010012	2262	LDEO
1010022	90	LDEO
1010023	1482	LDEO
1010054	2128	LDEO
1010081	1438	LDEO
1010082	1870	LDEO
1010083	259	LDEO
1010098	1500	LDEO
1010133	246	LDEO
1010137	1573	LDEO
1010254	444	LDEO
1020029	1312	LDEO
1030005	631	LDEO
1030041	1494	LDEO
1030066	1504	LDEO
1210016	10037	LDEO
1210029	715	LDEO
2010059	969	WHOI
2020026	3224	WHOI
3020005	2475	NOAA
3040002	250	NOAA
3040054	2030	NOAA
3040058	1955	NOAA
3040059	2802	NOAA
3040060	1790	NOAA
3040061	4338	NOAA
7010019	1079	Oregon State University
7010028	1807	Oregon State University

Table 1. Continued

NGDC ID Number	Number of Magnetic Survey Points	Source Institution or Country
7010030	3400	Oregon State University
7010032	2568	Oregon State University
7010037	1610	Oregon State University
7010056	3674	Oregon State University
7080005	3485	Oregon State University
8010007	3460	SOEST
8010009	3716	SOEST
8010018	1567	SOEST
8010021	1781	SOEST
8010022	1253	SOEST
8010025	1254	SOEST
8010027	2112	SOEST
8010028	1296	SOEST
8010053	507	SOEST
8020012	265	SOEST
8020042	1671	SOEST
8020043	195	SOEST
15010001	737	SIO
15010065	1837	SIO
15010067	250	SIO
15010069	1102	SIO
15020019	831	SIO
15020026	734	SIO
15020027	117	SIO
15020028	92	SIO
15020029	1956	SIO
15020046	1411	SIO
15020057	1886	SIO
15020077	1735	SIO
15020085	1170	SIO
15020087	560	SIO
15020088	287	SIO
15020134	868	SIO
15020135	189	SIO

Table 1. Continued.

NGDC ID Number	Number of Magnetic Survey Points	Source Institution or Country
15020137	420	SIO
15020146	381	SIO
15020147	818	SIO
15020152	109	SIO
15020153	4307	SIO
15020154	7	SIO
15020177	287	SIO
15040001	223	SIO
15040020	1205	SIO
15040024	3528	SIO
15040025	2993	SIO
15040027	95	SIO
15040045	574	SIO
15040046	152	SIO
15040047	62	SIO
15040048	2158	SIO
15040092	1290	SIO
15040141	795	SIO
15040142	76	SIO
15040143	1759	SIO
15040148	615	SIO
15040150	1573	SIO
15040161	803	SIO
15040171	1736	SIO
15040180	72	SIO
15040192	199	SIO
15040198	60	SIO
15040200	750	SIO
15040202	180	SIO
15040203	270	SIO
15040210	3554	SIO
15040221	1761	SIO
15050014	191	SIO

Table 1. Continued.

NGDC ID Number	Number of Magnetic Survey Points	Source Institution or Country
15050032	1541	SIO
15050067	90	SIO
15050092	1701	SIO
15060001	1491	SIO
15060002	2401	SIO
15060029	227	SIO
15060030	1647	SIO
15080007	233	SIO
19100022	2298	United Kingdom
19100023	2515	United Kingdom
19180007	1226	United Kingdom
23060042	1374	Texas A&M University
23060046	1253	Texas A&M University
67010087	395	France
67010088	1582	France
67010165	90	France
67010170	1702	France
67010171	359	France
67020003	1076	France
67020004	1508	France

bathymetry data were used primarily to validate the Smith and Sandwell [1997] predicted bathymetry, examine individual features for high resolution seafloor relief where needed, and for identifying bathymetric contributions to magnetic anomalies.

The NGDC magnetic data were projected perpendicular to the ship track, with amplitudes adjusted for clarity and ease of pattern identification. The locations of ship tracks for the magnetic data were the same used for the ship track bathymetry data and are shown in Figure 7 and identified by NGDC number in Table 1. Magnetic data were correlated by first plotting the data using Generic Mapping Tools (GMT) [Wessel and Smith, 1991, Wessel and Smith, 1995] as anomalies, where the trackline is considered to be the zero-line of the x-axis. The amplitude of the magnetic values is then plotted perpendicular to this axis as a continuous anomaly profile. Crossing of faults, seamounts, or other major tectonic features identified in the bathymetry were avoided in making anomaly correlations. Preference was given to profiles that crossed the Galapagos Rise ridge axis in a nearly perpendicular azimuth in order to minimize correlation errors based oblique ship track crossings. The anomalies are then correlated between tracks by eye, with picks based on matching anomaly shape, spacing, and pattern. Because the ship survey data were compiled from mostly random crossings of the Galapagos Rise by separate surveys over many years, navigational accuracy and resolution of the data is varied. Differences in shipboard instrumentation and parameter settings (most importantly, of data

resolution or density) increase the potential for error in the correlation of data from one ship track to another. This potential error results in correlations with a slightly larger magnitude of uncertainty than might be obtained by using the data from a single survey. More notably, some sections of the study area contain no correlation of magnetic anomaly patterns due to the lack of regular or numerous ship crossings of the Galapagos Rise, resulting in an inability to make correlations across long distances or bathymetric features such as fracture zones. Identifications of anomalies were made by correlation with the magnetic reversal scale established by Cande and Kent [1995].

A synthetic model of the total field magnetic reversal sequence was calculated using the method of Shouten and McCamy [1972]. A Fortran program called “synthanom” provided by Dr. Gary Acton calculated the synthetic anomaly pattern using this method over a two-dimensional horizontal structure by computing the Fast Fourier Transform of a square wave, multiplying it by an earth filter and then a phase shift filter, and finally computing the inverse Fast Fourier Transform. The time scale of magnetic field reversals used was that of Cande and Kent [1995] and Cande and Kent [1992]. Other parameters used in the calculation are shown in Table 2. The synthetic reversal sequence model is shown graphically in Figure 8. The observed (trackline) magnetic profiles were matched to the synthetic model where possible to identify individual anomaly sequences and ages from the magnetic reversal time scale.

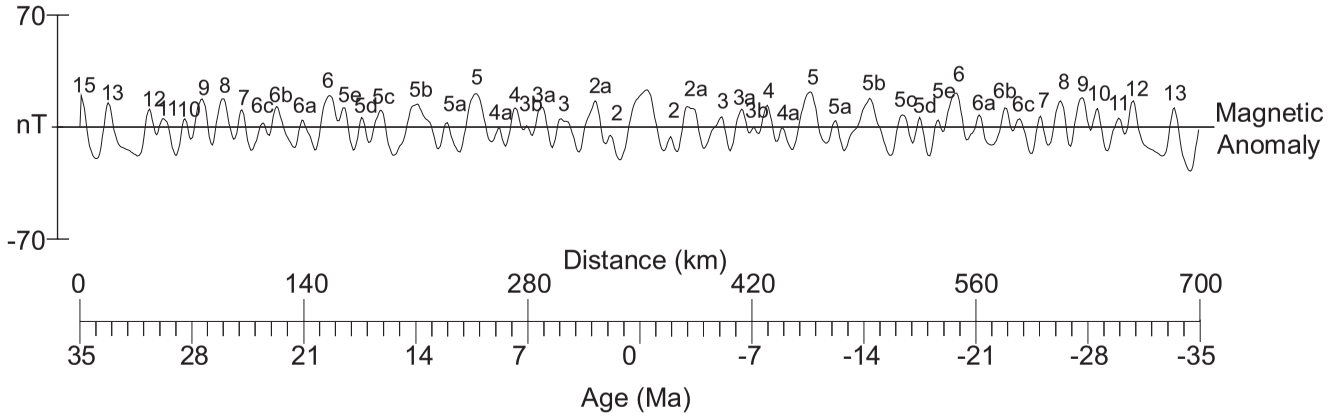

Figure 8. Synthetic model of the total field magnetic reversal sequence. Model parameters are given in Table 3. Distance and age scales provided for reference.

Table 2. List of parameters used to calculate synthetic magnetic anomaly profile.

Remnant Inclination:	-3.3°
Remnant Declination:	9.62°
Ambient Inclination:	-3.3°
Ambient Declination:	9.62°
Effective Remnant Inclination:	11.56°
Effective Ambient Inclination:	11.56°
Amplitude Factor:	0.0826
Spreading Direction:	116°
Lineation Azimuth:	206°
Depth to Top of Magnetic Layer:	4.5 km
Depth to Bottom of Magnetic Layer:	5 km

Predicted Bathymetry

Shipboard depth soundings and satellite altimetry data were combined by Sandwell and Smith [1994] and Smith and Sandwell [1997] to produce predicted gravity and bathymetry data (Figure 2) sets with 2-minute grid spacing. Satellite data from the United States' Geosat and Topex/Posidon altimeters, as well as from the European Space Agency's ERS-1 altimeter were used to detect variations from the ellipsoid form of the Earth's equipotential surface, or geoid. Multiple passes over each orbital path allow these values to be averaged, thereby removing transient effects such as waves and atmospheric distortions such as storms. The residual altimetry values over the oceans represent the perturbations of the ocean surface due to gravitational variation. The large-scale geoid elevations over the Earth can then be subtracted, resulting in a series of departures from the geoid elevations. These departures from the geoid are assumed to be the result of mass excesses and deficits on the seafloor. Inherent in this model are the assumptions that the mantle and core have uniform surfaces at a constant distance from the center of the Earth, and therefore the only gravity sources or sinks are from mass excesses and deficits due to seafloor variations. The predicted gravity values can then be calculated [Sandwell and Smith, 1997] based on the varying departures from the geoid as a grid with two-minute resolution. The slope of the gravity anomalies can be directly related to the topography of the seafloor in that area. In other words, sharp changes in the slope of predicted gravity represent corresponding

changes in seafloor bathymetry. Therefore, a regular 2-minute grid can then be constructed of predicted bathymetry based on the slopes of the calculated gravity data. This data set provides a high-density uniform grid coverage of the ocean floor. Previous global and regional gridded ocean depth data could only be interpolated from ship surveys, yielding low regional or global seafloor resolution. Shipboard depth soundings are combined with the satellite data to constrain the long wavelength bathymetric features.

Figure 9 compares ship track bathymetry with the Smith and Sandwell predicted bathymetry data interpreted along the same line to show the high degree of correlation between the data sets. While this is the expected outcome due to integration of the data sets, it is significant that even small features (~100 meters) visible in the ship survey data are repeated in profiles extracted from the grid data (Figure 9). Thus, there is little observable difference in the character of most bathymetric features obtained from the grid. The most significant departures are a slight underestimate in amplitude of some of the extreme bathymetric variations such as the extremely shallow (less than 500 meters below sea level) Galapagos Rise ridge crest, probably due to the effects of the low pass filter used to construct the grid. With such high correlation (least squares linear correlation coefficient 0.989 in Figure 9) of profiles extracted from the bathymetry grid along ship survey tracks with the shipboard bathymetry obtained from individual surveys, profiles obtained from regions with sparse ship survey coverage can be considered with confidence to represent the bathymetry

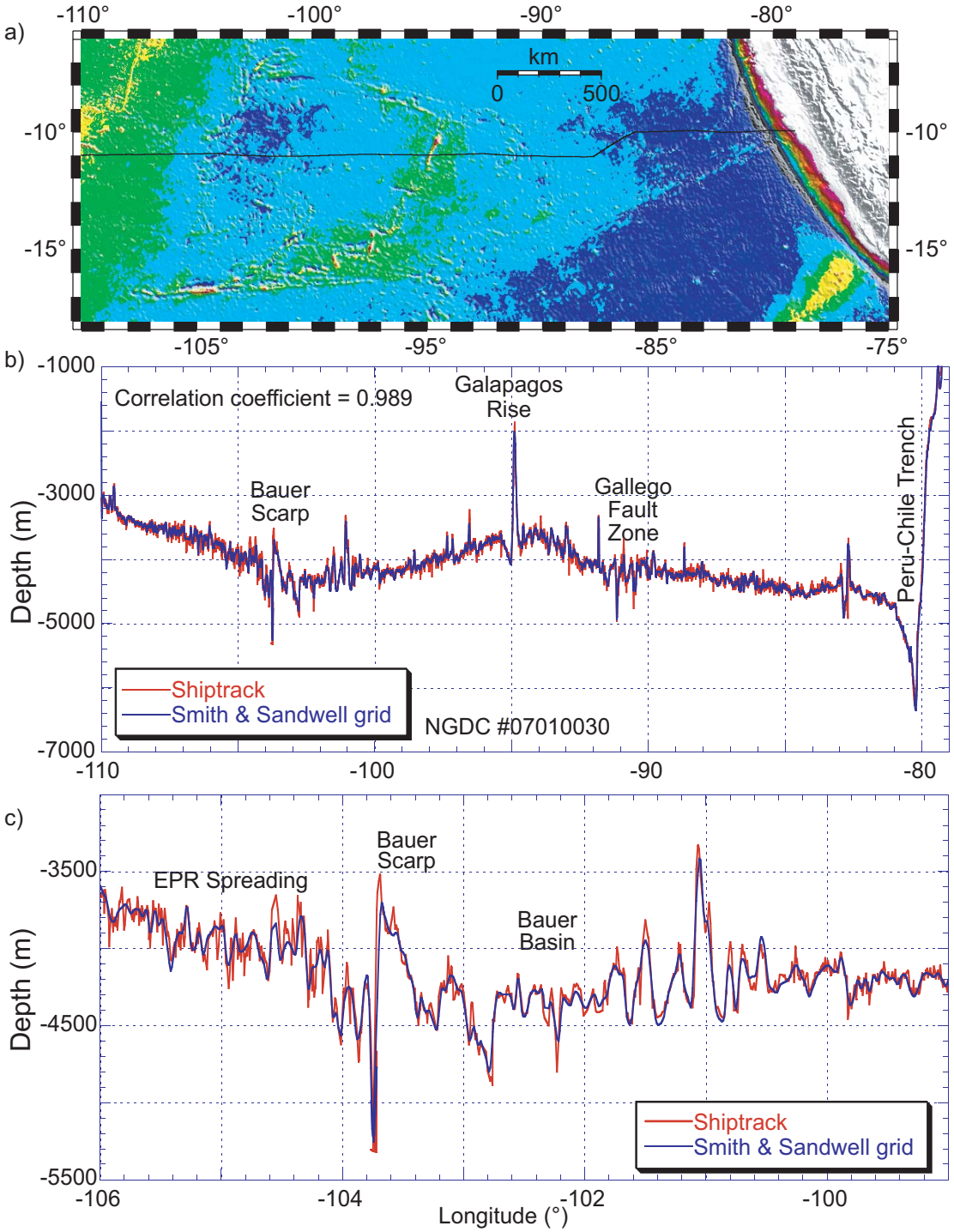

Figure 9. Comparison of shiptrack bathymetry locations from the R/V Yaquina cruise (1971) obtained from the NGDC plotted verses the same locations from the Smith and Sandwell (1997) predicted bathymetry grid. a) Map showing the ship track for the R/V Yaquina (1971), b) Shiptrack bathymetry profiles plotted vs. profile extracted from the Smith and Sandwell (1997) predicted bathymetry grid at same locations, and c) expanded profile of the Bauer Scarp and Bauer Basin.

in these regions. For example, a bathymetric profile obtained by the United Kingdom Navy in 1998 crossing both the Peru-Chile trench and the Nazca Ridge (Figure 10) has a 99.1% correlation with predicted depths extracted from the 2-minute grid. Since this data set was obtained after the publication of the Smith and Sandwell [1997] data, this ship track bathymetry data was not incorporated in the 2-minute grid and is therefore independent of the data incorporated in the predicted bathymetry grid. The extremely high correlation of the extracted predicted bathymetry with the ship track bathymetry demonstrates that profiles extracted from the grid are representative of the bathymetry in the region even in places where ship track data was not incorporated into the grid in that area.

Bathymetric profiles were extracted at the 2-minute grid resolution of the predicted bathymetry grid for analysis and plotted perpendicular to the track with a common vertical exaggeration. In places where the profiles were stacked, the geographic locations of the profile tracks are provided for reference. Stacked bathymetric profiles were used to establish topographic trends or characteristics to infer morphologic structure of the seafloor.

Seafloor Fabric

Depth distributions on the seafloor may be analyzed it terms of their relationships to the evolution of the various spreading centers by evaluating their “brightness” in an artificially illuminated seafloor image. The dense two minute predicted bathymetry grid provided by Smith and Sandwell [1997] allows shaded

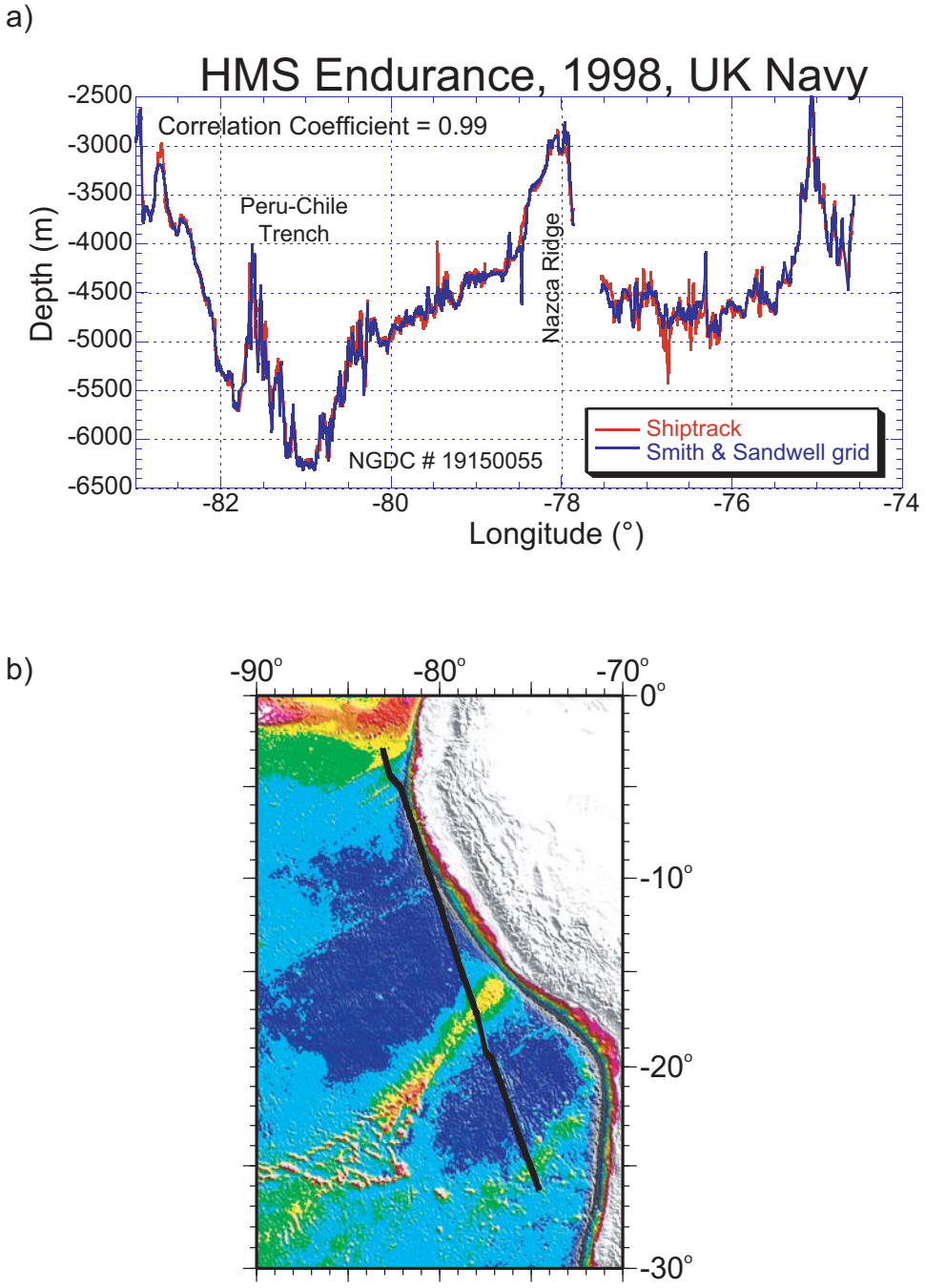

Figure 10. Comparison of independent ship track bathymetry and predicted bathymetry extracted at the same locations from the Smith and Sandwell [1997] grid. a) Note the high correlation between the two data sets (see text for description). b) Map showing location of the shiptrack data in part a.

relief images of the Galapagos Rise region to be constructed that are illuminated from various angles to highlight morphologic features on the seafloor (Figures 11, 12, 13). GMT was used to compute directional gradients at all of the points in the two-dimensional predicted bathymetry grid from a defined azimuth. The program calculates the value at every point according to the equation:

$$(x,y) = -[dz/dx*\sin(A) + dz/dy* \cos(A)] \quad (1)$$

where A is the azimuth measured clockwise from north and is the direction from which the artificial illumination appears. Slopes that are downhill toward the light source are given as positive values and slopes that are uphill toward the light source are negative. In an artificially illuminated grayscale image, the positive (downhill) gradients yield “bright” regions and the negative (uphill) gradients yield “dark” regions.

Bathymetric features with high relief would appear “bright” on a shaded relief image when the sloped surface of the feature is perpendicular to the direction of incident light. The incident light then appears as though it was reflected back toward the source, and the feature appears bright in the image. The opposite side of the feature, sloping away from the direction of incident light, therefore appears “dark,” as though it reflected any incident light away from the light source. Bathymetric features of relatively high relief whose trends are

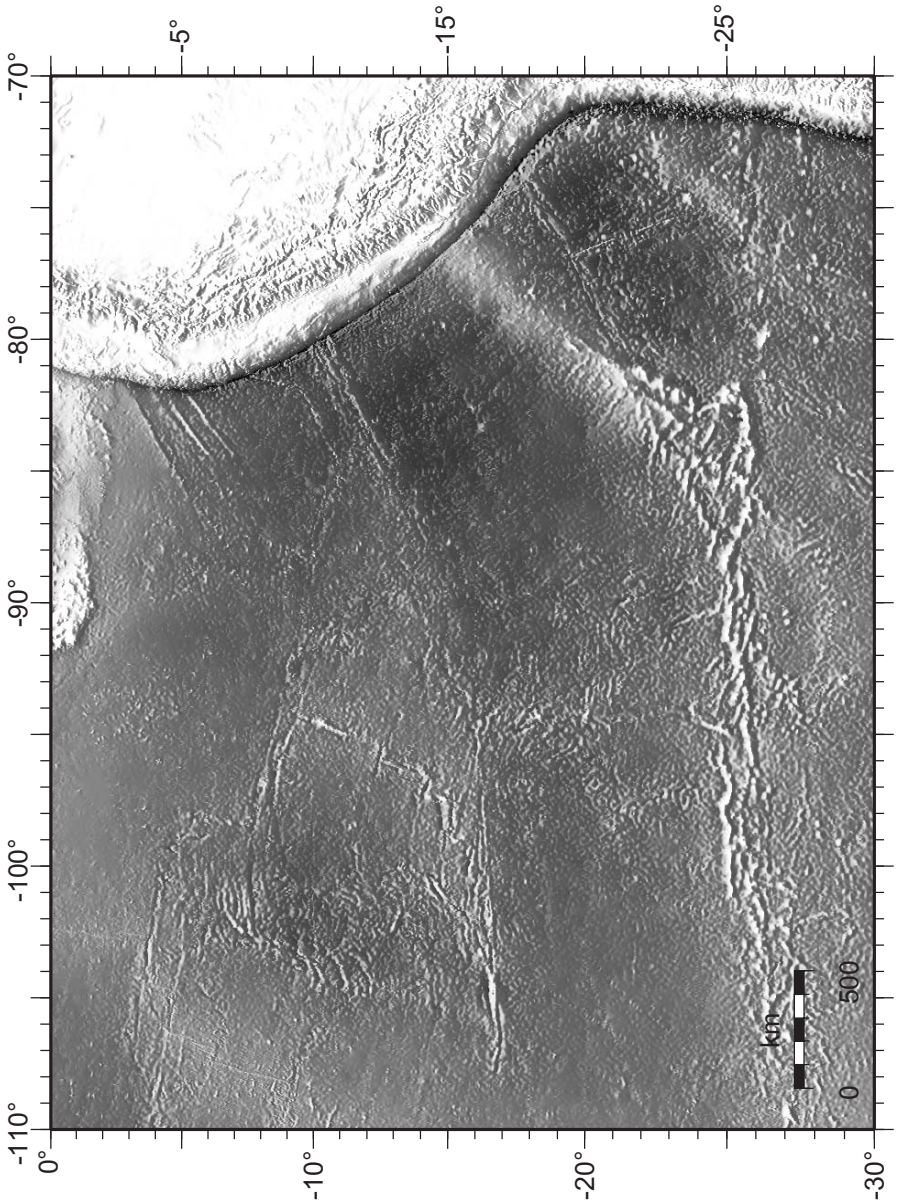

Figure 11. Shaded relief image of predicted bathymetry data from Smith and Sandwell [1997], illuminated from an azimuth of 0°

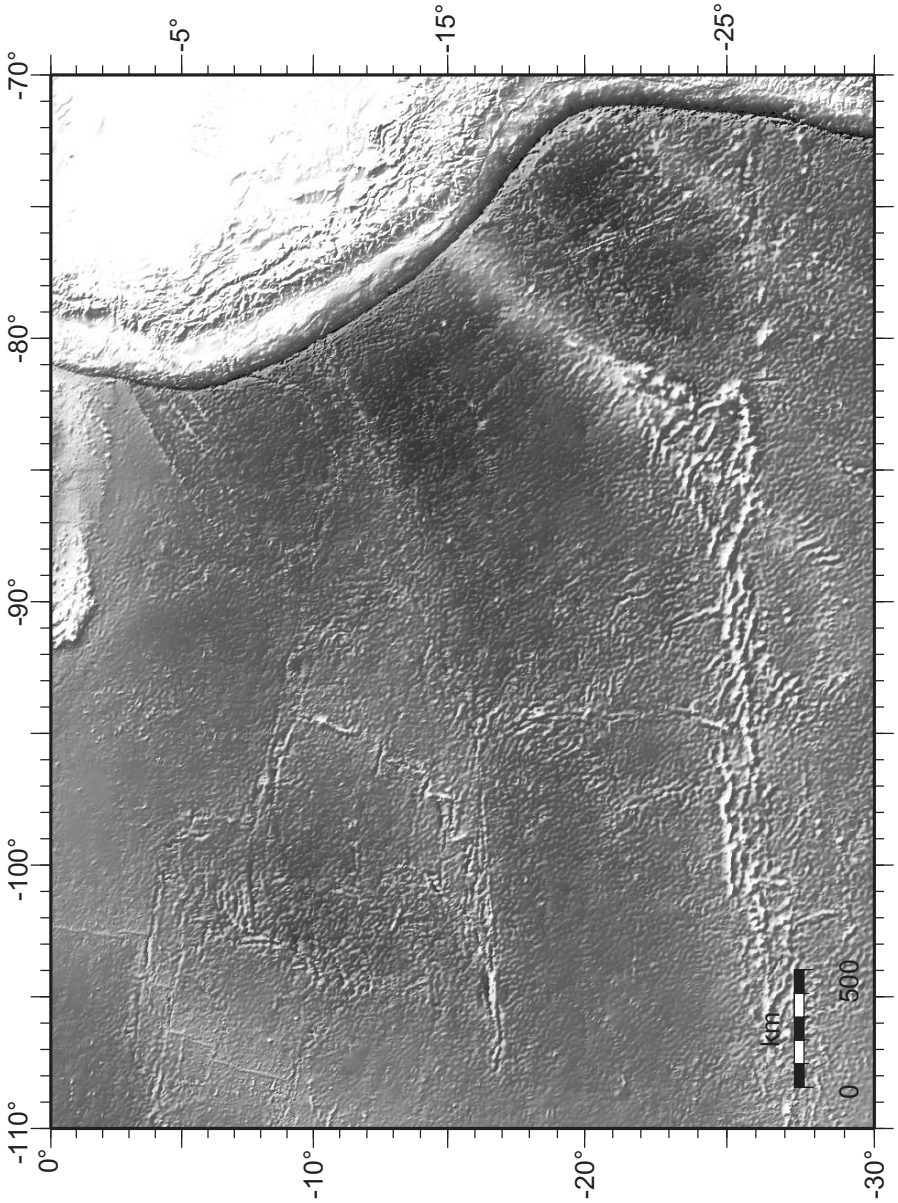

Figure 12. Shaded relief image of predicted bathymetry data from Smith and Sandwell [1997], illuminated from an azimuth of 45°

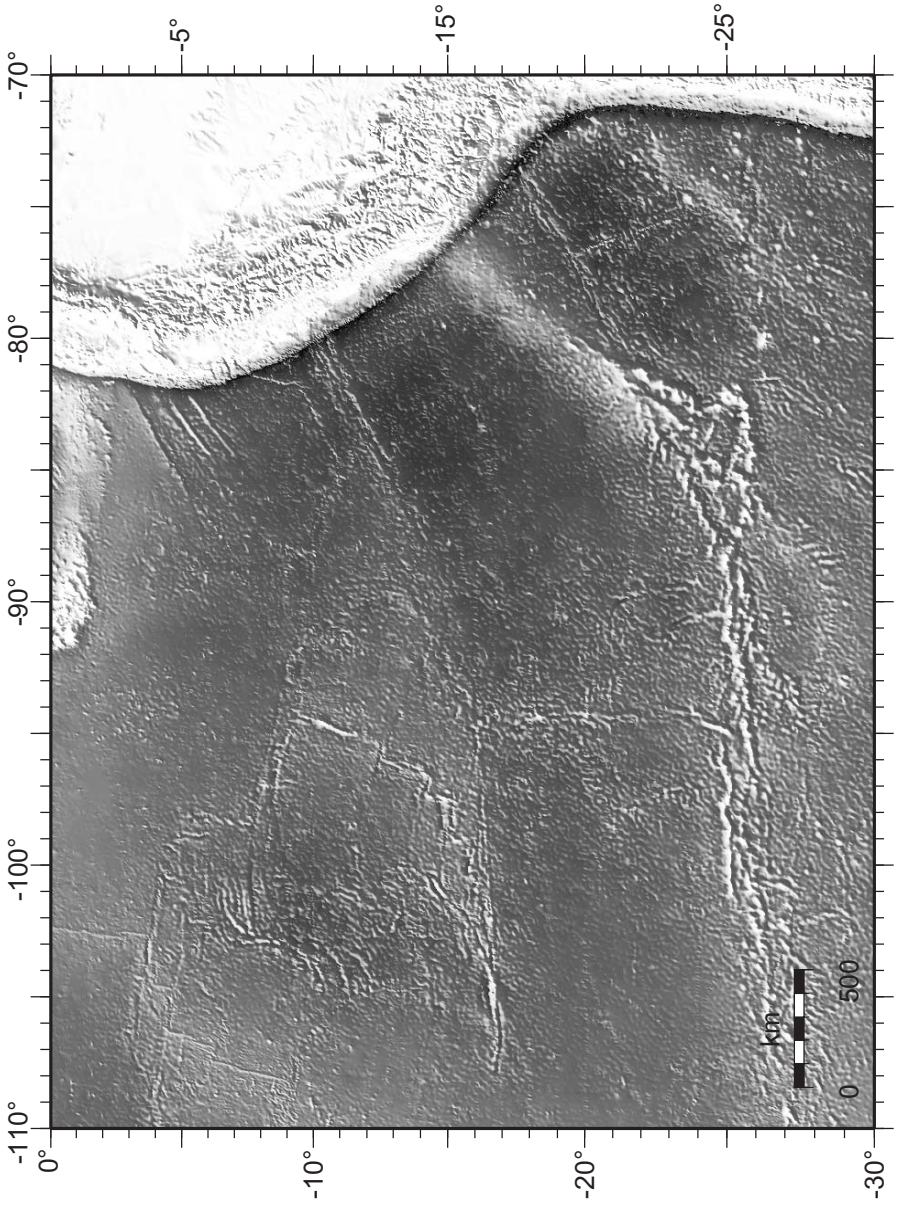

Figure 13. Shaded relief image of predicted bathymetry data from Smith and Sandwell [1997], illuminated from an azimuth of 315°

oriented roughly perpendicular to the direction of the incident light source are typically identified by paired bright and dark regions within the image, such as the approximately east-west trending Sala Y Gomez ridge in the lower portion of Figure 11 (see Figure 1 for location of ridge). Areas of seafloor with little relief, such as broad, flat plains or areas with gentle slopes tend to reflect a small portion of the incident light back toward the source. These areas typically appear in the mid-tonal range of the image, and contain few of the bright-dark paired regions associated with high relief features. The EPR for example (the northwest corner of Figure 12) displays regions of mid-tonal range seafloor that represents the low-relief seafloor created during the rapid spreading of the EPR system. This is most clearly seen in Figure 13, where the seafloor associated with the EPR still remains in the mid-tonal range, but the seafloor related to the Bauer Scarp appears bright on the northwestern side and darker on the southeastern side. This is because the incident light angle, at 315° (clockwise from north) is nearly perpendicular to the trend of the high relief Bauer Scarp. It is possible, therefore, to distinguish the seafloor produced during rapid spreading of the EPR from the bathymetric features that delineate the boundaries of the spreading in that area.

Earthquakes

Earthquake data for the Galapagos Rise region are available as public domain data from two sources: the National Earthquake Information Center and

the National Oceanic and Atmospheric Administration. Earthquake source locations for this region derived from the T-phase arrivals at underwater hydrophones were obtained from Dr. Christopher Fox at the National Oceanographic and Atmospheric Administration [Fox et al., 2001]. Many of the earthquakes detected by the hydrophones are much lower magnitude than is typically recorded by the world wide land-based seismometer net. These records therefore provide a unique insight to low-magnitude neotectonic activity in the seafloor. T-phases, or tertiary phase arrivals were recorded by hydrophone receivers suspended in the sound channel of the ocean. Source locations were triangulated based on hand-picked arrival times of the tertiary waves transmitted into the sound channel from earthquakes within the oceanic crust and received by a minimum of three and maximum of six receivers. Good correlation exists [Fox et al., 2001] between source location as determined for events recorded by hydrophones and epicenters for events that had sufficient magnitude to be recorded by land-based seismometers. More than 3000 micro-earthquakes, ranging in moment magnitude from as low as 2.5, were recorded in the region from the equator to 30°S and from 255° to 270°E. The locations of these earthquakes are shown in Figure 14.

Earthquake epicenter data were obtained from the National Earthquake Information Center at http://www.neic.gov. These earthquakes were determined from arrival times at land based seismometers. Earthquakes with moment magnitudes less than ~4 are generally not detected by land-based

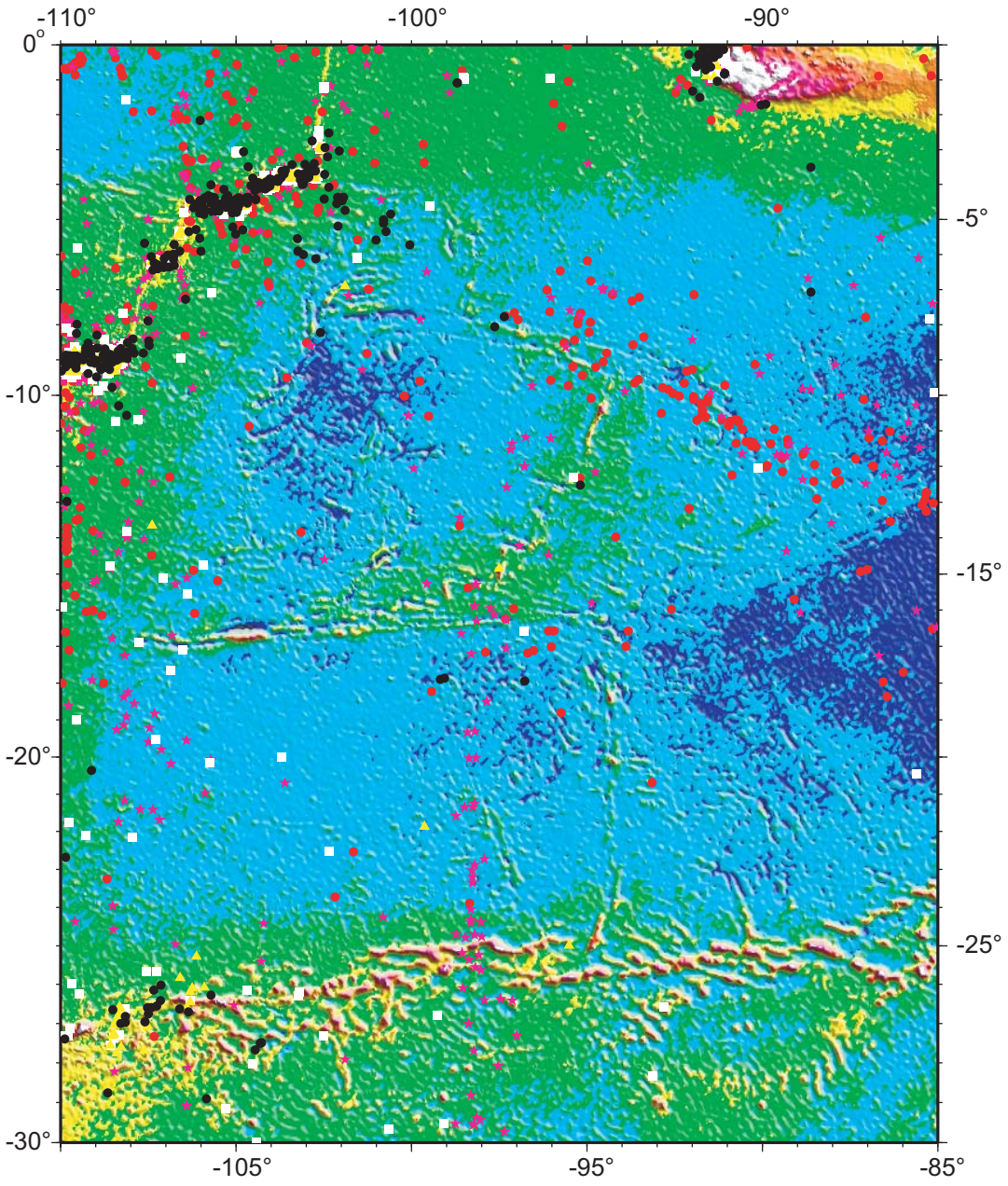

Figure 14. Map of the focus centers of earthquakes from the NEIC and NOAA hydrophone network in the study area relative to the Smith and Sandwell [1997] predicted bathymetry grid. Symbols represent earthquakes detected by land-based seismometers obtained from the NEIC database (black circles) and the NOAA hydrophone earthquakes recorded and correlated by three (red circles), four (pink circles), five (white squares), or six (yellow triangles) recording stations in the array.

seismometers.

The earthquake source locations (Figure 14) are generally located along fracture zone traces, such as the Gallego and Dana fracture zones. Since focal mechanisms cannot be determined at this time for the hydrophone-recorded earthquakes, it is not possible to establish the relative motion of the fault blocks for these events. The largest number of source locations, however, primarily coincides with the Gallego fracture zones. Source locations within the Gallego fracture zones imply that the seismic events are either transform events associated with further plate motion, or normal events associated with relative cooling and settling of seafloor across fracture zones. The multitude of events occurring along the EPR ridge segments and fracture zones (as a result of active spreading) are not observed on the Galapagos Rise ridge segments and fracture zones (except the eastern Gallego fracture zones). This lack of a similar distribution of seismic events is consistent with the suggestion that the Galapagos Rise system is an inactive (extinct) spreading system. Therefore, differential contraction and cooling due to seafloor age differences across the fracture zones is the likely explanation for the locations of low-magnitude earthquakes in the Galapagos Rise system.

The north-south trending series of earthquake source locations occurring at ~98°W and 18-30°S is unusual in this data. While the source locations seem adequately constrained [Fox et al., 2001, and personal communication], this series of source locations does not seem coincident with any significant

bathymetric features visible in the Smith and Sandwell [1997] data. In fact, the trend seems to cross major east-west trending features (see Figure 14) at approximately 25° S. This north-south trend lies along a similar longitude and is parallel with the trend of hydrophones used to collect this data [Fox et al., 2001]. As such, the locations of these source events remain suspect and, for the sake of interpretation of this work, have been ignored.

Euler Poles

The poles were determined graphically using small circles plotted on a stereonet using the method of Cox and Hart [1986]. The fracture zone lineations in the predicted bathymetry data were digitized to create sets of latitude and longitude points that defined the fracture zones. The stereonet was constructed in GMT, and the fracture zones used to determine the location of the Euler pole are labeled FZ1, FZ2, FZ3, and FZ4 on Figure 15. Other fracture zones present in the Galapagos Rise system were considered too short or too difficult to resolve adequately in the predicted bathymetry to contribute to the determination of the Euler pole. A small circle was then fitted by eye to each fracture zone trace as shown in Figure 16. The geographic center of each small circle is the location of the pole of rotation for the respective fracture zone trace. The average of the locations of the four poles of rotation (~22.5°S, ~99.5°W) was used in to rotate the Galapagos Rise and Bauer Basin as appropriate in the reconstructions.

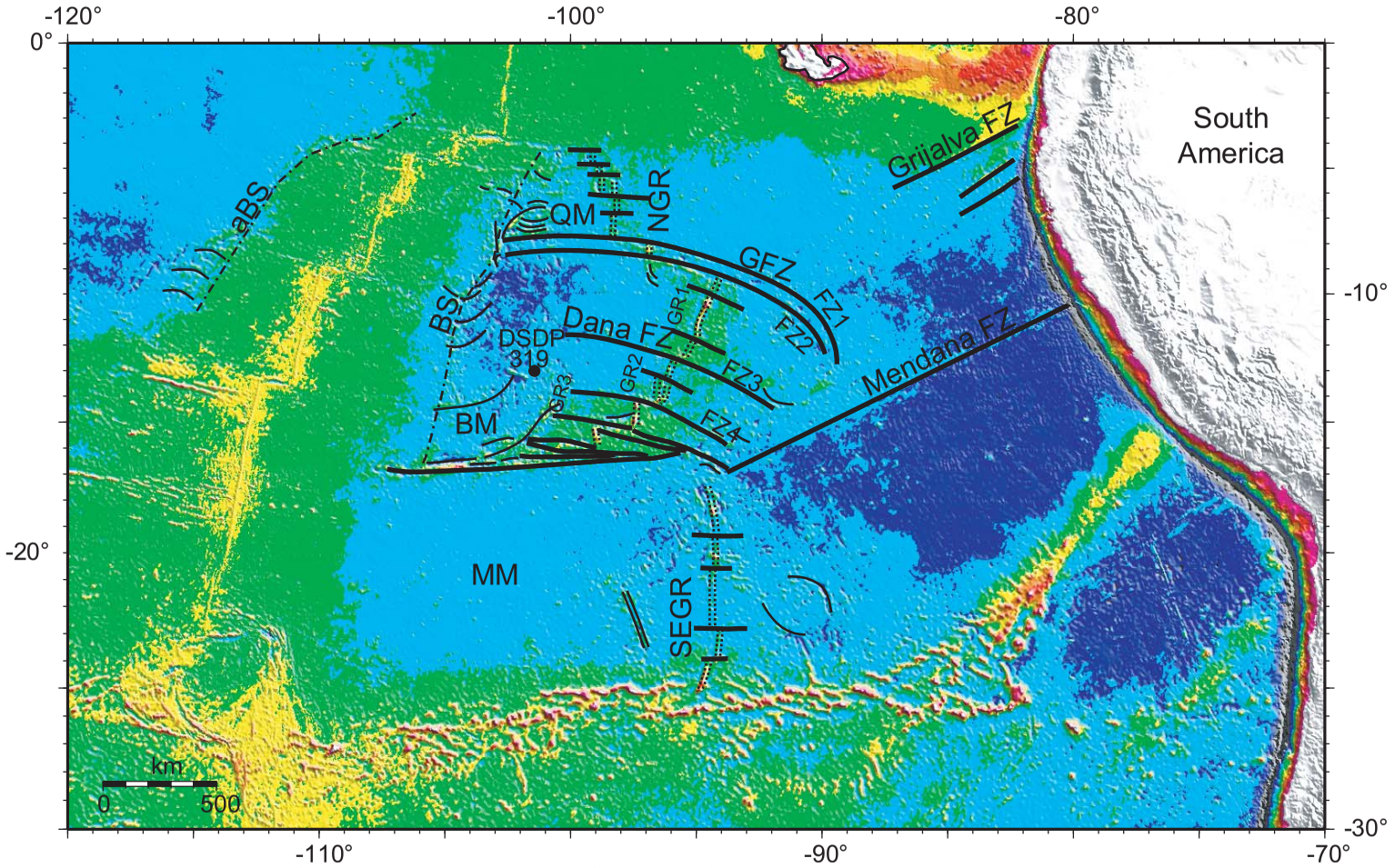

Figure 15. Location map of study area illustrating locations of bathymetric features discussed in text and Figures 21-23 and 25-27. Bathymetric scale the same as Figure Abbreviations employed are: GR = Galapagos Rise, SEGR = Southeast Galapagos Rise, NGR = North Galapagos Rise, BS = Bauer Scarp aBS = anti-Bauer Scarp, BM = Bauer Microplate, MM = Mendoza Microplate, QM = Quebrada Microplate. Double dotted lines indicate extinct spreading centers. Dash-dot lines indicate bathymetric scarps. FZ1, FZ2, FZ3, and FZ4 indicate fracture zones used to locate Euler pole.

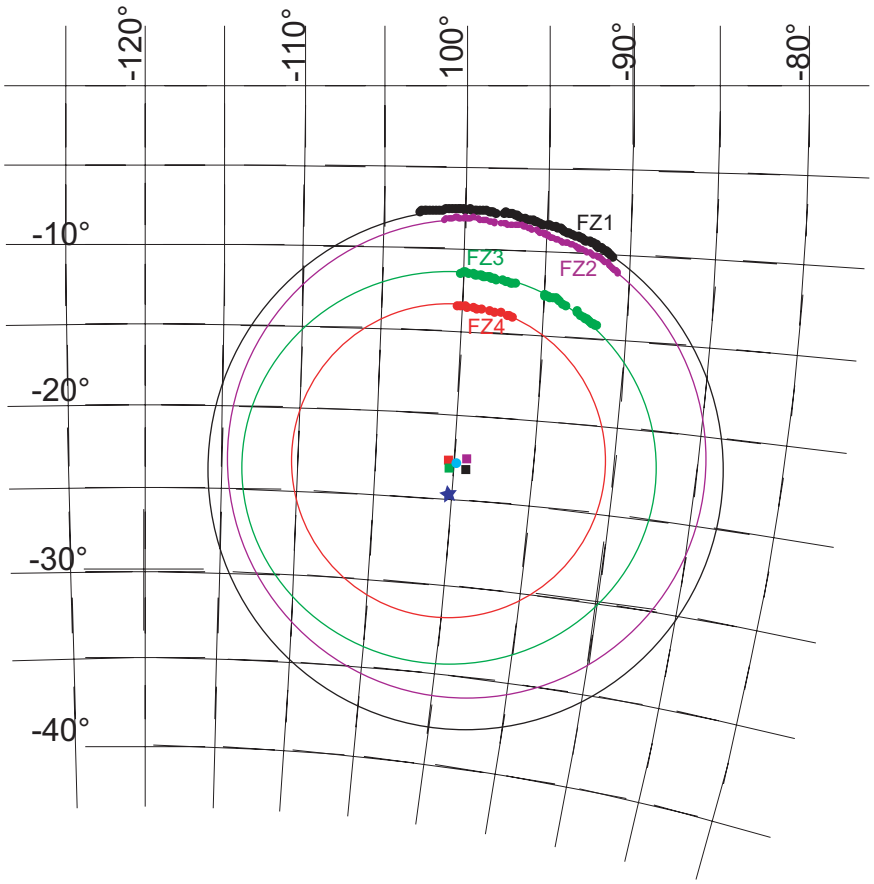

Figure 16. Equal area projection of graphically determined Euler pole locations based on curvature of Galapagos Rise fracture zones. Star indicates Euler pole estimated by Rea [1981]. Filled circles represent points digitized from predicted bathymetry along major fault traces in the Galapagos Rise system (labeled on Figure 1). Large circles represent best fit (by eye) small circle for digitized points. Squares are the corresponding pole location determined by the center of each large circle (see text). Euler pole was taken as average position of the large circle centers (squares).

Reconstructions

Seafloor age distribution determined from the predicted bathymetry, the magnetic anomaly lineations, and seafloor ages from the magnetic reversal time scale correlations from the Pacific, Farallon, and Nazca plates are reconstructed to several different ages. The only dates of value obtained from geologic samples in the region were from DSDP Site 319, but these dates yield limited constraint because of the large range of dates determined. Time steps were chosen for the reconstructions (23 Ma, 19.5 Ma, 14.7 Ma, 9.5 Ma, and 5.9 Ma) to correspond with reorientations of the Galapagos Ridge system [Meschede and Barckhausen, 2000] or the EPR [Goff and Cochran, 1996, and Mammerickx et al., 1980]. The Cocos plate and the Galapagos Ridge locations and orientations were incorporated into these reconstructions based on Meschede and Barckhausen [2000], and the locations of the magnetic anomalies. The reconstruction of the magnetic anomalies based on the Cande et al. [1989] map and the locations of land area shorelines were determined using the OSDN Plate Tectonic Reconstruction Service website (http://www.odsn.de/odsn/services/paleomap/paleomap.html). The program at this website uses plate tectonic reconstructions based on the Cox and Hart [1986] method to calculate the plate motions. The data files for terrane locations were obtained from Hay et al. [1999]. The plates are moved using the locations of the magnetic anomalies from Cande et al. [1989] relative to a hotspot reference frame based on Mueller et al. [1993]. The program used on the

website to calculate the reconstruction based on the input parameters was written by Emanuel Soeding and the maps were constructed using GMT. A detailed description of the parameters used in the reconstructions can be found on the above cited website. The parameters input by the user for each reconstruction (Table 3) were held constant except for the time of the reconstruction. Magnetic anomaly lineations digitized from Cande et al. [1989] were plotted on each map in the positions calculated by the program on the website for the age of each reconstruction. In addition, the present day shorelines were plotted in each reconstruction and moved according to the calculated plate motion. It is important to note that configuration of the shorelines shown in the reconstruction figures do not necessarily represent the shorelines of the reconstruction age; they are the present day shorelines reconstructed according to calculated plate motion.

Table 3. List of parameters used in the tectonic reconstruction program.

Age to be Reconstructed (Ma):	23, 19.5, 14.7, 9.5, 5.9, and 0 Ma
Move plates relative to:	Hotspot Reference Frame 2 (Mueller et al., 1993)
Boundaries (North, South, East, West):	20°, -40°, -140°, -60°
Annotation Interval:	20°
Gridline Interval:	10°
Projection:	Mercator
Frame Type:	Thin Lines
Plot:	Magnetic Lineations Present Day Shore Lines

ANALYSIS

Age/Depth Relationships

The predicted bathymetry data of Smith and Sandwell [1997] present an exceptional opportunity to evaluate the distribution of seafloor depth as an indication of the seafloor age distribution. The predicted bathymetry grid was sampled at the same locations as the identified magnetic anomaly lineations of Cande et al. [1989] within the study area as shown in Figure 17. Therefore, for each point at which an age value has been determined along the magnetic anomaly lineation, a depth value was determined from the predicted bathymetry grid. The age/depth relationship in the study area was then determined by fitting a curve of the form:

$$\text{Depth} = M1 + M2\,(\text{Time})^{1/2} \qquad (2)$$

to the available data, where M1 and M2 are the constants determined by the curve fit. The curve fit is shown graphically in Figure 18. M1 (-2822.8 m) represents the zero-age depth of the seafloor, and has an error of +/- 5.8586 m. M2 (-301.36 m/Ma) has an error of 1.8016 m/Ma. A linear correlation coefficient for the least squares curve fit was determined to be 0.95637.

There is an additional set of magnetic anomaly lineations identified in Cande et al. [1989] just west of the Peru-Chile Trench and between 6° and

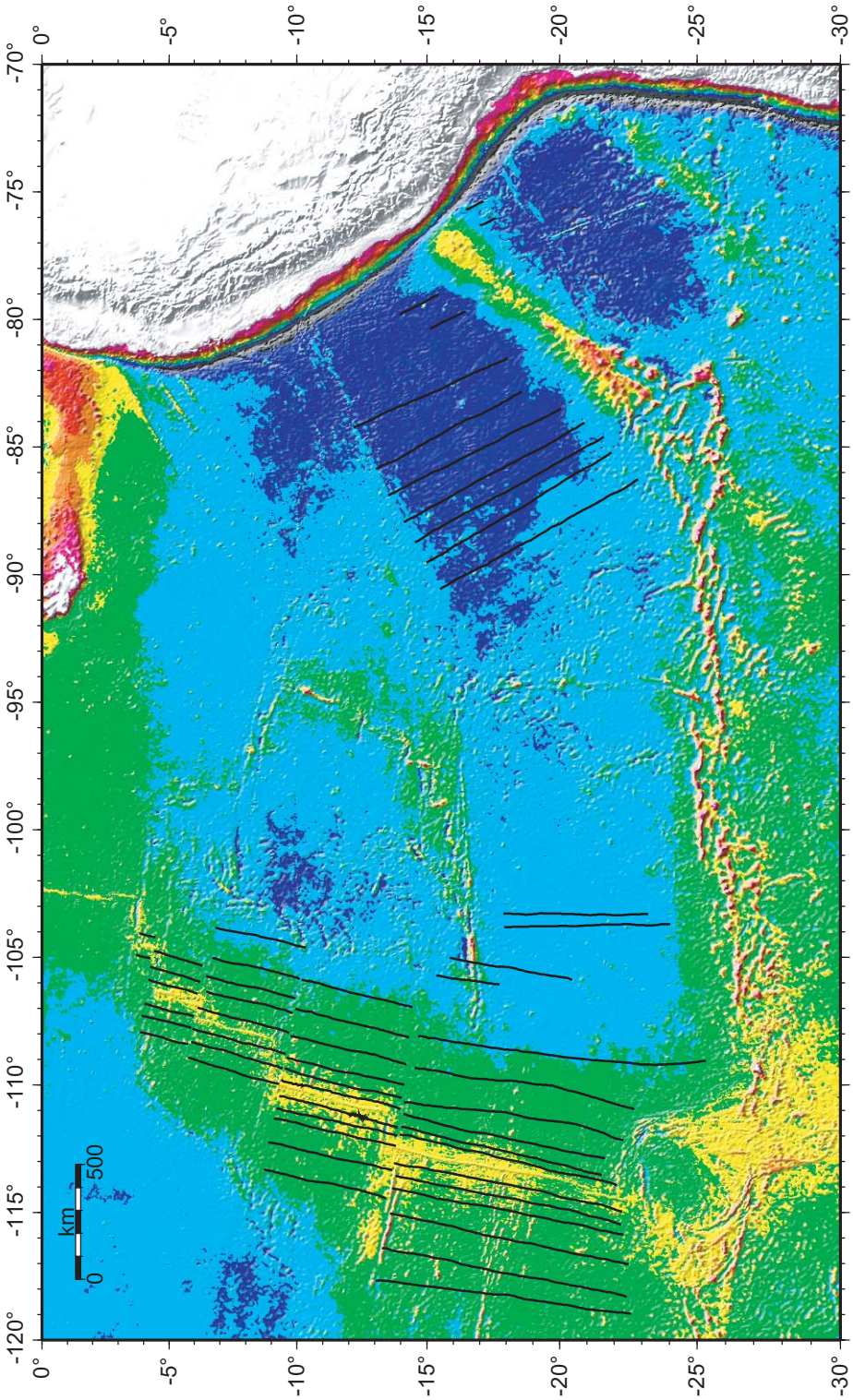

Figure 17. Predicted bathymetry map from the Smith and Sandwell [1997] grid showing the locations of the magnetic anomaly lineations used to determine the age/depth relationship for the study area.

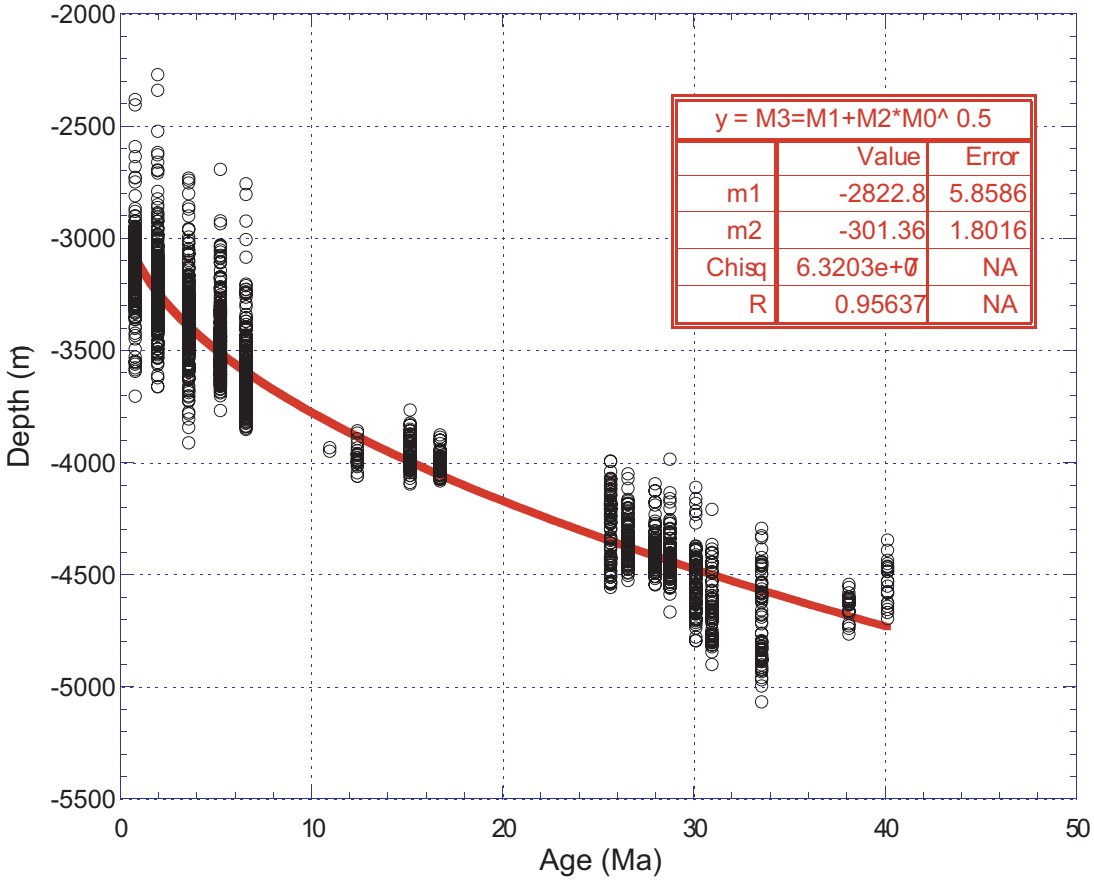

Figure 18. Curve fit to age data obtained from Cande et al. [1989] magnetic anomaly lineations and associated depth values from the predicted bathymetry grid. Black circles are data points. Red line represents the curve fit. Curve fit parameters are shown in red.

11°S, but they were not included in the age-depth determination because of the great variation of bathymetric depth along the trend of the lineation. Large variations in depth along the constant age of a magnetic anomaly lineation contribute a large source of error to the depth/age conversion, and therefore were excluded from the calculation.

The parameters determined by the curve were then used to convert the predicted bathymetry grid into a predicted age grid of the same two minute resolution, shown in Figure 19. To better resolve the age boundaries for interpretation, the predicted age grid was filtered to a 25 kilometer geographic radius and the age values were binned to the time steps used in the reconstructions (Figure 20). Age boundaries can then be used to aid in the interpretation of the predicated age map in the reconstructions of the study area.

Bathymetry and Seafloor Structure

Identification of the ridge crests, as well as the extent of the associated seafloor produced by the Galapagos Rise, allows age and geographical boundaries to be established as part of the evolution of the Nazca plate. The predicted bathymetry grid was therefore studied to evaluate the nature of the bathymetric expression of the ridge crests, fracture zones, and boundaries of seafloor produced by the Galapagos Rise during its evolution (Figure 15), and these details were considered in the reconstructions of the region. Stacked bathymetric profiles of the ridge crests were used to identify the unusually

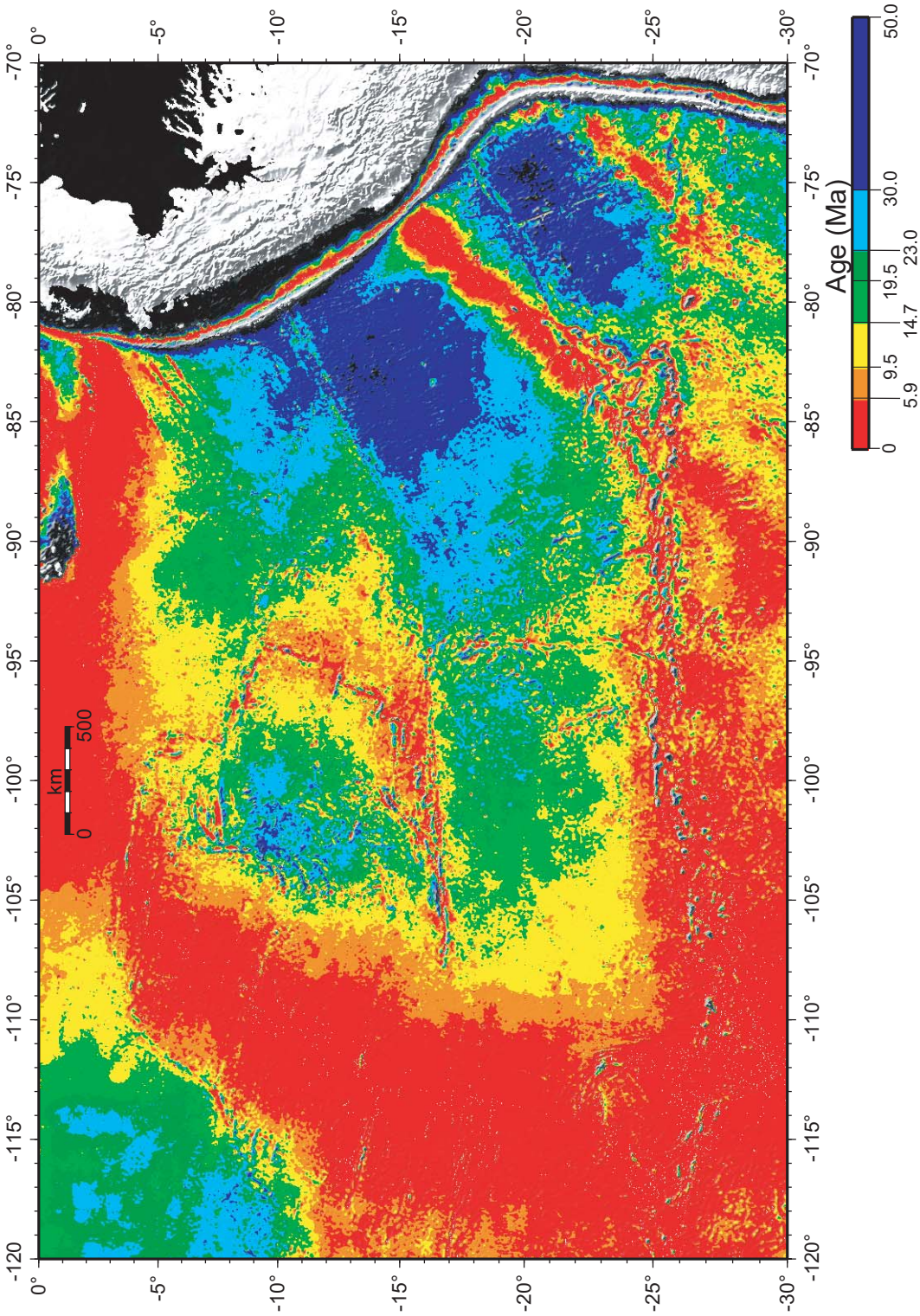

Figure 19. Depth-predicted age map of the study area.

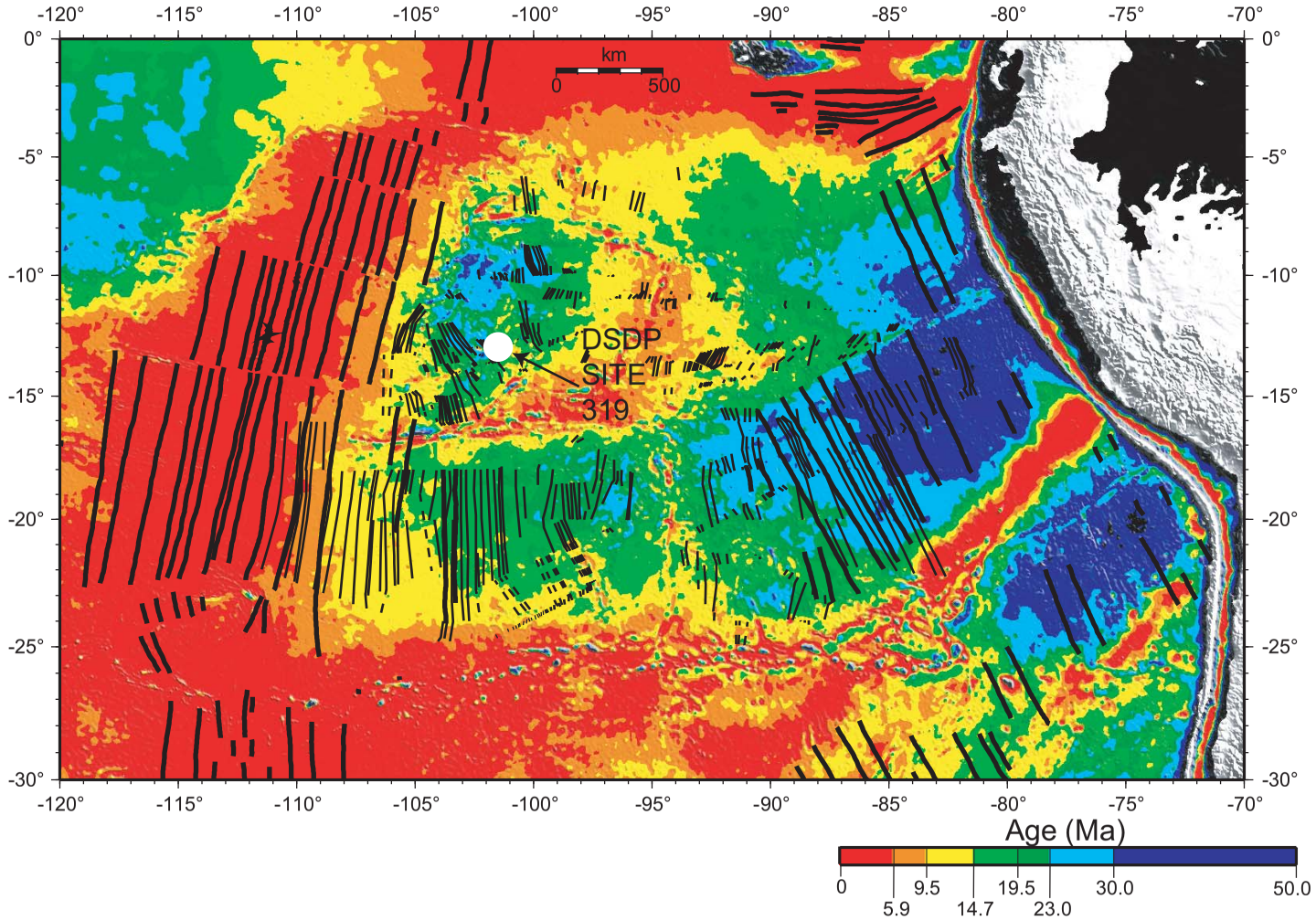

Figure 20. Depth-predicted age map filtered to a 25 km radius to better resolve age boundaries. Color scale correlates with the time steps of reconstructions determined in this study. Thick black lines represent magnetic anomaly lineations from Cande et al.[1989]. Thin black lines represent magnetic anomaly lineations determined in this study.

shallow peaks of the GR1 (~550 m) and GR2 (~750 m) ridge crests, as well as the changes in depth along the GR1 segment from its extremely shallow peaks to a depth of ~3000 near the Dana fracture zone. The lengths of the ridge crest segments were shorter in the southern part of the Galapagos Rise system, and the trends of these segments varied from the northwest trend of the northern segments. Boundaries of seafloor spreading produced by the uniformly spreading ridge segments were identified by locating abrupt depth discontinuities in the ocean floor. The Mendaña fracture zone bounds the Galapagos Rise on the east, the Gallego fracture zones in the north, and the Bauer fracture zone in the south. The Bauer and anti-Bauer Scarps display differences in morphology that suggest a complex initiation to the EPR spreading in this area.

The ridge crest segment immediately south of the Gallego fracture zones is the most prominent section (GR1) of the Galapagos Rise (Figure 21), and displays unique morphologic characteristics. An extremely shallow peak exists at the northern tip of the ridge segment. Reaching depths as shallow as ~550 m [Mammerickx et al., 1980 and this work, Figure 21], this peak is significantly shallower than even the zero-age depths that are predicted by the [Parsons and Sclater, 1977] age-depth relationship. There is no evident axial valley in profiles that cross the ridge axis, as would be expected when magma is withdrawn during spreading system failure. South of FZ2 segment, and along the same trend, a small rise in the seafloor exists that may constitute the bathymetric

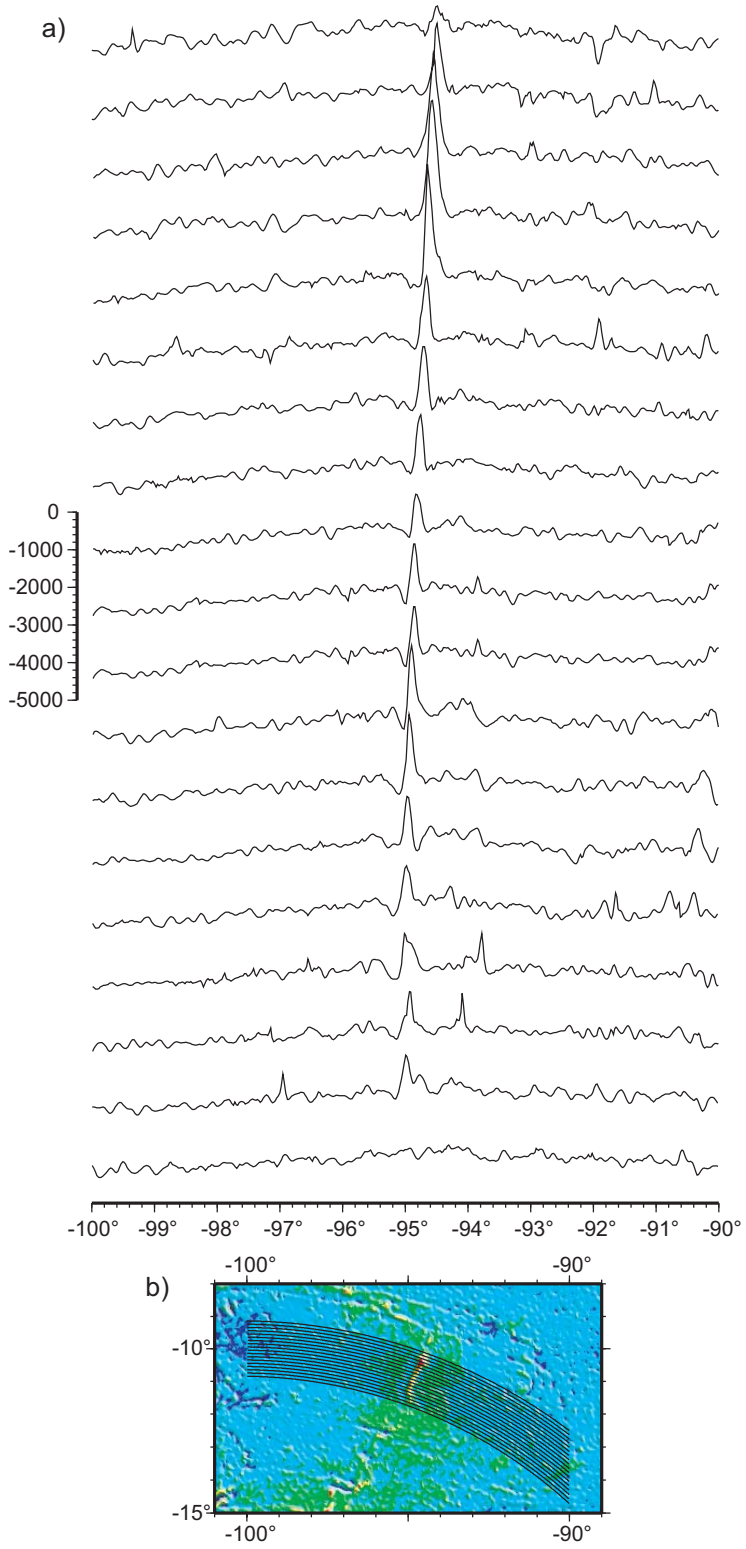

Figure 21. a) Bathymetric profile stack from north (top) to south (bottom) of the GR1 ridge crest. b) Profiles were extracted from the gridded Smith and Sandwell (1997) predicted bathymetry set at 2-minute resolution along profile path.

expression of the ridge crest. However, there are no significant comparable bathymetric highs for ~125 km between the southern tip of the GR1 segment and the Dana fracture zone. There is some question, then, as to how the seafloor crust was generated in these areas without the shallow bathymetry that would indicate a ridge structure. It is possible that a fissure-like structure could have existed to allow magma to reach the surface in these areas, but the rough seafloor typically associated with this type of structure is not evident. It is not clear why the GR1 ridge would not have simply extended toward the fracture zones to accommodate the extension.

The seafloor immediately surrounding the GR1 segment on all sides displays a trough in the bathymetric profiles that likely represents flexure of the local seafloor due to loading from the mass of the GR1 segment itself. The width of this flexure ranges from ~10 km at the northern and southern tips to as much as 25 km along the eastern and western sides of the ridge segment.

The ridge crest segment immediately south of the Dana fracture zone (referred to as the GR2 segment in Figure 15) of the Galapagos Rise (Figure 22) is broken by another previously unidentified fracture zone at 14°S. The presence of this fracture zone is suggested by a valley in the bathymetry, as well as the interruption in the continuity of the ridge segment extending south from the Dana fracture zone. South of the fracture zone at 14°S, the ridge segments are expressed in the bathymetry data as overlapping spreading centers, as indicated by the curved nature of the ridge crest (Figure 22). None of the

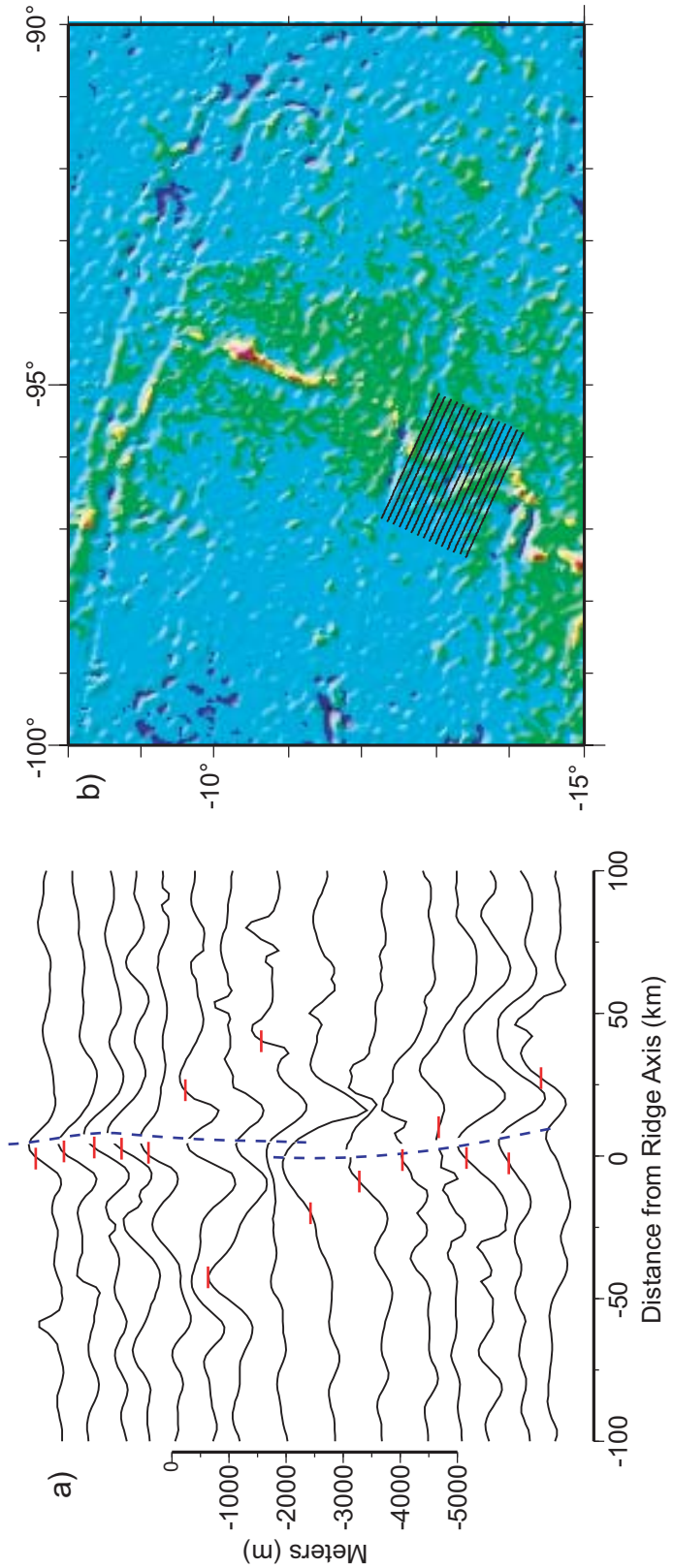

Figure 22. a) Bathymetric profile stack from north (top) to south (bottom) of the GR2 ridge crest. Blue lines indicate the ridge crest of the overlapping spreading centers. Red lines indicate the -1000 m contour on each profile for calibration with the depth scale. b) Profiles were extracted from the gridded Smith and Sandwell (1997) predicted bathymetry set at 2-minute resolution along the profile path.

segments of the GR2 ridge crest reaches the extremely shallow bathymetric values found in the GR1 segment.

South of the GR2 ridge segment, another prominent fracture zone (referred to here as the FZ2 fracture zone, see Figure 15) is evident in the bathymetry. South of this fracture zone, the GR3 ridge segment is expressed in the gridded bathymetry as a rise with two prominent bathymetric highs from 14.5-15.5°S (Figure 23). The northward trend of the southern GR3 rise is a significant departure from the northeast trend of the GR1 and GR2 segments. The change in trend of this segment indicates that southern portions of the Galapagos Rise system possibly rotated at a different rate than the segments in the northern portions of the system. South of the GR3 segment, the bathymetric rises visible in the gridded bathymetry data trend increasingly eastward from the northern segments. The fracture zones bounding these bathymetric highs are longer relative to the length of the spreading segments than that observed in GR1 and GR2. The southern segments of the Galapagos Rise, therefore, exhibit significantly different trend than the northern segments, suggesting that the tectonic forces in this area were more complex, and likely related to the rotational motion of the Galapagos Rise system and the Bauer microplate. Similar regions with long fracture zones and short ridge segments were noted by Tebbens et al. [1997] along the Chile Rise, and can also be seen near the Gofar fracture zone on the EPR (Figure 24).

The Bauer and anti-Bauer Scarps (Figure 15) identify the location of

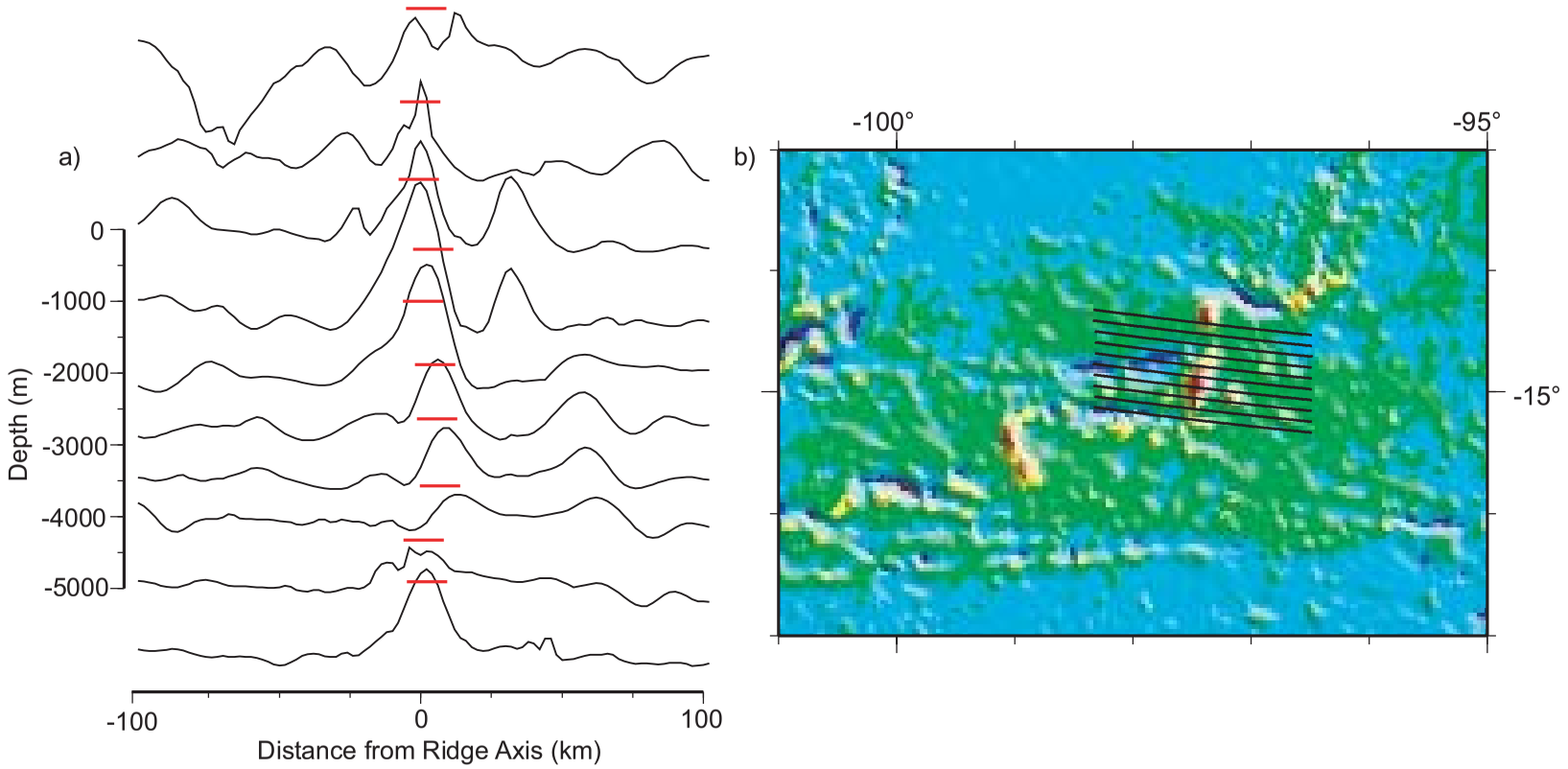

Figure 23. a) Bathymetric profile stack from north (top) to south (bottom) of the GR3 ridge crest. Red lines indicate the -2500 m contour on each profile for calibration with the depth scale. b) Profiles were extracted from the gridded Smith and Sandwell (1997) predicted bathymetry set at 2-minute resolution along the profile path.

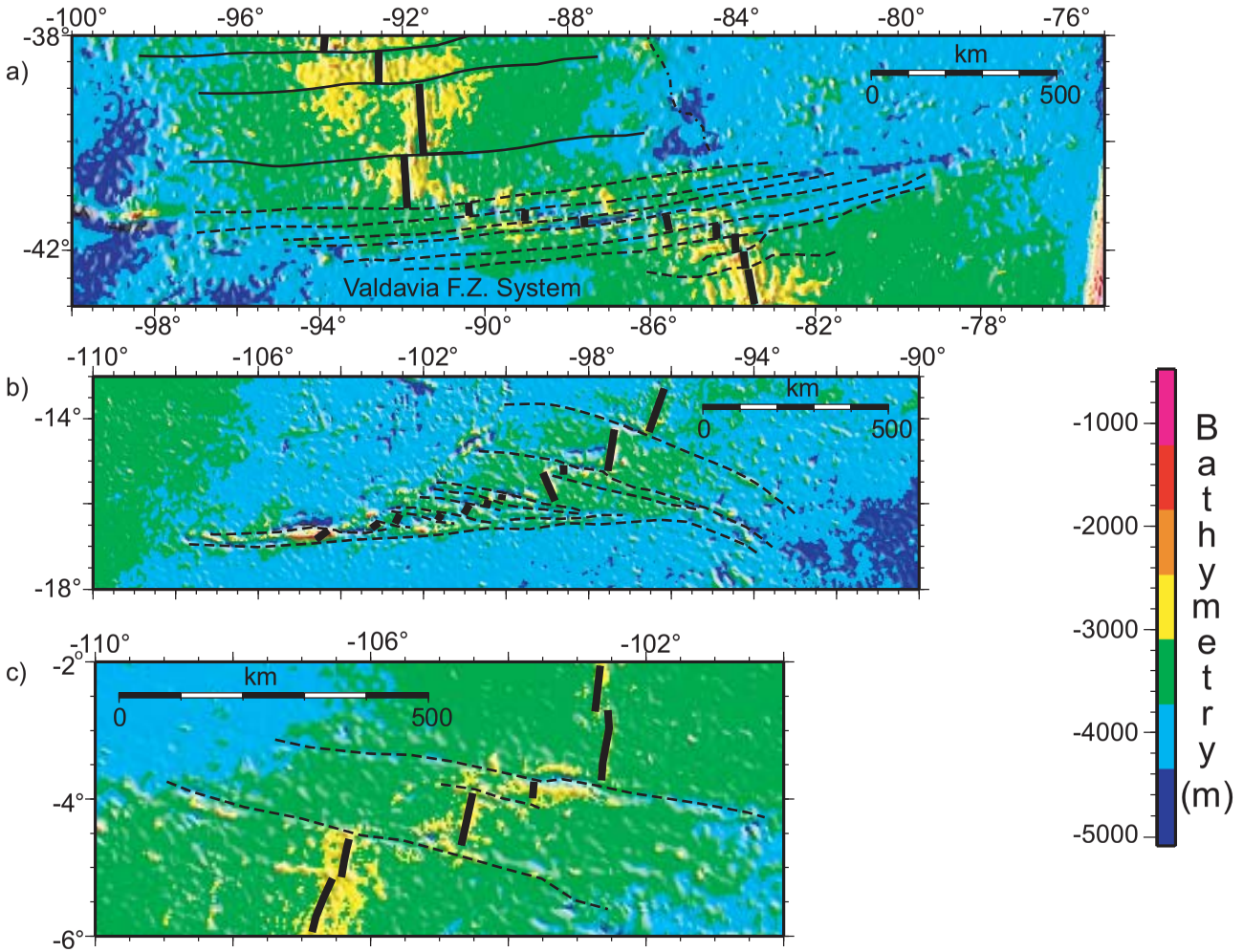

Figure 24. Comparison of a) the Valdavia fracture zone system on the Chile Rise to b) the transition zone of the southern Galapagos Rise and c) the Gofar and Quebrada fracture zones on the EPR. Note the long fracture zone traces relative to the short ridge segments that are characteristic of all these regions.

initiation of EPR spreading, and yields insight into the nature of the transition from Galapagos Rise spreading to EPR spreading. Mammerickx and Sandwell [1986] suggest that a principle evidence of the initiation of spreading in older oceanic lithosphere is the presence of conjugate troughs marking the limits of subsequent seafloor spreading. The Bauer and "anti-Bauer" Scarps (Figure 1) were identified as the pair of conjugate troughs created at the initiation of EPR spreading in this study region [Goff and Cochran, 1996, Mammerickx, 1980, Lonsdale, 1989]. Both escarpments are nearly linear with a sharp increase in depth (~900 m) marking the extents of EPR spreading. Both the Bauer and anti-Bauer scarps lie increasingly closer to the EPR ridge axis with progression northward (Figure 2). This is consistent with previous observations and reconstructions involving the northward propagating ridge tip of the EPR as spreading was established along the current EPR system [Goff and Cochran, 1996, Mammerickx and Sandwell, 1986, Hey, 1980, Lonsdale, 1989, Herron, 1972]. The morphology of the Bauer Scarp, however, appears more complex. The Bauer Scarp contains multiple offsets along its length, as well as a wider zone of associated rough topography (Figure 25). The relief across both escarpments is primarily caused by the difference in age of the seafloor (and therefore depth) between the older seafloor (Bauer Basin and the seafloor west of the anti-Bauer Scarp) and the 8.5-6.2 Ma seafloor produced by the early spreading of the EPR (see Figure 2).

More subtle, yet apparent, bathymetric features mark the northern and

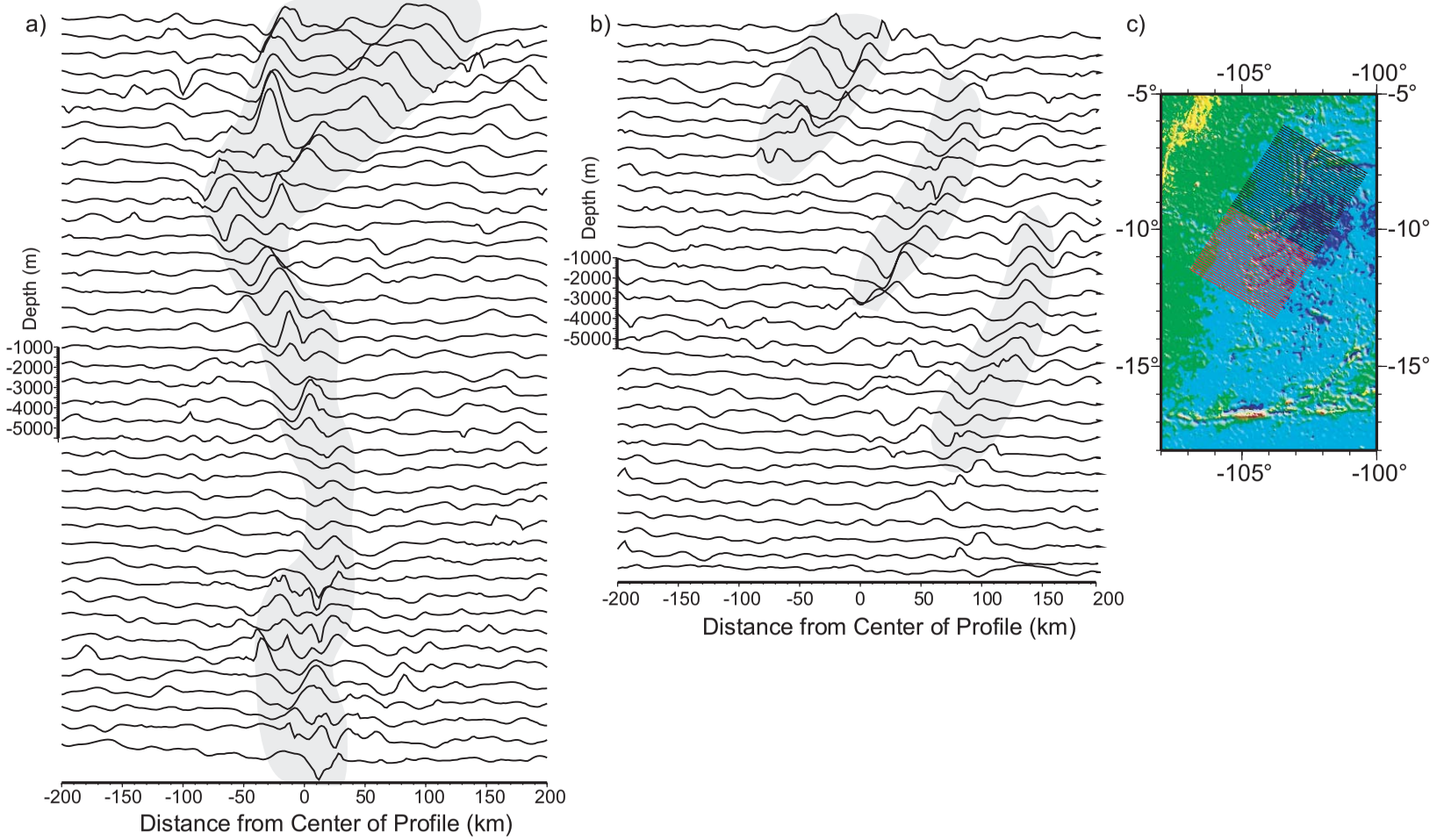

Figure 25. Stacked bathymetry profiles extracted from the predicted bathymetry grid to illustrate the morpho-structural features of the Bauer Scarp. a) Gray area indicates the location of the Bauer Scarp, b) gray area indicates tectonic lineations identified by Goff and Cochran [1996], and c) locations of profiles from part a) in black, from part b) in red.

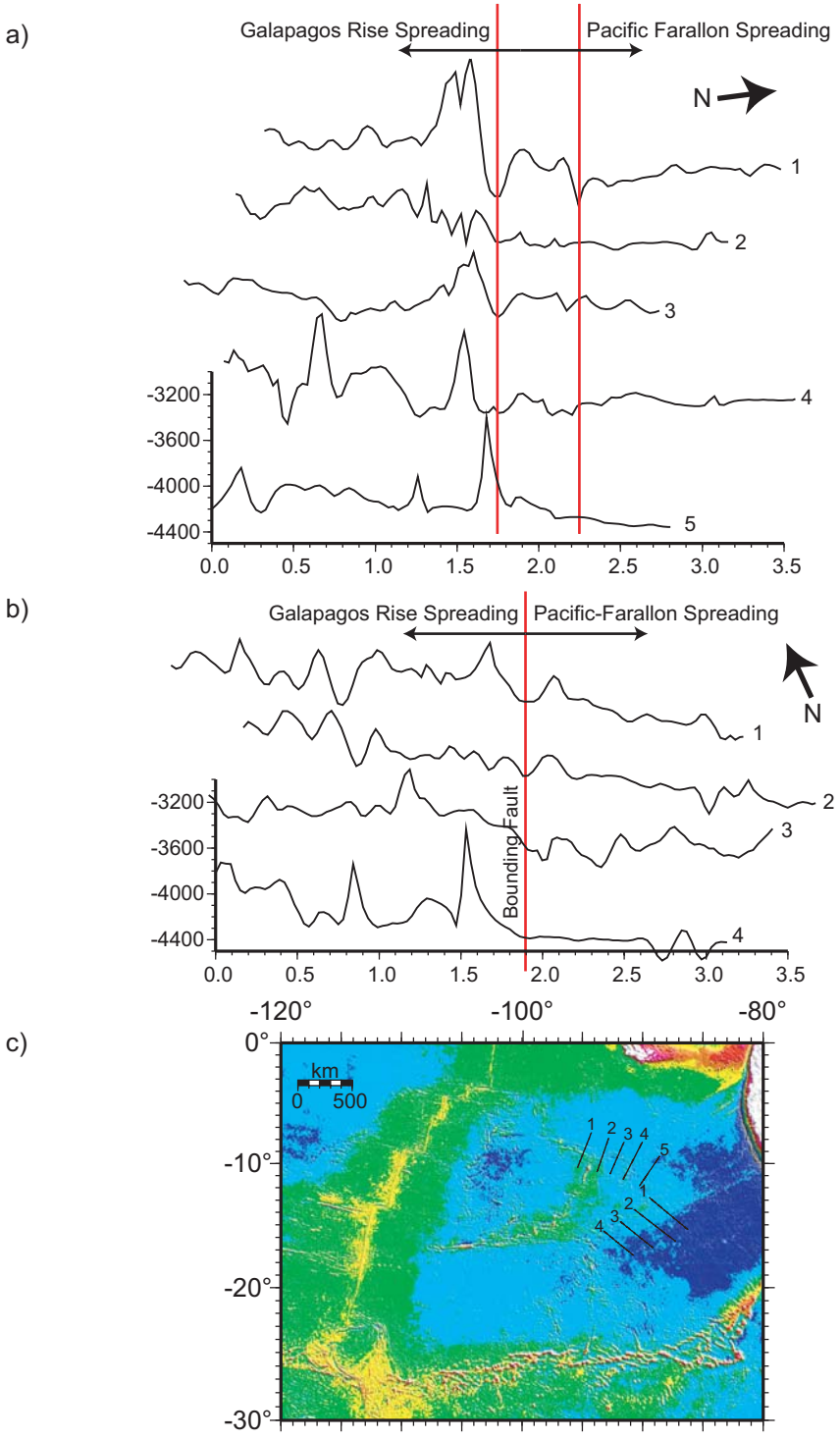

Figure 26. Stacked bathymetry profiles extracted from the predicted bathymetry grid to illustrate discontinuities present at the a) northern and b) eastern tectonic boundaries of the Galapagos Rise system. c) Locations of profiles plotted for reference. Red lines indicate the location of fault traces.

eastern limits of Galapagos Rise spreading, as defined by profiles extracted from the predicted bathymetry grid (Figure 26). The northern boundary is defined primarily by the Gallego fracture zones, observed in the northernmost profile in Figure 26a as twin troughs. North of the Gallego fracture zones, the character of the bathymetry abruptly changes, becoming deeper with lower amplitude variations. The character is consistent with older, subsided seafloor as would be produced by Pacific-Farallon spreading in this location. East of the Galapagos Rise spreading, the bathymetric character of the boundary is similar to the northern boundary. Eastern portions of the profiles display distinctly lower relief and greater depth associated with older seafloor. There is an associated zone of "rough topography" identified by Goff and Cochran [1996] north of the Mendaña fracture zone, which is likely the result of the initiation of spreading along the Galapagos Rise [Mammerickx and Sandwell, 1986].

South of 16°S and the complex east-west fracture zone (the Bauer fracture zone, Figure 1) that marks the southern boundary of Bauer Basin, the transition from Pacific-Farallon spreading to EPR spreading appears to be less complex than the Galapagos Rise spreading history to the north. Here, the first Pacific-Nazca spreading is marked by the Southeast Galapagos Rise Propagator (SEGR), a wedge shaped zone of higher-amplitude bathymetry south of the Galapagos Rise segments and north of the Sala Y Gomez ridge (Figure 27). The SEGR is suggested to have been a northward propagating ridge segment that predates the EPR spreading south of the Garrett fracture

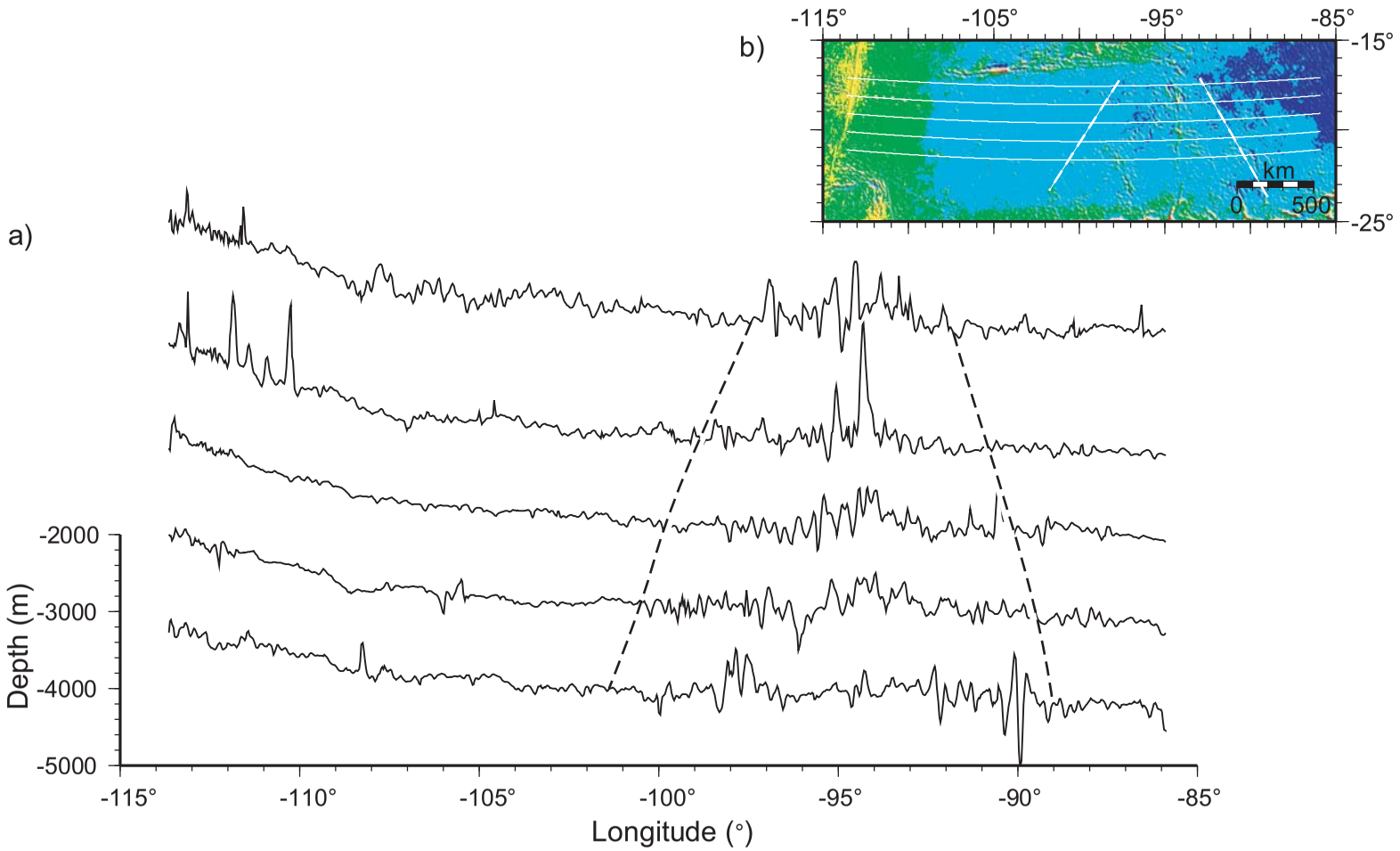

Figure 27. a) Stacked bathymetry profiles extracted from the predicted bathymetry grid to illustrate the morpho-structural features of the SEGR. b) Locations of profiles plotted for reference. Dashed lines in a) and b) indicate the boundaries of the SEGR spreading.

zone and north of the Easter microplate. The spreading along the SEGR was relatively short-lived, and, as indicated by the wedge shape and strike of magnetic anomaly lineations to the east and west (Figure 28), fully accommodated the change between Pacific-Farallon and Pacific-Nazca spreading from 16-26°S. The spreading along the SEGR was likely of short duration (~7 Ma), involving the rapid propagation of the EPR from what is now the Easter microplate to the Garrett fracture zone. Depth distributions and magnetic lineations indicate that this 16-26°S section of the EPR was established earlier and more rapidly than the EPR to the north. The SEGR was the transition zone to EPR spreading at these latitudes.

Seafloor Fabric

Artificially illuminated shaded relief images of the predicted bathymetry in the study area provide an additional opportunity to evaluate the portions of the seafloor that are related to the evolution of the Galapagos Rise system. Boundaries that may produce distinct changes in the slope of the seafloor include fracture zones (the double Gallego fracture zones, for example), and scarps produced by the difference in age and therefore depth (such as the Bauer Scarp).

With illumination from the north in Figure 11, the central portions of the Gallego fracture zones, as well as the G2, G3, and Bauer fracture zones, are most prominent. It is important to note that the G2 and G3 fracture zones are

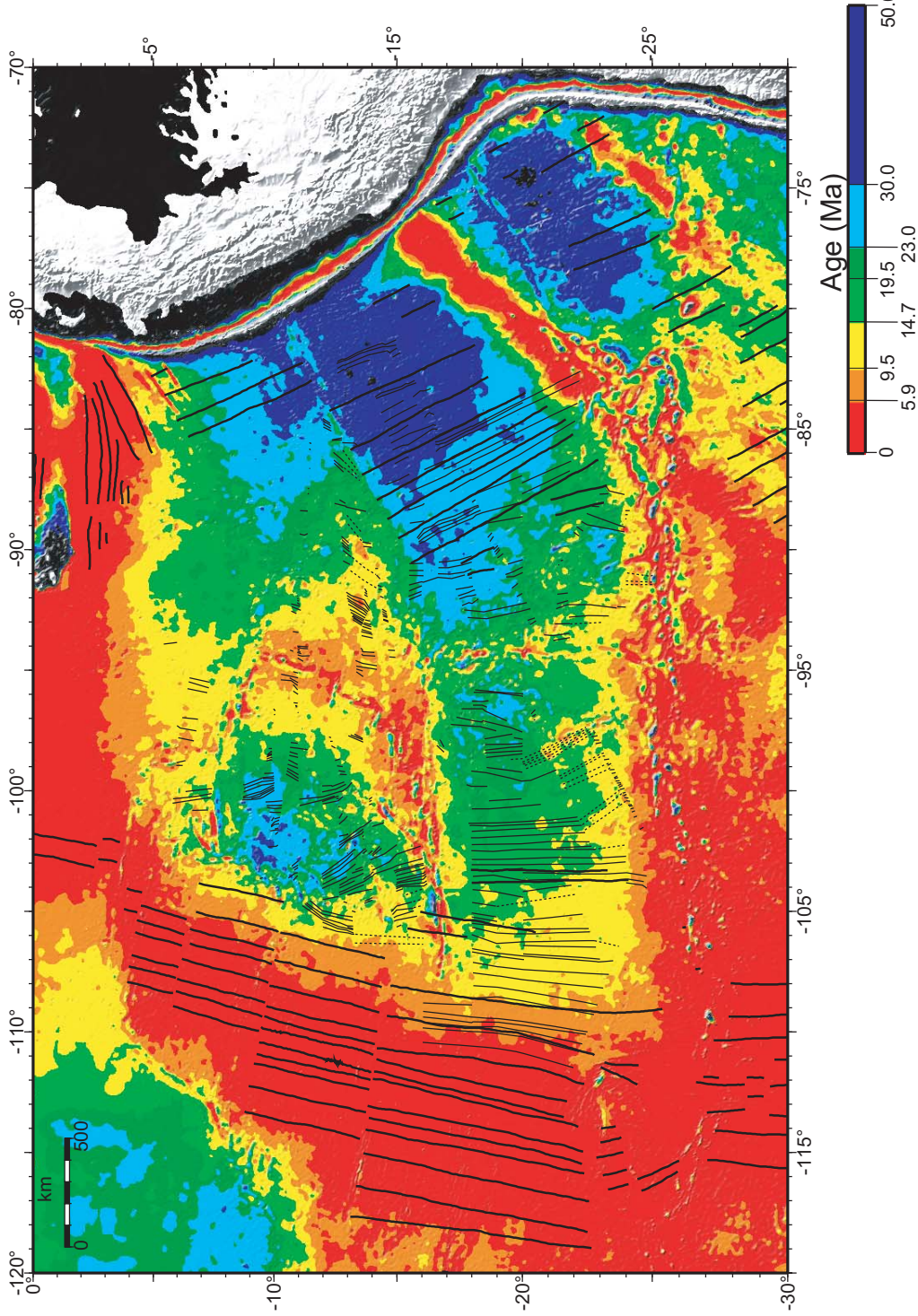

Figure 28. Magnetic anomaly trends from available ship track data in the study area. Thick lines are trends from Cande et al. [1989].. Thin lines are trends mapped in this work. Dashed lines are uncertain correlations.

prominent both east and west of their associated spreading centers, but that neither fracture zone can be easily traced across the Bauer Basin to the Bauer Scarp. This suggests that the part of the Bauer Basin west of FZ3 and FZ4 (Figure 15) may not have been produced by the Galapagos Rise, but was possibly “captured” seafloor produced by Pacific-Farallon spreading and accreted to the Pacific plate (during Galapagos Rise spreading) and the Nazca plate (during EPR spreading). It is, however difficult to trace the exact limits of the fracture zones in the southern Galapagos Rise, and therefore possible that the bathymetric expression of the western parts of these fracture zone were affected by the rotation of Bauer Basin.

The Bauer fracture zone, however, is prominent westward of the southern Galapagos rise past Bauer Scarp and into apparent seafloor produced by the EPR. This suggests that there may have been relative motion between the seafloor produced by the EPR south of the westward extent of the Bauer fracture zone and the seafloor produced by the Galapagos Rise, and therefore that these spreading systems were simultaneously active. The curved troughs noted by Goff and Cochran [1996] (Figure 6) are most clearly visible in Figures 12 and 13. In addition, similarly curved tectonic lineations are visible just north of the Gallego fracture zones on the Quebrada microplate. These curved bathymetric lineations suggest rotation of the seafloor adjacent to the Bauer Scarp that was likely related to the initiation of the EPR and the creation of the Bauer Scarp itself. If this seafloor was rotated at the initiation of the EPR

spreading, then it is likely that the NGR segments were also active during the initiation of the EPR.

The eastern part of the Gallego fracture zones display a distinct change in curvature relative to the rest of the Gallego fracture zones. While the bathymetric expression of the Gallego fracture zone is more complex, a higher degree of curvature can be traced on the eastern end of the fracture zones than is visible on western end near Bauer Scarp. Since the Galapagos Rise initiated subparallel to the Mendana fracture zone, and rotated counter-clockwise, this suggests that there may have been an initial pole of rotation closer to the Galapagos Rise than the pole determined in Figure 14. This pole was short lived, as evidenced by the short trace of the higher curvature on the eastern end of the fracture zones. The pole determined in Figure 14 was active for most of the spreading of the Galapagos Rise and therefore remains the dominant Euler pole.

Magnetic Anomalies

Correlation of the magnetic anomaly profiles across the Galapagos Rise and Bauer Basin was possible in limited areas (Figures 28 and 29). The available magnetic anomaly data were obtained from past ship tracks crossing the study area during transit to the EPR. The ship track orientations often cross the bathymetric features at oblique angles. Perpendicular crossings of bathymetric features (such as those found in a dedicated survey of a region)

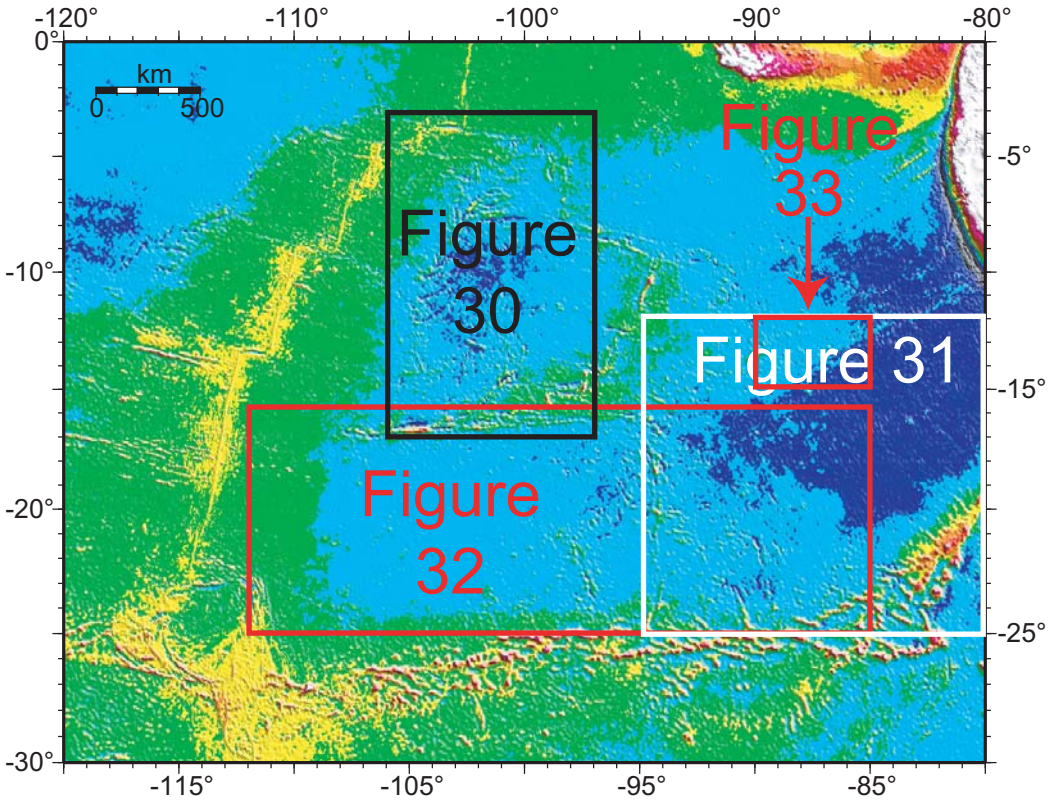

Figure 29. Index map for magnetic anomaly correlations in Figures 30, 31, 32, and 33.

yield the best correlation of magnetic anomalies. The random orientation of most ship tracks, variable frequency of recording magnetic values from cruise to cruise, and the abundance of fracture zones and other bathymetric features made correlation of magnetic anomalies over long distances extremely difficult most ship tracks, variable frequency of recording magnetic values from cruise to cruise, and the abundance of fracture zones and other bathymetric features made correlation of magnetic anomalies over long distances extremely difficult within the Galapagos Rise spreading region. As a result of the combination of these factors, correlations to the synthetic magnetic anomaly profile were problematic. Magnetic anomaly trends, or correlations of pattern and amplitude between lines, were made however, and contributed significantly to the determination of seafloor spreading patterns and pattern changes. Correlating magnetic anomaly lineation trends across distances provided an orientation of seafloor fabric that corresponded with the trends of bathymetric features.

Close to the ridge crests, the magnetic anomaly trends were subparallel to the bathymetric trend of the ridge segment (Figure 28). Farther from the ridge crest, these trends remained roughly perpendicular to the fracture zones in the area, further confirming the rotation of the ridge segments during spreading. On the eastern side of the Galapagos Rise, a pattern of magnetic anomalies was identified on both the northern and southern sides of the Dana fracture zone (Figure 30). This set of magnetic anomaly correlations does not represent the true trend of the magnetic anomalies, as the lineations would cross the Dana

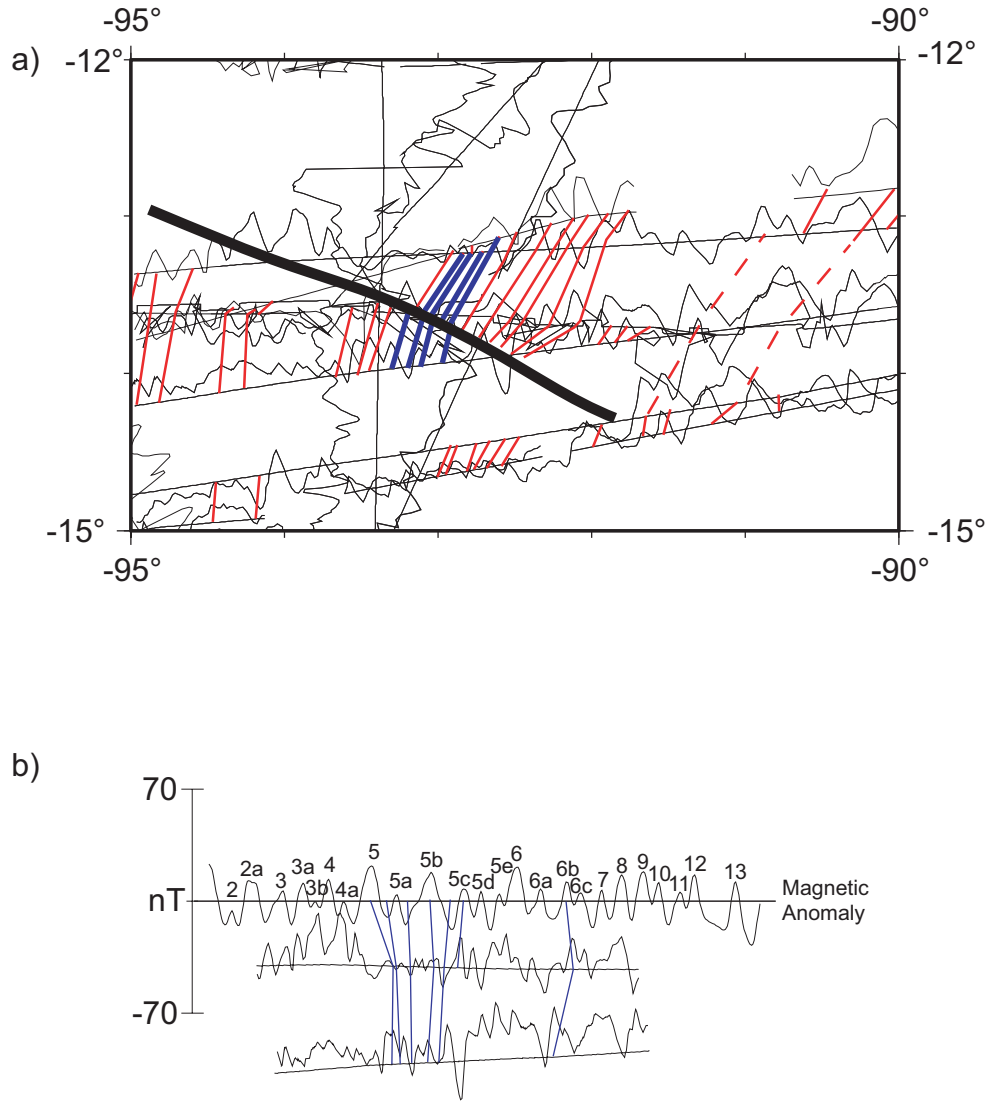

Figure 30. Correlation of identified magnetic anomaly lineations mapped in the study area to synthetic magnetic reversal sequence. a) Red lines indicate correlation of magnetic anomaly patterns. Thick black line indicates location of GR2 fracture zone. Thin black lines represent magnetic anomalies and associated ship tracks. b) Correlation of magnetic anomaly patterns indicated by blue lines in part (a) to synthetic model of the magnetic reversal sequence of Cande and Kent [1995]. See text for details on model parameters.

fracture zone, but represents the offset produced by the different ridge segments (the northern anomalies by GR1 and the southern anomalies by GR2).

The trends of the magnetic anomalies mapped in the Bauer Basin region vary considerably in orientation, and are consistent with seafloor produced from different spreading centers, as well as the possibility of rotation of the seafloor in the Bauer Basin (Figure 31). Between 12°S and 14°S and 101°W and 105°W, a set of magnetic anomaly lineations trend north-northwest, and are located on seafloor that is significantly deeper than the nearby EPR lineations. This area of seafloor is east of the Bauer Scarp, which is the deepest seafloor in the Bauer Basin, and therefore likely the oldest seafloor of the Bauer Basin. These lineation trends are subparallel to the orientations of the magnetic anomaly lineations on the eastern Nazca plate produced by Pacific Farallon spreading. The result of the ages determined by isotope dating from the DSDP Site 319 (see Figure 1 for location) cores suggest that the ages of the basement samples for Site 319 are ~15-19 Ma [Hogan and Dymond, 1976, Lanphere and Dalrymple, 1976, Seidermann, 1976, Reynolds, 1976, Macdougall, 1976, Mitchell and Aumento, 1976, Yeats et al., 1976], which places that portion of the southern Bauer Basin in the age range of active spreading on the Galapagos Rise system (~23-5.9 Ma). These ages are consistent with the predicted ages determined in this study (Figure 20). There is a discrepancy, then, between the age of the southern Bauer Basin as established by magnetic anomaly lineation trends and predicted ages for the northern Bauer Basin (23-30 Ma).

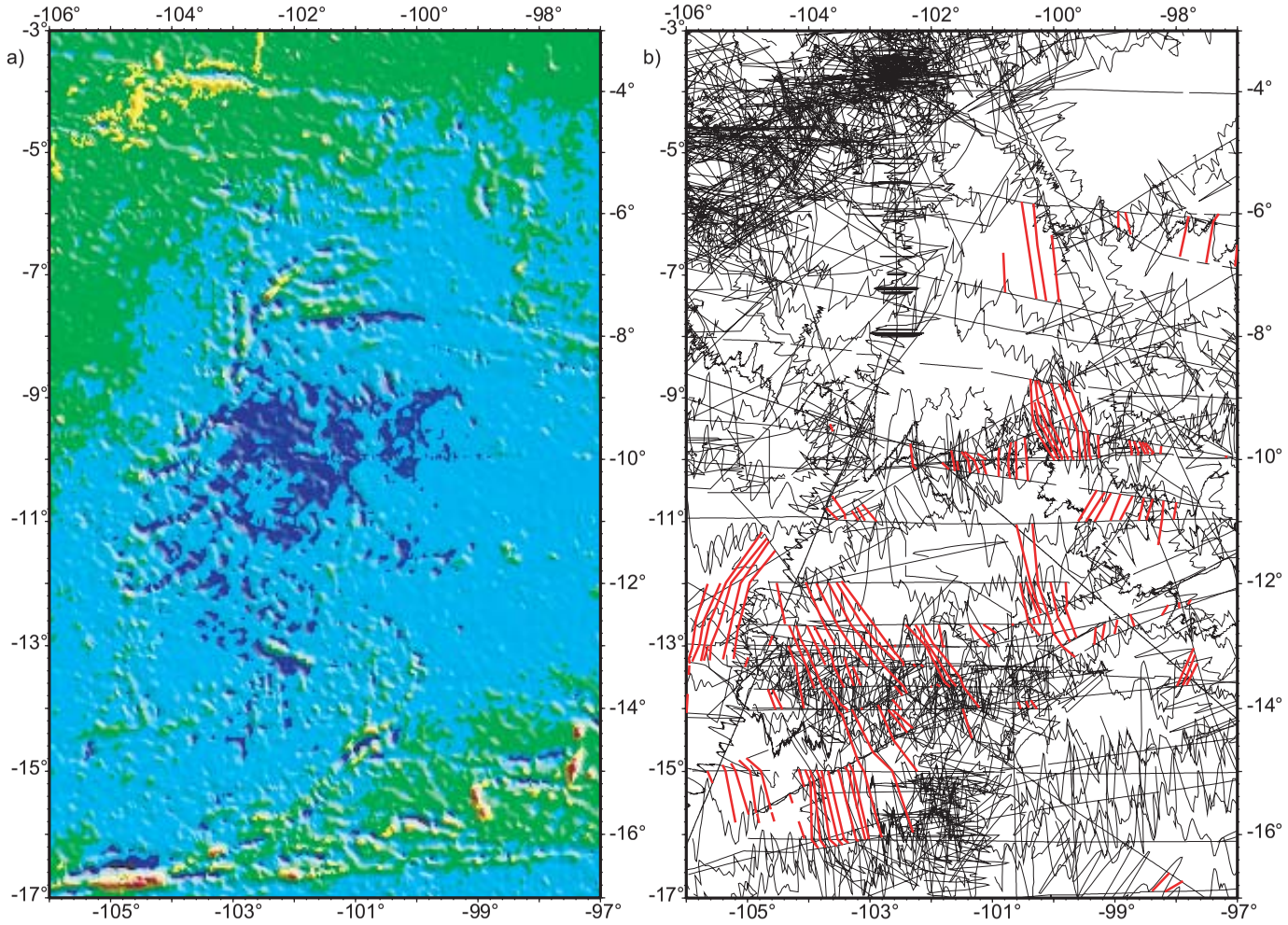

Figure 31. Magnetic anomaly trends mapped in the Bauer Basin area. a) Black lines represent magnetic anomaly values projected perpendicular to ship track. Red lines indicate magnetic anomaly pattern correlations between ship tracks. b) Predicted bathymetry map of the same area for reference.

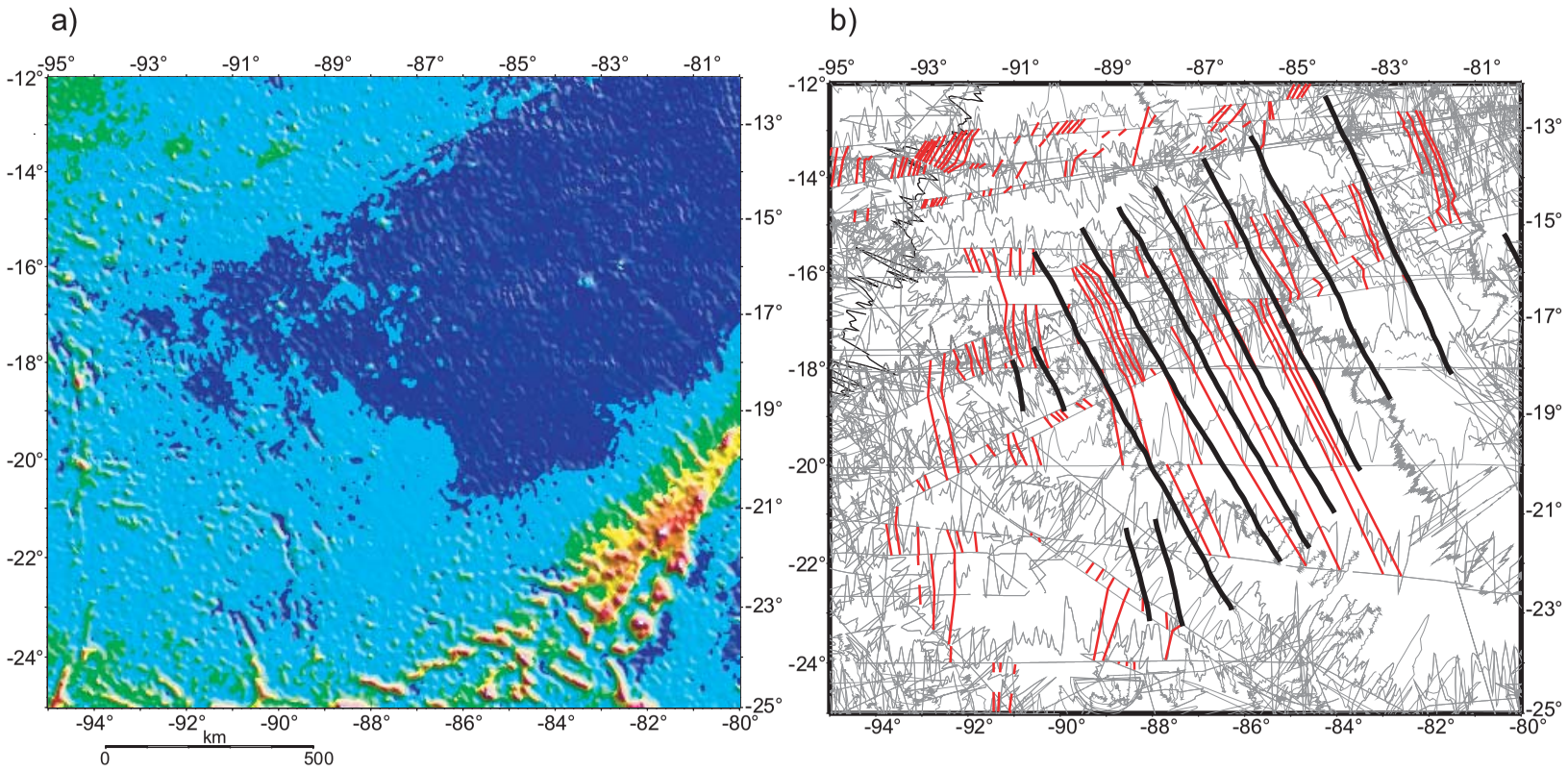

Figure 32. Magnetic anomaly trends mapped in the eastern portion of the Nazca plate. a) Black lines represent magnetic anomaly values projected perpendicular to ship track. Thick black lines represent magnetic anomalies mapped by Cande et al. [1989]. Thin red lines indicate magnetic anomaly pattern correlations between ship tracks mapped in this work. b) Predicted bathymetry map of the same area for reference.

The magnetic anomaly lineation trends on the eastern part of the Nazca plate (Figure 32) are consistent with the trends established by Cande et al. [1989], striking NW. The peaks and troughs of the magnetic anomalies in this area are relatively easy to correlate, and match to the magnetic reversal time scale. This area, from ~88°W to the Peru Trench is occupied by reversals 7 to 10, dating from 24.7 to 28.7 Ma, and was formed as part of the Farallon plate, prior to development of the Galapagos Rise and the EPR to the west.

The magnetic anomaly lineation trends in the area south of the Galapagos Rise system consistently strike north-south to the west of 101°W and northwest east of 88°W. These lineations (Figure 33) can be attributed to EPR and Pacific-Farallon spreading, respectively [Cande et al., 1989]. Between these sets of lineations, from 88°W and 101°W, the magnetic anomaly patterns are more complex, making it difficult to resolve comprehensive lineation trends. It is this zone that corresponds to the SEGR and the complex, high amplitude bathymetry illustrated in Figure 27. This region of “rough topography” may represent the slower spreading predicted by Mammerickx and Sandwell [1986] for the initiation of new spreading centers. It is fairly clear, however, that the SEGR represented a transition from the northwest-trending Pacific-Farallon spreading to the north-trending EPR spreading, and accommodated the rotation between these spreading centers from 18-26°S.

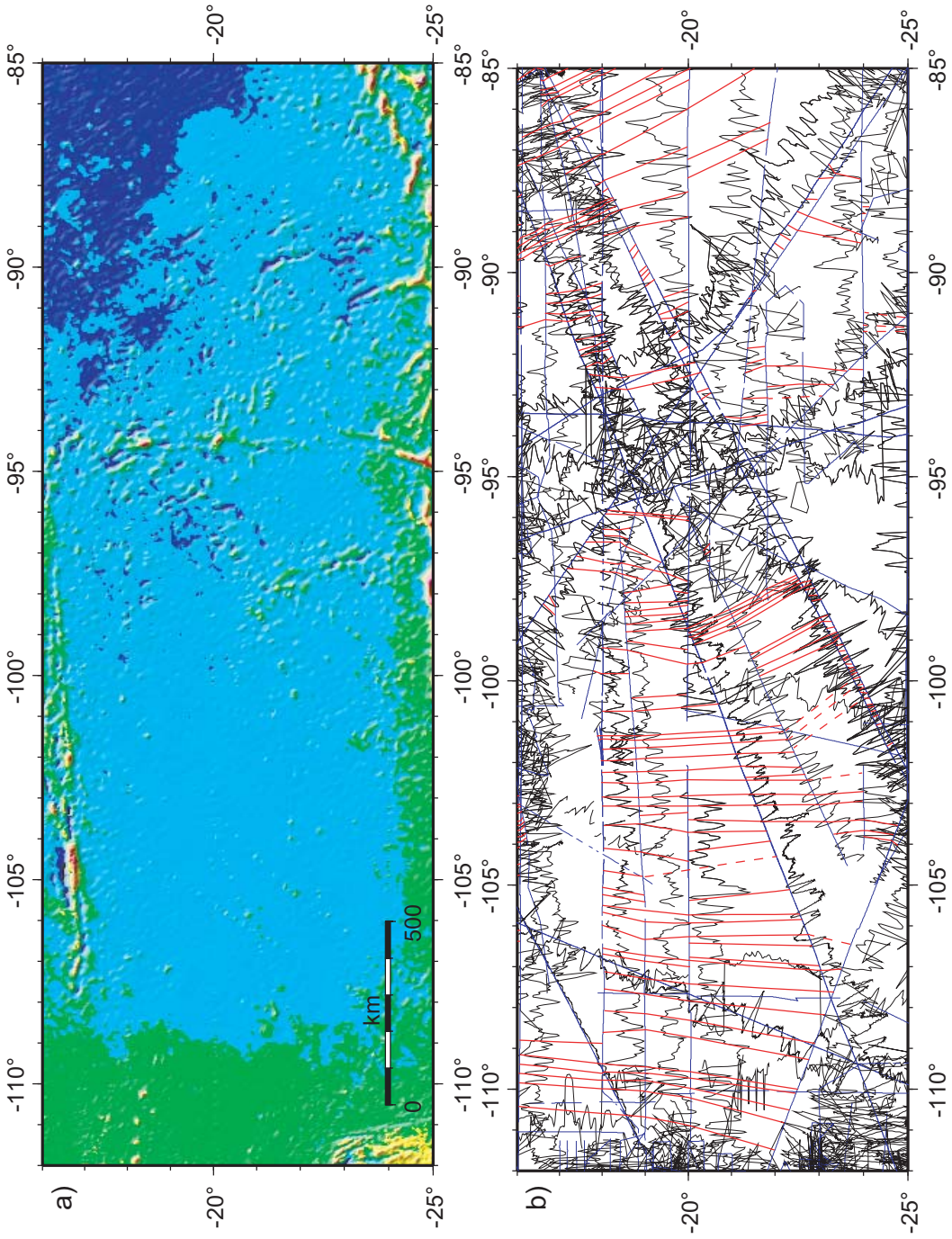

Figure 33. Magnetic anomaly trends mapped in the SEGR region. a) Black lines represent magnetic anomaly values projected perpendicular to ship track. Red lines indicate magnetic anomaly pattern correlations between ship tracks. b) Predicted bathymetry map of the same area for reference.

The magnetic anomaly trends mapped throughout the study area (Figure 28) were used in conjunction with the seafloor depth distribution and previously mapped magnetic anomalies of Cande et al. [1989] as the basis for the reconstructions developed in this work. Seafloor ages and structural or tectonic features were integrated to make the reconstructions that follow.

Reconstructions

Depth-determined age of the seafloor, combined with magnetic lineation trends of the Bauer Basin and Galapagos Rise system are the primary basis for interpretation of the tectonic evolution of the region. Dated magnetic anomaly lineations and age/depth relationships are better correlated surrounding the Bauer Basin and Galapagos Rise system.

The ridge segments and transform fault traces of the Galapagos Rise system identified in the bathymetry were placed in the appropriate geographical positions relative to the locations of spreading centers, magnetic anomaly lineations and transform fault zones from Cande et al. [1989], beginning with the present day and working backward in time. The predicted age maps were used in conjunction with the reconstructed magnetic anomaly lineation locations from the OSDN program to help identify the presence and location of portions of seafloor and prominent bathymetric features at the indicated time steps. The color coded predicted age maps indicate which parts of the seafloor were present at the time of each reconstruction. For example, after removal of

seafloor younger than the reconstructed age in the predicted age map, the remaining seafloor moved according to the reconstructed location of magnetic anomalies present at the time of the reconstruction. The locations of ridge segments, transform fault zones, and identified magnetic anomaly lineations within the Galapagos Rise system can then be inferred from the relative locations of the previously identified seafloor features and magnetic anomaly lineations.

The time steps, 23 Ma (Figure 34), 19.5 Ma (Figure 35), and 14.7 Ma (Figure 36) for the reconstructions were chosen to correlate with major ridge system reorientations as indicated in Meschede and Barckhausen [2000] for the Pacific- Farallon system and the Galapagos Ridge. The 9.5 Ma (Figure 37) and 5.9 Ma (Figure 38) steps were selected to correlate with major EPR reorientations suggested by Goff and Cochran [1996] and Mammerickx et al. [1980]. Finally, the present-day orientations of the active and extinct ridge systems are shown in Figure 39.

The 23 Million Years Reconstruction

At 23 Ma (Figure 34), the Pacific-Farallon system was the only active spreading system in the region. The ridge axis segments were long and straight with little curvature along strike, as indicated by the consistent strike and the correlation of magnetic anomalies (7 through 15 on the west side of the ridge and 7 through 18 or older on the east of the ridge). The trends of the ridge axes

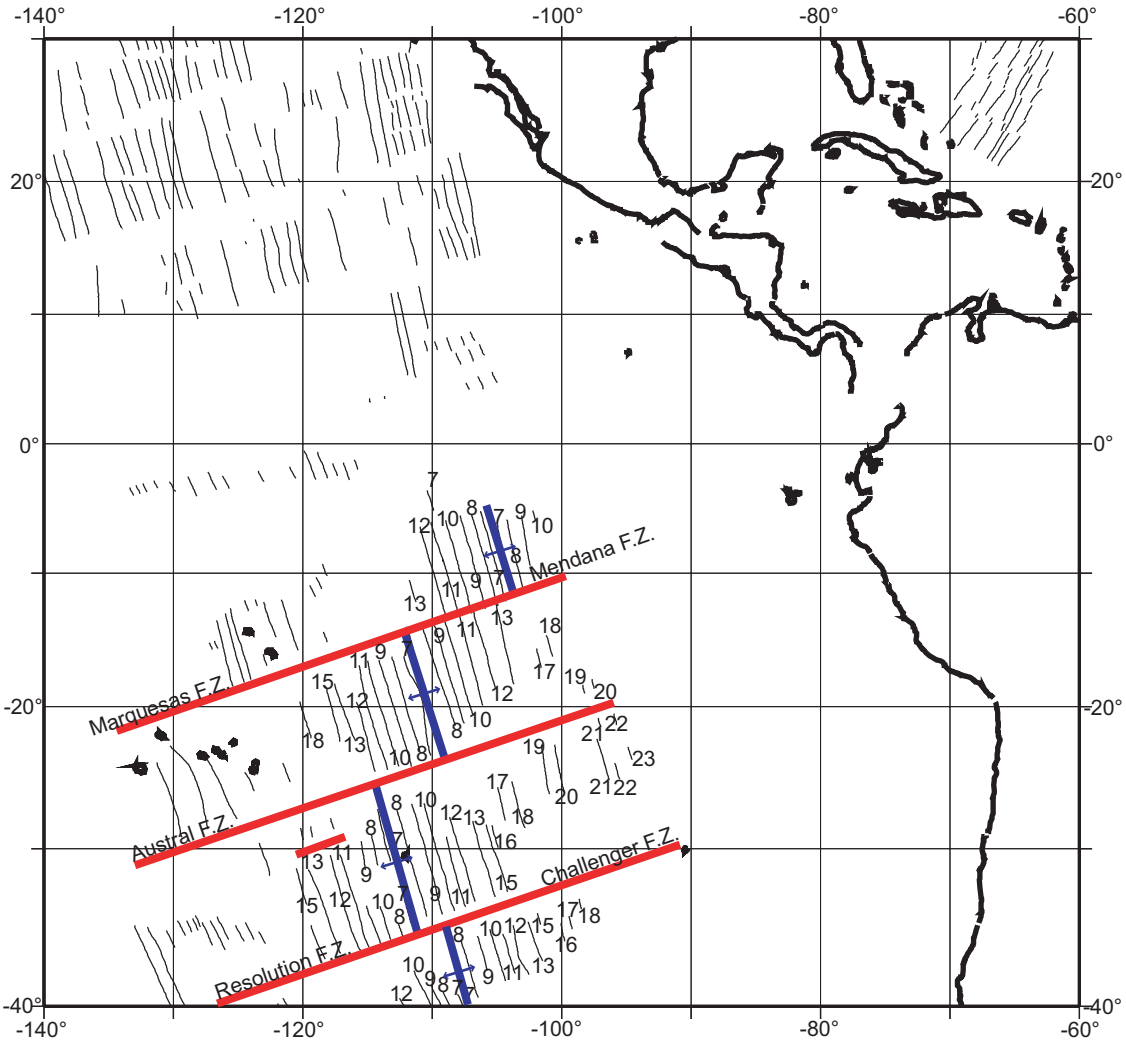

Figure 34. Reconstruction of the Galapagos Rise at 23 Ma. Red lines indicate fracture zones. Blue lines indicate spreading centers, with arrows to indicate direction of spreading. Thin black lines indicate magnetic anomaly lineations of Cande et al. [1989], and are numbered where appropriate. Thick black lines indicate shore lines.

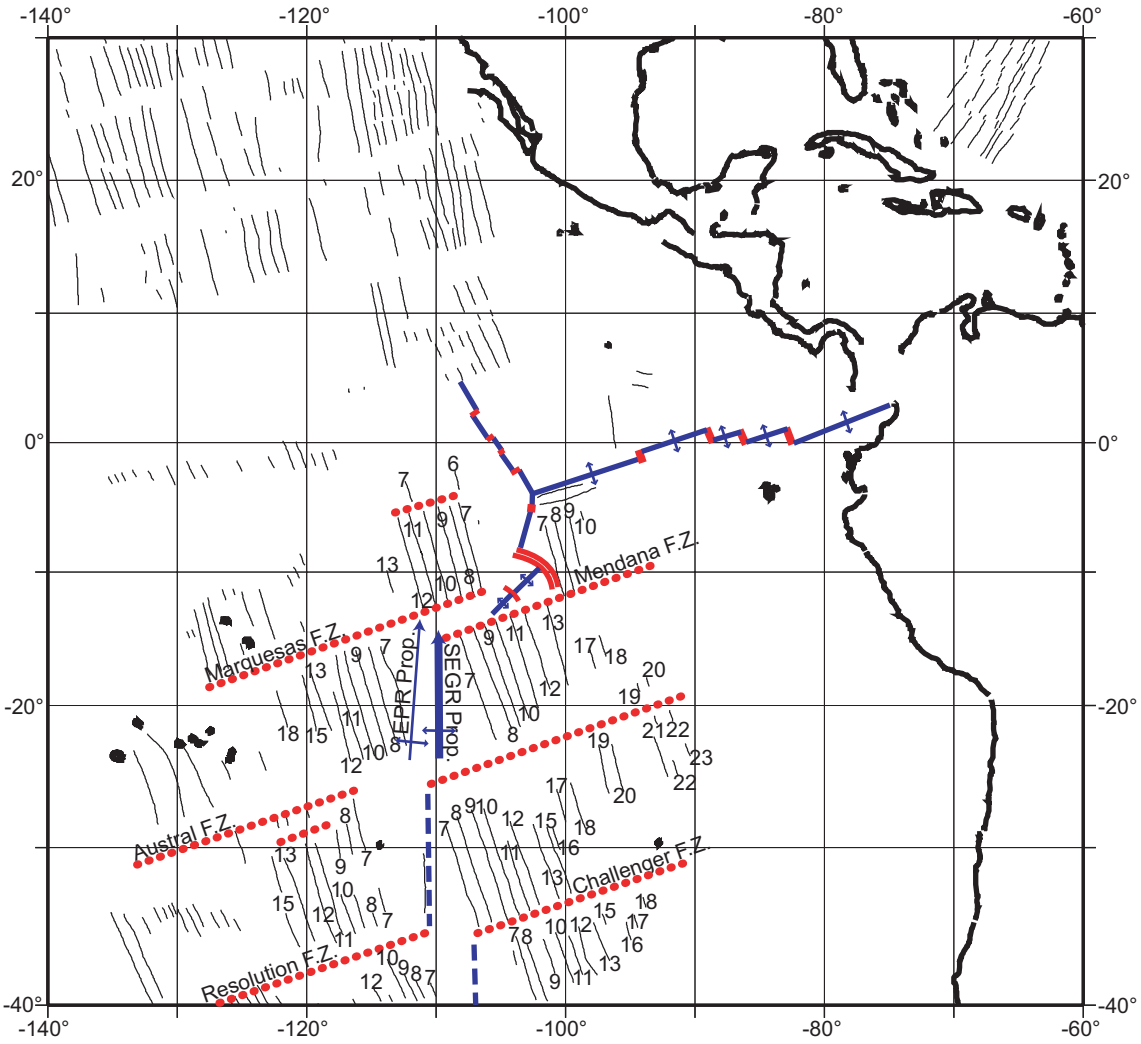

Figure 35. Reconstruction of the Galapagos Rise at 19.5 Ma. Blue lines indicate active spreading centers, with arrows showing direction of spreading. Dashed blue lines indicate interpreted locations of spreading centers outside the study area. Solid red lines indicate active transform plate boundaries. Dotted red lines indicate inactive fracture zones.

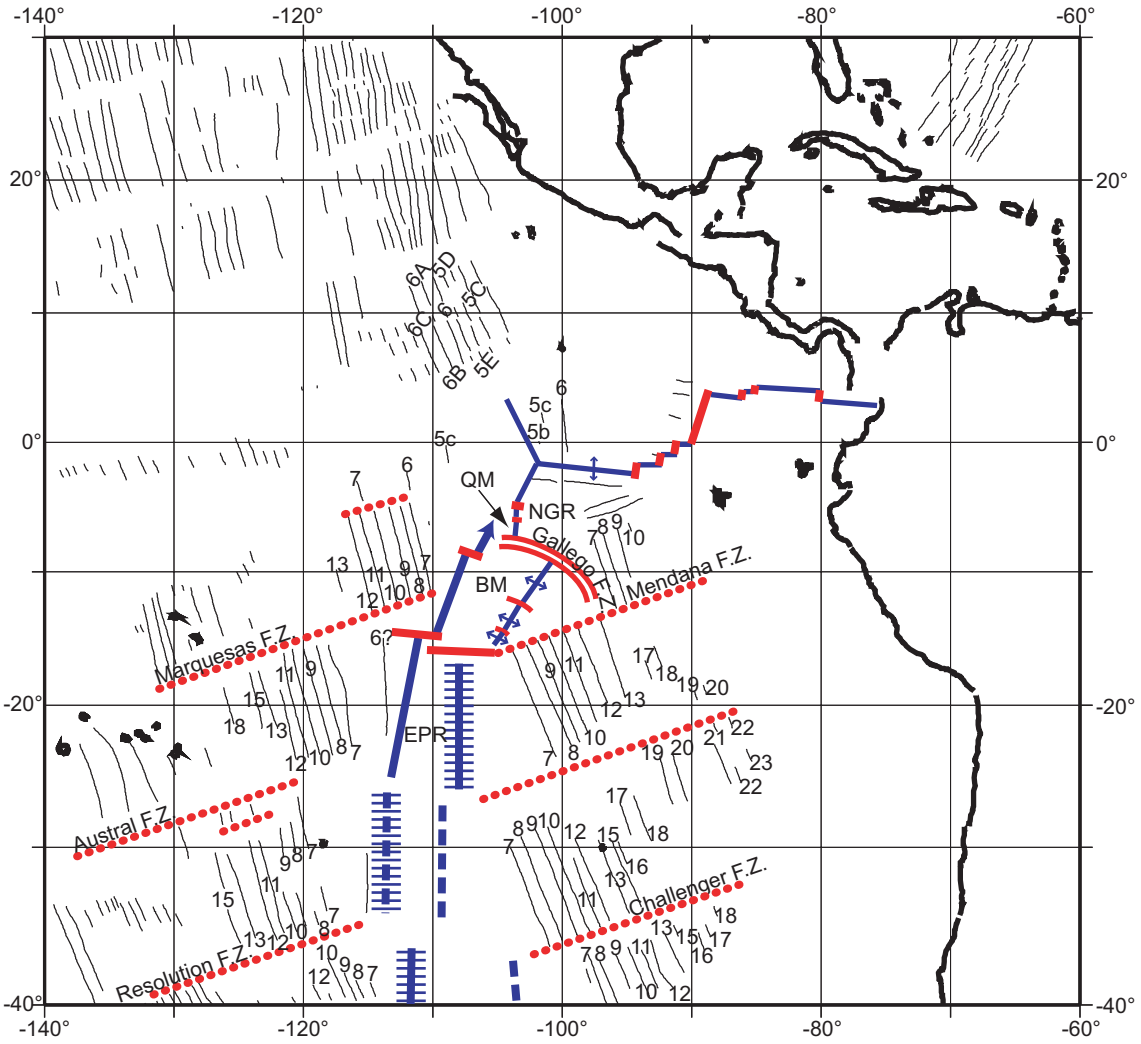

Figure 36. Reconstruction of the Galapagos Rise at 14.7 Ma. Hachured blue lines indicate extinct spreading centers. All other lines are as in Figure 34. BM = Bauer Microplate, NGR = North Galapagos Rise, QM = Quebrada Microplate.

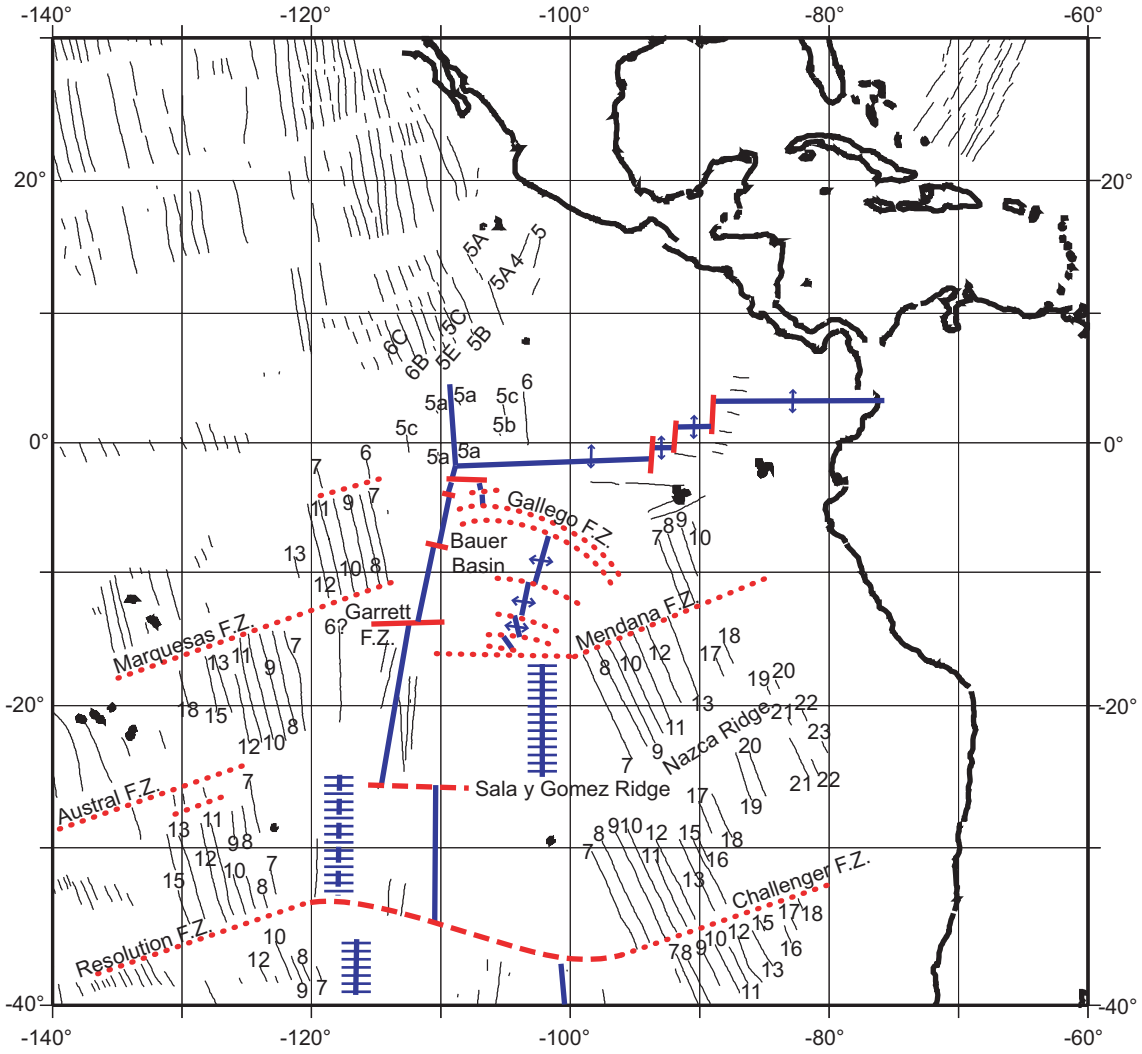

Figure 37. Reconstruction of the Galapagos Rise at 9.5 Ma. Hachured blue lines indicate extinct spreading centers. All other lines are as in Figure 34.

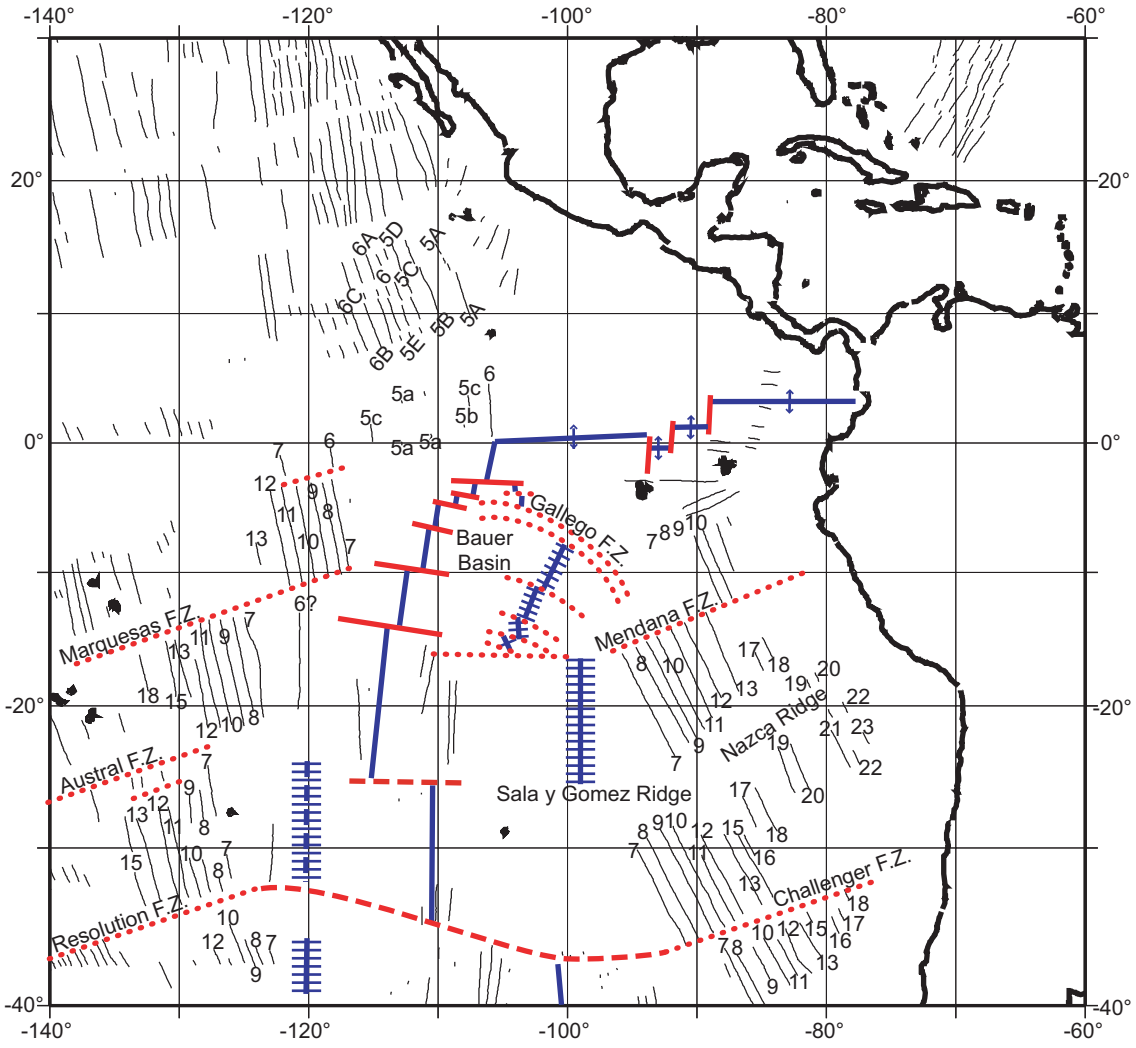

Figure 38. Reconstruction of the Galapagos Rise at 5.9 Ma. Hachured blue lines indicate extinct spreading centers. All other lines are as in Figure 34.

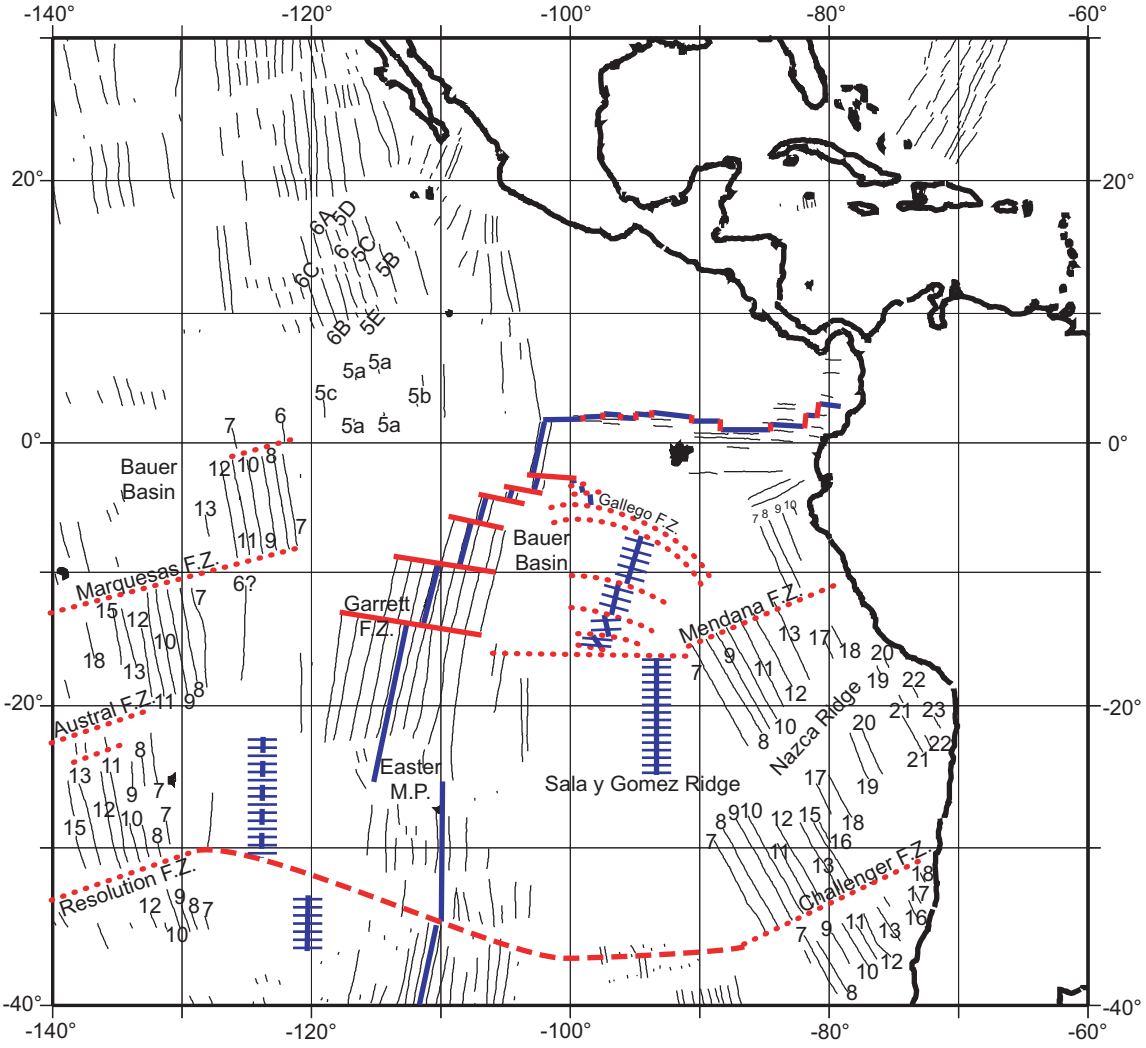

Figure 39. Present-day configuration of the study area. Hachured blue lines indicate extinct spreading centers. All other lines are as in Figure 34.

were consistently north-northwest, with perpendicular spreading. Transform faults (Marquesas, Austral, Challenger, and Resolution fracture zones) also appear to have very little curvature (or a very distant pole of rotation), indicating a stable ridge/transform system for this time period.

The spreading rates of the Pacific-Farallon system, estimated from the distance between identified magnetic anomalies, ranged from ~80-115 mm/yr [Hey et al., 1977, Mammerickx, 1980], which is consistent with medium to fast spreading centers observed today. The simplicity of the magnetic lineation pattern makes it likely that the Pacific-Farallon system was the only spreading system in the region at that time. The Meschede and Barckhausen [2000] reconstruction at 23 Ma shows an established Pacific-Cocos-Nazca triple junction. While the initial breakup of the Farallon plate and the initial formation of the Galapagos Ridge was possibly beginning at the Farallon plate's eastern margin at this time, the Pacific-Farallon spreading system orientation indicated by the reconstruction of magnetic anomaly 7 (Figure 34) indicates the Pacific-Farallon plate boundary had not yet been altered and the Farallon plate not yet completely broken into the Cocos and Nazca plates.

The long, consistent-trending ridge segments and fracture zones with low curvature indicated by the magnetic anomalies in Figure 34, along with rapid spreading rates in this region suggest that the Pacific-Farallon spreading system was stable at 23 Ma. Any plate reorganization that would produce active spreading on a ridge system with a significantly different orientation has not

produced related morphological seafloor features or magnetic lineations indicative of plate breakup or reorientation. The only possible 23 Ma seafloor produced by Galapagos Ridge spreading is found at the east edge of the Galapagos Ridge system just north of Grijalva scarp [Meschede and Barkhausen, 2000]. Therefore, the Galapagos Rise and the Galapagos Ridge spreading, as well as the breakup of the Farallon plate were not fully established until after 23 Ma.

The 19.5 Million Years Reconstruction

By this time, the Farallon plate had broken and new spreading centers were established (Figure 35). The Galapagos Ridge, the northern boundary of the Nazca plate, propagated westward, breaking the Farallon plate into the Cocos and Nazca plates [Hey et al., 1977]. To the south, along the former Pacific-Farallon ridge, there was a reorientation from the NW-SE striking spreading center system to NE-SW to N-S trending spreading center segments. This is the new Pacific-Nazca spreading system.

South of the Austral and Challenger-Resolution fracture zones (Figure 35), the new ridge segments formed with a N-S strike. As will be shown later, ridge jumps will occur on the segments but they will maintain their N-S strike. North of the Austral fracture zone (and Sala Y Gomez ridge), the new spreading system was more complex. The SEGR propagator initiated, propagating northward from the Austral fracture zone, and becoming the dominant spreading

system at that latitude. This segment was oriented approximately due north, and produced a wedge-shaped segment of seafloor. Shortly after this time, a new EPR segment between the present Easter microplate and Garrett fracture zone was initiated and propagated NNE. This ridge segment, located west of the SEGR, has continued spreading to the present. While the SEGR was short-lived, it accommodated the rotation between the Pacific-Farallon and EPR spreading (Figure 33). The EPR segment spreading likely increased quickly to the full spreading rate, as indicated by the amount of seafloor produced by the ridge. The SEGR, therefore, began to fail a short time (less than 10 Ma) after initiation. The central SEGR segments, however, are shallow relative to the adjacent seafloor (similar to the fossil ridge crests of the Galapagos Rise system), suggesting possible post-spreading volcanism. The region between the SEGR and the EPR is the area of the proposed Mendoza microplate (postulated by Lonsdale [1989], Figure 5). The magnetic anomaly tentatively identified in Cande et al. [1989] as anomaly 6 (south of the Austral and to the northeast of the Resolution fracture zones), indicates that ridge segments initiated with a due-north trend that breaks the Austral fracture zone into eastern and western components, and the Resolution-Challenger fracture zone into individual fracture zones. The greatest area of seafloor was produced by the GR1 segment of the Galapagos Rise (~750 km of seafloor produced on the eastern side of GR1). The GR2 segment produced less seafloor (~650 km on the eastern side of GR2), which suggests that it was initiated slightly later than

the GR1 segment. The Galapagos Rise most likely initiated at the Gallego fracture zones and propagated southward. These segments came to constitute the Nazca-Pacific spreading system and represented the proto-EPR, propagating from south to north between the former fracture zones in this region.

The most significant ridge segment for this study is the initiation of the GR1 segment of the Galapagos Rise system. The smaller radius of curvature on the eastern portion of the Gallego fracture zones and the trends of magnetic anomaly lineations in the Bauer Basin indicate that the GR1 ridge segment initiated parallel to the Mendaña fracture zone, trending east-northeast, and propagating west-southwest. Magnetic anomaly lineation trends in the Bauer Basin are not parallel to either the EPR or the Galapagos Rise ridge segments, the former Pacific-Farallon magnetic anomaly lineations, suggesting that these lineations were rotated with the rotation of the Galapagos Rise. At this time step (19.5 Ma), only the GR1 segment has initiated, and the Dana fracture zone is not yet present, as estimated from age/depth relationships (Figure 20). The initiation of the GR1 segment parallel to the Mendaña fracture zone (suggested by Goff and Cochran [1996]) produced the region of rough topography and depth/age discontinuities observed across the Mendaña fracture zone, as predicted by Mammerickx and Sandwell [1986]. The Galapagos Ridge and the Galapagos Rise spreading systems have both initiated and been established as an accommodation to the Farallon plate breaking into the Cocos and Nazca plates, likely by subduction forces along Central and South America,

respectively [Warsi and Hilde, 1983]. The propagation of the GR1 segment initiated the formation of the Bauer Basin, and the Gallego fracture zones. The NGR segments also began producing seafloor north of the Gallego fractures zones at this time, connecting the Galapagos Rise system to the Galapagos Ridge system.

The 14.7 Million Years Reconstruction

By 14.7 Ma, the Marquesas and Mendaña fracture zones were significantly displaced by Galapagos Rise spreading and the formation of the Bauer microplate (Figure 36). Since the curved bathymetric troughs (identified by Goff and Cochran [1996]) along the deeper sides of the Bauer and anti-Bauer Scarps are located at the farthest extent of EPR spreading, and thus predate or are related to the initial the propagation of the EPR in this area. The absence of similar structures in the younger crust produced by the EPR suggests that the kinematics that created these structures were short lived.

The Galapagos Rise system rotated counter-clockwise relative to the Mendaña fracture zone, producing the Gallego, Dana, and GR3 fracture zones prominent in the bathymetry, as the GR2 and GR3 ridge segments formed by southwest ridge propagation (Figure 2). The SEGR propagator reached failure stage by this time, fully transferring its spreading to the EPR. This segment of the EPR was rapidly established at fast spreading rates, as indicated by the magnetic anomaly lineations [Herron, 1972], and consistent with the short span

of spreading (~7 Ma) suggested by the predicted age map (Figure 20). The EPR segments south of the Galapagos Rise all trended almost due north by this time, consistent with the trend of anomaly 6 from Cande et al. [1989].

The 9.5 Million Years Reconstruction

By this stage, the EPR has propagated northward from the newly developed Garrett fracture zone, (Figure 37). The Galapagos Rise was still the dominant spreading center north of ~17°S and south of the Galapagos Ridge, with the EPR spreading slowly [Goff and Cochran, 1996]. The SEGR segment had failed by this time, and active spreading on the sub-parallel EPR segment to the west reached full spreading rate, as indicated by the depth/age relationships and magnetic anomalies and the near the SEGR (Figures 27 and 33). South of the Austral fracture zone, the Pacific-Farallon spreading ridges were abandoned and spreading transferred eastward to the southern EPR [Tebbens and Cande, 1997, Tebbens et al., 1997]. The Galapagos Ridge reorganized to an approximately due east direction [Meschede and Barckhausen, 2000].

The counter-clockwise rotation of the Galapagos Rise segments and the Bauer microplate continued as the Nazca and Pacific plates reorganized. The EPR system has propagated northward to the Quebrada fracture zone. The Quebrada fracture zone connects the northern segments of the NGR with the EPR by means of a transform fault, creating another microplate labeled in this study as the Quebrada microplate (Figure 1). The NGR segments stopped

producing seafloor shortly afterward, as suggested by the predicted age map in Figure 20, and Quebrada microplate accreted to the Nazca plate. Interestingly, curved bathymetric structures north of the Gallego fracture zones immediately east of the Yaquina fracture zone (Figure 1) strongly resemble the bathymetric expressions of the Bauer (concave-northward) and anti-Bauer (concave-southward) structures. This similarity in bathymetric expression suggests that there may have been rotation of the EPR propagator tip in this area as well.

The 5.9 Million Years Reconstruction

The EPR was established as the dominant spreading system in the study area (Figure 38). Prior to this (at ~9.5 Ma), the active Pacific-Nazca spreading system from south to north included the EPR from south of 25^{o}S, the EPR segment from the future Easter microplate to the Garrett fracture zone, and the Galapagos Rise (including the NGR). North of Quebrada fracture zone, the EPR and the Galapagos Ridge were the dominant spreading systems. Propagation of the EPR north of Garrett fracture zone was suggested by Mammerickx et al. [1980] to have occurred later (at 6.8 Ma) than proposed in the Goff and Cochran [1996] reconstruction. In either case, the propagation of the EPR north of Garrett fracture zone created spreading at the same latitudes as the Galapagos Rise, contributing to the progressive cessation of Galapagos Rise spreading as the EPR propagated northward. The Galapagos Rise spreading transferred to the EPR in progressively northward stages. As the Galapagos Rise segments

failed, the EPR spreading accelerated to full spreading rates. The GR1 segment was the last of the Galapagos Rise segments to fail, and therefore spread the longest, with the widest distribution of associated seafloor related to spreading. Spreading ceased on the Galapagos Rise between 5.9 and ~8 Ma.

The Present Day

By this stage, all active spreading along the Galapagos Rise has failed (Figure 39). The extremely shallow ridge crests along the Galapagos Rise segments (Figure 2) suggest the possibility that there may be small amount of magma supplying the northern Galapagos Rise ridge segment (GR1) that supports the shallow ridge crest structures, but does not contribute to any spreading along the ridge segments. The EPR is the sole spreading system between the Pacific and Nazca plates. The identification the earliest spreading along the EPR, from Garrett fracture zone to the Galapagos Ridge, progressively from 3a (6.57 Ma) to 2 (1.95 Ma) documents the sequential transfer of spreading from the Galapagos Rise to the EPR. The presence of earthquake seismicity all along this part of the EPR and lack of seismicity along the Galapagos Rise indicates that the transfer of spreading was completed. Seismic activity along the eastern portions of the double Gallego fracture zones (Figure 14) consists of small magnitude earthquakes likely due to differential subsidence of seafloor of different ages across the fracture zones. Earthquakes recorded along the fossil ridge segments are suggested to be the result of

subsidence of the seafloor due to failure of magma supply to the ridge segment.

DISCUSSION

The breakup of the Farallon plate into the Nazca and Cocos plates was a result of subduction forces along the Peru-Chile and Middle America trenches. Major ridge jumps in the eastern Pacific occurred following the breakup of the Farallon plate into the Nazca and Cocos plates and the corresponding new relative motion between these plates and the Pacific plate. The study of the Galapagos Rise yields insight into the nature of plate fragmentation and subsequent spreading center initiation as a result of the plate motion changes. The transition from Pacific-Farallon to the current Pacific-Nazca spreading along the EPR involved the creation of several microplates, rotation during spreading, and the nucleation of multiple ridge systems as evidenced by the bathymetric features and magnetic anomaly lineation patterns that make up the current western Nazca plate north of 25°S. In the 23 million years since the Farallon plate breakup, the Galapagos Rise constituted a major component of the active seafloor spreading between the Pacific and Nazca plates between 3° and 25°S [Mammerickx et al., 1980, Hey, 1980, Lonsdale, 1989, Goff and Cochran, 1996, McGuire and Hilde, 1999, McGuire and Hilde, 2002].

Prior to 23 Ma, the Pacific-Farallon system was the sole source of seafloor spreading in the eastern Pacific Ocean. The Pacific-Farallon ridge segments were oriented northwest, with few fracture zone transforms. The motions of the Pacific and Farallon plates were perpendicular to the ridge segments. The long

fracture zone traces are not curved, indicating there was a distant pole of rotation and a stable, simple Pacific-Farallon mid-ocean ridge system.

The initiation of the Galapagos Rise just after 23 Ma, however, marked the beginning of more complex spreading in transition from Pacific-Farallon to Pacific-Nazca plate motion. The spreading systems that developed as a result of the Farallon plate breakup incorporate rotations (Gallego and Dana fracture zones), short-lived (SEGR) and long-lived (Galapagos Rise and the NGR) spreading centers, and multiple instances of microplate formation (Mendoza, Quebrada, and Bauer microplates). All of these structures were initiated with the formation and propagation of the Galapagos Rise parallel to the Mendaña fracture zone. The zones of "rough topography" parallel to the Mendaña fracture zone in the east and the eastern boundary of the Bauer microplate in the west identified by Goff and Cochran [1996] (Figure 6) are consistent with the rough topography predicted by Mammerickx and Sandwell [1986] for the initiation of spreading centers, and were the result of the initial slow spreading on the new ridge. The Galapagos Rise propagated southward starting at the Gallego fracture zones, consistent with the highest extensional paleo-stresses for this region as calculated in the finite element analysis of Wortel and Cloetingh [1983]. Previous reconstructions of the Galapagos Rise system suggest that the propagation began at or near the Garrett fracture zone [Mammerick, 1980, Lonsdale, 1989, Goff and Cochran, 1996], and involved the northward propagation of the EPR, the SEGR, and the NGR spreading systems. In particular, the Goff and Cochran [1996] reconstruction suggests the propagation

of simultaneous spreading centers (EPR and Galapagos Rise) from the Garrett fracture zone. This reconstruction involves the rotation of both spreading systems, but is inconsistent with the straight fracture zones apparent in the bathymetry of the EPR.

The fan-shaped spreading boundaries of the Galapagos Rise, however, suggest a southward propagation as the widest area of seafloor (~750 km) from the rise crest to the Mendaña fracture zone produced by the Galapagos Rise is associated with the northern (GR1) ridge crest. The seafloor produced from the central (GR2) segment is ~650 km from the ridge crest to the Mendaña fracture zone. An explanation for this would be that the GR1 segment was active for the longest period of time, which is consistent with both the southward propagation of the ridge segments and the progressively northward failure of active spreading as full spreading rates were transferred to the EPR. It is also possible, however, that the fan-shaped boundaries of this system were produced by different spreading rates along different segments of the ridge system. The nearby pole of rotation (Figure 16) indicates that the fastest spreading rates would have occurred on the GR1 segment, with progressively slower spreading rates on the southern segments. This is consistent with the higher extensional stresses in the northern part of the Nazca plate, as calculated by Wortel and Cloetingh [1983]. The rough topography zones proposed by Goff and Cochran [1996] that indicate the initial spreading of the Galapagos Rise also form a wedge shape that narrows to the south, consistent with slower spreading rates on the more southern segments.

The propagation of the SEGR began at approximately the same time as the initiation of the Galapagos Rise (~20 Ma), but this system propagated northward to the Bauer fracture zone. The small offsets in the ridge crest segments visible in the bathymetry display little evidence of rotation during spreading (no curved fracture zones). This system failed earlier than the Galapagos Rise (~13 Ma). The slope of the seafloor eastward from the EPR at the same latitudes (18-26°S) indicates that this segment of the EPR was active at the same time as the SEGR. Magnetic anomaly lineations in this area are oriented due north, consistent with the trend of the EPR. With both the EPR and the SEGR actively spreading, the seafloor in between them becomes a microplate (Mendoza) bounded on the north by the Bauer fracture zone and on the south by the Sala Y Gomez ridge. Curved fracture zones and ridge crests, such as those seen in the Galapagos Rise and the Easter microplate [Larson et al., 1992, Searle et al., 1993, Rusby and Searle, 1995, Bird et al., 1998] are not apparent on the Mendoza microplate, indicating that little rotation of this microplate occurred. The westward curve at the northern tip of the SEGR ridge segments suggests interaction of this segment with the Bauer fracture zone. The presence of the Bauer fracture zone during the propagation of the SEGR constrains the initiation of the Galapagos Rise as being earlier than or concurrent with the propagation of the SEGR. The SEGR segment represents a clearly defined transitional phase in the accommodation of the Nazca plate to the new plate motions that resulted from the Farallon breakup.

Also initiating at the time of the Galapagos Rise was the NGR. These segments are associated with seafloor that deepens (ages) with distance eastward, indicating that these segments were active from ~20 Ma. The EPR eventually (at ~1.95 Ma) began spreading rapidly west of the NGR ridge crests, propagating through seafloor produced on the western side of the NGR. This section of seafloor between the NGR and EPR must be trapped Pacific plate. It is, however, difficult to recognize the depth/age distribution or magnetic anomalies that would identify the captured seafloor on the Pacific plate. It is possible then that the seafloor produced on the eastern side of the NGR was the product of asymmetric spreading, but spreading rate required to produce the observed seafloor would be approximately ten times higher on the eastern side of the NGR than the western side. This degree of asymmetry is not observed on other systems, and is therefore unlikely to be the cause of the seafloor depth distributions observed near the NGR. There is a large area of shallow, gently sloping seafloor from 3-7°S and west of ~112°W (Figure 20) that may have been produced by the western side of the NGR and accreted to the Pacific plate. Further investigation is needed to identify this section of seafloor and its relationship to the Pacific-Nazca spreading systems.

One of the major components of the Galapagos Rise reconstructions (both in previous literature and this study) was the evolution of the Bauer Basin. The two competing explanations for the formation of the Bauer Basin are 1) that the entire Bauer Basin was “captured” seafloor produced by the Pacific-Farallon spreading center added to the Pacific plate when the Galapagos Rise initiated,

then captured to the Nazca plate when the EPR started, and 2) that the entire Bauer Basin was produced by the Galapagos Rise during the early spreading stage of the system. By ~15-16 Ma, the seafloor sampled at DSDP Site 319 had been produced in the southwestern Bauer Basin, according to the age determinations from K-Ar, and ^{40}Ar-^{39}Ar dating of cored basalts [Hogan and Dymond, 1976, Lanphere and Dalrymple, 1976, Seidermann, 1976, Reynolds, 1976, Macdougall, 1976, Mitchell and Aumento, 1976]. The northern part of the Bauer Basin is likely "captured" Farallon plate seafloor based on its 23-30 Ma depth-predicted age. The southern Bauer Basin is younger than the northern region, determined both by depth-predicted age and isotope dating of the seafloor basalts at DSDP Site 319, suggesting that it was produced by the earliest spreading along the Galapagos Rise. The Bauer Basin is therefore a combination of the "captured" older seafloor and the accreted Galapagos Rise seafloor.

The failure of the Galapagos Rise occurred in stages, with the spreading between the Pacific and Nazca plates progressively transferred to the EPR, as it propagated to the north from the Garrett fracture zone. The GR1 segment was the last of the Galapagos Rise segments to cease spreading. By 5.9 Ma, the EPR had accelerated to the fast spreading rates it has today (~110 mm/yr) [Herron, 1972, Handschumacher, 1976, Mammerickx et al., 1975, Mammerickx et al., 1980, Engebretson, 1984, Cande, 1986, Rosa and Molnar, 1988, Lonsdale, 1989, Mayes et al. 1990, Cande and Haxby, 1991, Goff and Cochran, 1996, Jordahl et al., 1998] and the Galapagos Rise had failed completely. The

prominent northern ridge segments, as shallow as ~600 m, were most likely produced by post-spreading volcanism and bordered by ~200 m deep moats. The only remaining activity on structures related to the Galapagos Rise was earthquakes detected by the hydrophones in the equatorial Pacific [Fox et al., 2001]. This seismic activity is generally confined to the Gallego fracture zones and most likely related to differential seafloor subsidence due to age differences across the fracture zones.

The transition from Pacific-Farallon spreading to Pacific-Nazca spreading involved a progression of intermediate spreading configurations between 23 Ma and 1.95 Ma. These included general northward-propagation of the EPR, ridge jumps, and microplate formation. Galapagos Rise and Bauer Basin constitute the largest and most complex parts of these transitional stages.

CONCLUSIONS

The conversion of the predicted bathymetry grid [Smith and Sandwell, 1997] to a predicted age grid based on the calibration with dated magnetic anomalies on the Nazca plate and western slope of the seafloor produced by the EPR [Cande et al., 1989] yields a systematic age distribution of seafloor spreading history in the study area. The predicted age grid is therefore a useful tool in determining the evolution of the southeast Pacific following the breakup of the Farallon plate.

The Galapagos Rise represented the transitional stage of seafloor spreading from 3-18°S between the Pacific-Farallon spreading system that was active at 23 Ma and the current EPR system. The Galapagos Rise system was active from shortly after 23 Ma until the EPR became the dominant spreading system at the same latitudes at 5.9 Ma. Spreading initiated along the Galapagos Rise system subparallel to the Mendaña fracture zone, and propagated southward to the Bauer fracture zone. As suggested by the curvature of the Gallego fracture zones, the orientations of the magnetic anomaly lineations mapped within the Galapagos Rise seafloor spreading boundaries, and the fan shaped boundaries of the Galapagos Rise system, the Galapagos Rise rotated rapidly counter-clockwise about a nearby pole of rotation (~22.5°S, ~99.5°W) relative to the Nazca plate. This rapid “local” rotation of the Galapagos Rise, and thus necessarily the Bauer Basin, therefore

requires Bauer Basin to have been a rotating microplate. A southward direction of propagation is consistent with the distribution of tensional stresses in the region as suggested by Wortel and Cloetingh [1983].

North of the Bauer Basin and the Gallego fracture zones, the NGR segments of the Galapagos Rise produced a vast part of the Nazca plate, south of 5°S and east to 85°W, as indicated by the depth distribution in the region north of the Gallego fracture zones. These segments connected the Galapagos Rise system to the Galapagos Ridge system until the EPR propagated through the seafloor produced on the western side of the NGR, 1.95 Ma to the present. The Bauer Scarp from 3-7°S displays curved bathymetric trough structures similar to those further south, suggesting that there were rotational stresses all along the northward propagation of the EPR through then-Pacific seafloor, everywhere west of the Galapagos Rise.

The SEGR was the primary transitional stage of seafloor spreading between the Pacific-Farallon spreading system and the current EPR system between 18°S and 26°S, and was active for a short period from ~19.5 to shortly after 14.7 Ma. This system propagated northward from the Sala Y Gomez ridge to the Bauer fracture zone, and accommodated the full rotation between the Pacific-Farallon and the Nazca-Pacific spreading systems. Unlike the Galapagos Rise, the SEGR was a northward propagating system producing a wide wedge of seafloor at the south along the Sala Y Gomez ridge and narrowing to the north at the Bauer fracture zone (Figure 27). The EPR from 18-

26°S was also spreading rapidly at this time, indicated by the long gradual slope on the eastern side of the EPR. The simultaneous spreading of the EPR and the SEGR was short-lived, with the EPR taking over the full spreading rate by 14.7 Ma.

The evolution of the Galapagos Rise system involved the creation of several microplates bounded by the Galapagos Rise spreading system to the east and the EPR spreading system to the west. The largest of these, the Bauer Microplate, consisted of seafloor produced by the Pacific-Farallon system, and is bounded on the north by the Gallego fracture zones and on the south by the Bauer fracture zone. The cessation of Galapagos Rise spreading caused the accretion of the Bauer Microplate to the Nazca plate on the eastern side of the EPR. The Mendoza microplate (Figure 1) was originally proposed by Lonsdale [1989] to have been bounded by the Mendoza Rise (part of the Pacific-Farallon spreading system) and the EPR from 18-26°S. The SEGR is concluded here to have been the eastern boundary of the Mendoza microplate. The Mendoza Microplate was bounded on the south by the Sala Y Gomez ridge, on the north by the Bauer fracture zone, and on the west by the EPR from ~19.5 to shortly after 14.7 Ma. When the SEGR failed, the Mendoza microplate was accreted to the Nazca plate. The third microplate associated with the Galapagos Rise system is the Quebrada microplate (Figure 1). This microplate was bounded by the NGR segments to the east, the Gallego fracture zones to the south, and the Quebrada fracture zone to the north. The bathymetric troughs visible on the

western side of the microplate, related to EPR propagation, are structures similar to those identified on the Bauer and anti-Bauer Scarps suggested by Goff and Cochran [1996] and suggest the presence of rotational kinematics during the propagation of the EPR through this area.

Failure of the Galapagos Rise occurred in stages progressing from south to north, transferring seafloor spreading by means of a series of ridge jumps to the EPR. Magnetic anomaly lineations identified as Anomaly 2 (1.95 Ma) in the north and 3a (6.57 Ma) near Garrett fracture zone along the EPR [Cande et al., 1989] document the full transfer of spreading to the EPR.

REFERENCES

Barrett, T. J., and H. Friedrichsen (1982), Elemental and isotopic compositions of some metalliferous and pelagic sediments from the Galapagos mound area, DSDP Leg 70, *Chem. Geol.*, *36*, 275-298.

Bird, R. T., D. F. Naar, R. L. Larson, R. C. Searle, and C. R. Scotese (1998), Plate tectonic reconstructions of the Juan Fernandez microplate: Transformation from internal shear to rigid rotation, *J. Geophys. Res.*, *103*, 7049-7067.

Calcagno, P. and A. Cazenave (1994), Subsidence of the seafloor in the Atlantic and Pacific oceans; regional and large-scale variations, *Earth Planet. Sci. Lett., 126,* 473-492.

Cande, S. C., and W. H. Haxby (1991), Eocene propagating rifts in the southwest Pacific and their conjugate features on the Nazca plate, *J. Geophys. Res., 96,* 19,609-19,622.

Cande, S. C., and D. V. Kent (1992), A new geomagnetic polarity time scale for the Cretaceous and Cenozoic, *J. Geophys. Res., 97,* 13,917-13,951.

Cande, S. C., and D. V. Kent (1995), Revised calibration of the geomagnetic polarity timescale for the Late Cretaceous and Cenozoic, *J. Geophys. Res., 100*(4), 6093-6095.

Cande, S. C., and R. B. Leslie (1986), Late Cenozoic tectonics of the southern Chile Trench, *J. Geophys. Res. B, 91*(1), 471-496.

Cande, S. C., E. M. Herron, and B. R. Hall (1982), The early Cenozoic tectonic history of the Southeast Pacific, *Earth Planet. Sci. Lett., 57*(1), 63-74.

Cande, S. C., J. L. LaBrecque, R. L. Larson, W. C. Pitmann III, X Golovchenko, and W. F. Haxby, (1989), Magnetic lineations of the world's ocean basins, *AAPG Map Ser., 131,* Tulsa, Oklahoma.

Cochran, J. R. (1986), Variations in subsidence rates along intermediate and fast spreading mid-ocean ridges, *Geophys. J. R. Astron. Soc., 87*, 421-454.

Cox, A., and R. B. Hart (1986), *Plate Tectonics: How It Works*, 392 pp., Blackwell Scientific Publications, Palo Alto, California.

Davis, E. E. and C. R. B. Lister (1974), Fundamentals of ridge crest topography, *Earth Planet. Sci. Lett., 21*, 405-413.

DeLaughter, J., S. Stein, C. A. Stein (1999), Extraction of a lithospheric cooling signal from oceanwide geoid data, *Earth Planet. Sci. Lett., 174*, 173-181.

Engebretson, D. C., A. Cox, and R. G. Gordon (1984), Relative motions between oceanic plates of the Pacific Basin, *J. Geophys. Res., 89,* 10,291-10,310.

Fox, C. G., H. Matsumoto, and T-K.A. Lau (2001), Monitoring Pacific Ocean seismicity from an autonomous hydrophone array, *J. Geophys. Res., 106,* 4183-4206.

Goff, J. A., and J. R. Cochran (1996), The Bauer Scarp ridge jump: a complex tectonic sequence revealed in satellite altimetry, *Earth Planet. Sci. Lett., 141*, 21-33.

Handschumacher, D. (1976), Post-Eocene plate tectonics of the eastern Pacific, *Am. Geophys. Union, Geophys. Monogr., 19*, 177-202.

Hay, W. W., R. DeConto, C. N. Wold, K. M. Wilson, S. Voigt, M. Schulz, A. Wold-Rossby, W. C. Dullo, A. B. Ronov, A. N. Balukhovsky, and E. Soeding (1999), Alternative global Cretaceous paleogeography, in *Evolution of Cretaceous Ocean/Climate Systems,* edited by E. Barrera, and C. Johnson, Geological Society of America Special Paper 332, pp. 1-47.

Hayes, D. E. (1992), Age-depth relationships and depth anomalies in the southeast Indian Ocean and South Atlantic Ocean, *J. Geophys. Res.*, 97, 17317-17330.

Herron, E. M. (1972), Sea-floor spreading and the Cenozoic history of the East-Central Pacific, *Geol. Soc. Am. Bull., 83*, 1671-1692.

Hey, R. N. (1977), Tectonic evolution of the Cocos-Nazca spreading center. *Geol. Soc. Am. Bull., 88,* 1404-1420.

Hey, R. N., F. K. Duennebier, and W. J. Morgan, (1980), Propagating rifts on midocean ridges, *J. Geophys. Res., 85*, 3647–3658.

Hogan, L., and J. Dymond (1976), K-Ar and ^{40}Ar ^{39} Ar dating of Site 319 and 321 basalts, in *Init. Repts. DSDP, 34,* edited by R. S. Yeats and S. R. Hart, pp. 439-442, Texas A & M University, Ocean Drilling Program, College Station, Texas.

Jordahl, K. A., M. K. McNutt, and H. Zorn (1998), Pacific-Farallon relative motion 42-59 Ma determined from magnetic and tectonic data from the southern Austral Islands, *Geophys. Res. Lett., 25*, 2869-2872.

Lanphere, M. A., and G. B. Dalrymple (1976), Potassium-argon age of a basalt from Hole 319A, DSDP Leg 34, in *Init. Repts. DSDP, 34,* edited by R. S. Yeats and S. R. Hart, pp. 443-444, Texas A & M University, Ocean Drilling Program, College Station, Texas.

Larson, R. L., R. C. Searle, M. C. Kleinrock, H. Schouten, R. T. Bird, D. F. Naar, R. I. Rusby, E. E. Hooft, and H. Lasthiotakis (1992), Roller-bearing tectonic evolution of the Juan Fernandez microplate, *Nature*, *356*, 571-576.

Levitt, D. A., and D. T. Sandwell (1996), Modal depth anomalies from multibeam bathymetry: Is there a South Pacific superswell?, *Earth Planet. Sci. Lett., 139*, 1-16.

Lonsdale, P. (1989), Segmentation of the Pacific-Nazca Spreading Center, 1°N-20°S, *J. Geophys. Res., 94*, 12,197-12,225.

Macdougall, D. (1976), Fission track studies of basalt from Leg 34, in *Init. Repts. DSDP, 34,* edited by R. S. Yeats and S. R. Hart, 45 pp., Texas A & M University, Ocean Drilling Program, College Station, Texas.

Mammerickx, J., and D. Sandwell (1986), Rifting of old oceanic lithosphere, *J. Geophys. Res., 91* (B2), 1975-1988.

Mammerickx, J., R. N. Anderson, H. W. Menard, and S. M. Smith (1975), Morphology and tectonic evolution of the East-Central Pacific, *Geol. Soc. Am. Bull., 86*(1), 111-117.

Mammerickx, J., E. Herron, and L. Dorman (1980), Evidence for two fossil spreading ridges in the southeast Pacific, *Geol. Soc. Am. Bull., 91*, 263-271.

Marks, K. M., and J. M. Stock (1994), Variations in ridge morphology and depth-age relationships on the Pacific-Antarctic ridge, *J. Geophys., Res. 99*, 531-541.

Marty, J. C., and A. Cazenave (1989), Regional variations in subsidence rate of oceanic plate: a global analysis, *Earth Planet. Sci. Lett., 94*, 301-315.

Mayes, C. L., L. A. Lawver, and D. S. Sandwell (1990), Tectonic history and new isochron chart of the South Pacific, *J. Geophys. Res., 95*, 8543-8567.

McGuire, J. C., and T. W. C. Hilde (1999), Tortured early history of the Nazca plate, *EOS Trans. AGU, 80*(46), 1070.

McGuire, J. C., and T. W. C. Hilde (2002), Galapagos Rise to East Pacific Rise spreading history, *EOS Trans. AGU, 83*(47), 1359.

Menard, H. W. (1978), Fragmentation of the Farallon Plate by pivoting subduction, *J. of Geology*, *86*(1), 99-110.

Menard, H. W., T. E. Chase, and S. M. Smith (1964), Galapagos Rise in the southeastern Pacific, *Deep-Sea Research*, *83*, 233-242.

Meschede, M., and U. Barckhausen, (2000), Plate tectonic evolution of theCocos-Nazca spreading center, in *Proc. ODP, Sci. Results,* 170, edited by E. A. Silver, G. Kimura, and T. H. Shipley, pp. 1-10, Texas A & M University, Ocean Drilling Program, College Station, Texas.

Mitchell, W. S., and F. Aumento (1976), Fission track chronology and uranium content of basalts from DSDP Leg 34, in *Init. Repts. DSDP, 34,* edited by R. S. Yeats and S. R. Hart, pp. 451-453, Texas A & M University, Ocean Drilling Program, College Station, Texas.

Mueller, R. D., J.-Y. Royer, and L. A. Lawver (1993), Revised plate motions relative to the hotspots from combined Atlantic and Indian Ocean hotspot tracks, *Geology, 21*, 275-278.

Pardo-Casas, F., and P. Molnar (1987), Relative motion of the Nazca (Farallon) and South American plates since late Cretaceous time, *Tectonics 6*(3), 233-248.

Parsons, B., and J. G. Sclater (1977), An analysis of the variation of ocean floor bathymetry and heat flow with age, *J. Geophys. Res., 82*(5), 803-827.

Perrot, K., J. Francheteau, M. Maia, and C. Tisseau (1998), Spatial and temporal variations of subsidence of the East Pacific Rise (0-23°S), *Earth Planet. Sci. Lett. 160*, 593-607.

Phipps Morgan, J., and W. H. F. Smith (1992), Flattening of the age-depth as a response to asthenospheric flow, *Nature 359*, 5524-527.

Rea, D. K. (1978), Evolution of the East Pacific Rise between 3°S and 13°S since the middle Miocene, *Geophys. Res. Lett., 5*(7), 561-564.

Rea, D. K. (1981), Tectonics of the Nazca-Pacific divergent plate boundary, *Mem. Geo. Soc. Am.*, *154*, 27-62.

Reynolds, P. H. (1976), ^{40}Ar ^{39}Ar dating of Leg 34 basalts, in *Init. Repts. DSDP, 34,* edited by R. S. Yeats and S. R. Hart, pp. 449-450, Texas A & M University, Ocean Drilling Program, College Station, Texas.

Rosa, J. W. C., and P. Molnar (1988), Uncertainties in reconstructions of the Pacific, Farallon, Vancouver, and Kula plates and constraints on the rigidity of the Pacific and Farallon (and Vancouver) plates between 72 and 35 Ma, *J. Geophysical Res., 93*, 2997-3008.

Rusby, R. I., and R. C. Searle (1995), A history of the Easter Microplate, 5.25 Ma to Present, *J. Geophys. Res*, *100*, 12,617-12,640.

Sandwell, D. T. (1990), Geophysical applications of satellite altimetry, *Rev. of Geophys. Supp.*, 132-137. Available at: http://www.ngdc.noaa.gov/mgg/bathymetry/predicted/explore.HTML

Sandwell, David T., and Walter H. F. Smith (1994), Marine gravity anomaly from Geosat and ERS-1 satellite altimetry, *J. Geophysical Res., 102*, 10,039-10,054.

Schouten, H., and K. McCamy (1972), Filtering marine magnetic anomalies, *J. Geophys. Res. 77*, 7089-7099.

Sclater, J. G., R. N. Anderson, and M. L. Bell (1971), Elevation of ridges and evolution of the Central Eastern Pacific, *J. Geophysical Res., 76* (32), 7888-7915.

Searle, R. C. (1989), Location and segmentation of the Cocos-Nazca spreading centre west of 95°W. *Mar. Geophys. Res. 11*, 15-26.

Searle, R. C. and J. Francheteau (1986), Morphology and tectonics of the Galapagos triple junction, *Mar. Geophys. Res. 8*, 95-129.

Searle, R. C., R. T. Bird, R. I. Rusby, and D. F. Naar (1993), The development of two oceanic microplates: Easter and Juan Fernandez microplates, East Pacific Rise, *J. of the Geo. Soc. London*, *150*, 965-976.

Seidemann, D. E. (1976), K-Ar date for basaltic rocks from Site 319 and 321, Leg 34, in *Init. Repts. DSDP, 34,* edited by R. S. Yeats and S. R. Hart, pp. 445-447, Texas A & M University, Ocean Drilling Program, College Station, Texas.

Smith, W. H. F. (1993), On the accuracy of digital bathymetric data, J*. Geophys. Res. 98*, 9591-9603.

Smith, W. H. F., and D. T. Sandwell (1997), Global seafloor topography from satellite altimetry and ship depth soundings, *Science, 277,* 1957-1962.

Stein, C. A., and S. Stein (1992), A model for the global variation in oceanic depth and heat flow with lithospheric age, *Nature 359*, 123-129.

Tebbens, S. F., and S. C. Cande (1997), Southeast Pacific tectonic evolution from early Oligocene to present, *J. Geophys. Res., 102* (6), 12,061-12,084.

Tebbens, S. F., S. C. Cande, L. Kovacs, J. C. Parra, J. L. LaBrecque, and H. Vergara (1997), The Chile Ridge; a tectonic framework, *J. Geophys. Res., 102* (6), 12,035-12,059.

Warsi, W. E. K., T. W. C. Hilde, and R. C. Searle (1983), Convergence structures of the Peru Trench between 10°S. and 14°S. *Tectonophysics, 99, 313-329*.

Wessel, P., and W. H. F. Smith (1991), Free software helps map and display data, *Eos, Trans., AGU, 72,* 445-446.

Wessel, P., and W. H. F. Smith (1995), New version of the generic mapping tools released, *Eos Trans., AGU*, *76*, 329.

Wortel, R., and S. Cloetingh (1983), A mechanism for fragmentation of oceanic plates, in *Studies of Continental Margin Geology,* Memoir 34, edited by J. S. Watkins and C. L. Drake, pp. 793-801, AAPG, Tulsa, Oklahoma.

Yeats R. S., S. R. Hart, J. M. Ade-Hall, M. N. Bass, W. E. Benson, R. Hart, P. G. Quilty, H. M. Sachs, M. H. Salisbury, T. L. Vallier (1976), Site 319, in *Init. Repts. DSDP , 34,* edited by R. S. Yeats and S. R. Hart, pp. 19-80, Texas A & M University, Ocean Drilling Program, College Station, Texas.

VITA

The author, Jennifer Catherine McGuire Wright, was born on January 11, 1973, in Albany, New York, to Mr. and Mrs. John E. McGuire, Sr. From 1991 to 1995, she attended the State University of New York at Stony Brook, where she obtained a B.S. degree in Geology with a minor in English in May 1995. During the summer of 1997, she worked as a geophysical intern for Arco Exploration and Production Co. in Plano, Texas. In the summer of 1998, she joined Shell Oil Co. Deepwater Division in New Orleans, Louisiana, as a geophysical intern. In the fall of 2001, she sailed as a Physical Properties Specialist aboard the *JOIDES Resolution* on Ocean Drilling Program Leg 198. From 1995 to 2004, she attended Texas A&M University, where she pursued a Ph. D. degree in Geophysics. Address any correspondence to the author at 146 Holcomb Rd, Averill Park, NY 12018